# Performance testing of an axial flow fan in an A-frame test facility

by
Johannes van Eck

*Thesis presented in partial fulfilment of the requirements for the degree of Master of Mechanical Engineering in the Faculty of Engineering at Stellenbosch University*

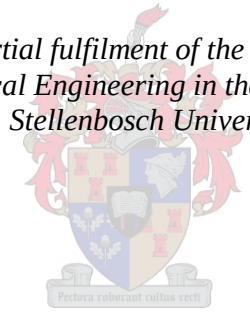


Supervisor: Dr J. Muiyser
Co-supervisor: Dr D.N.J Els

April 2019

# Declaration

By submitting this thesis electronically, I declare that the entirety of the work contained therein is my own, original work, that I am the sole author thereof (save to the extent explicitly otherwise stated), that reproduction and publication thereof by Stellenbosch University will not infringe any third party rights and that I have not previously in its entirety or in part submitted it for obtaining any qualification.

Date: April 2019

UNIVERSITEIT·STELLENBOSCH·UNIVERSITY
jou kennisvennoot • your knowledge partner

# Plagiaatverklaring / *Plagiarism Declaration*

1 Plagiaat is die oorneem en gebruik van die idees, materiaal en ander intellektuele eiendom van ander persone asof dit jou eie werk is.
*Plagiarism is the use of ideas, material and other intellectual property of another's work and to present is as my own.*

2 Ek erken dat die pleeg van plagiaat 'n strafbare oortreding is aangesien dit 'n vorm van diefstal is.
*I agree that plagiarism is a punishable offence because it constitutes theft.*

3 Ek verstaan ook dat direkte vertalings plagiaat is.
*I also understand that direct translations are plagiarism.*

4 Dienooreenkomstig is alle aanhalings en bydraes vanuit enige bron (ingesluit die internet) volledig verwys (erken). Ek erken dat die woordelikse aanhaal van teks sonder aanhalingstekens (selfs al word die bron volledig erken) plagiaat is.
*Accordingly all quotations and contributions from any source whatsoever (including the internet) have been cited fully. I understand that the reproduction of text without quotation marks (even when the source is cited) is plagiarism.*

5 Ek verklaar dat die werk in hierdie skryfstuk vervat, behalwe waar anders aangedui, my eie oorspronklike werk is en dat ek dit nie vantevore in die geheel of gedeeltelik ingehandig het vir bepunting in hierdie module/werkstuk of 'n ander module/werkstuk nie.
*I declare that the work contained in this assignment, except otherwise stated, is my original work and that I have not previously (in its entirety or in part) submitted it for grading in this module/assignment or another module/assignment.*

| | |
|---|---|
| J van Eck<br>Voorletters en van / *Initials and surname* | Datum / *Date* April 2019 |

# Abstract

**Performance testing of an axial flow fan in an A-frame test facility**

The primary objective of this research and experimental investigation is to determine the performance of an axial flow fan in an A-frame test facility. Commissioning of the A-frame test facility required certain modifications which allowed the facility to be used for testing purposes. Modifications include a new fan drive system, fan bridge, heat exchanger and structural supports. The bell mouth roundness was improved upon, achieving a more constant tip clearance around the casing, and all air leaks around the facility were sealed to prevent loss of mass flow. Tests were conducted on the B2-fan, according to standardised fan testing procedures in ISO 5801 (2007) Type-A, to obtain the fan characteristics at selected blade angles. The measurements recorded at the A-frame test facility included outlet velocity, inlet velocity, fan torque and rotational speed measurements. The outlet velocity profiles differ for the two heat exchanger outlets, but the total volumetric flow rate differs only by 3% for the two sides. It was also found that the velocity profile stays similar with a change in blade angle, but increases in magnitude as the blade angle is increased. Pressure measurements according to ISO 5802 (2008), at the walls of the plenum chamber, were regarded as unusable due to it being much lower than the expected pressure.

With the use of the system draft equation from Kröger (2004, 8.1.30) it was possible to calculate a recovery coefficient for the A-frame plenum chamber at different blade angle settings of the B2-fan, with values of 0.505, 0.685 and 0.412 for the 28º, 31º and 34º blade angles respectively. The recovery coefficient calculated for the M-fan equalled 0.143 and 0.322 for the 34º and 35º blade angles respectively. This value represents the portion of kinetic energy that is converted back into a pressure. The sensitivity of the recovery coefficient to change in volumetric flow rate and heat exchanger loss coefficient was also investigated with the use of a Monte Carlo simulation. The importance of accurately measuring the volumetric flow rate is shown by a normal distribution of the recovery value with the use of the mean and standard deviation of the volumetric flow rate. A functional A-frame test facility can now be used to test different heat exchanger and fan configurations. By changing the fan, heat exchanger type or area, the performance of the A-frame setup can be analysed for various heat exchanger and fan configurations.

# Uittreksel

**Toets van ‘n aksiaalwaaier in ‘n A-raam toets fasiliteit**

Die primêre doelwit van hierdie navorsing en experimentele ondersoek is om die werking van ‘n aksiaal waaier binne ‘n A-raam toets fasiliteit te bepaal. Die ingebruikstelling van die A-raam toetsfasiliteit het sekere aanpassings benodig wat die fasiliteit bruikbaar vir toets doeleindes gestel het. Aanpassings sluit ‘n nuwe waaier aandryfstelsel, waaier brug, warmte uitruiler en strukturele versterkings in. Die klokmond inlaat se rondheid is verbeter wat daartoe gelei het dat ‘n meer konstante waaier lempunt spasiëring binne die omhulsel bereik is. Verder is alle lekplekke verseel sodat daar geen massavloei verlore gaan nie. Toetse is gedoen op die B2-waaier volgens die standard waaier toets prosedures soos in ISO 5801 (2007) Tipe A om die waaier karakteristieke by sekere lem hoeke te verkry. Die metings wat by die A-raam fasilitiet geneem is sluit die uitlaat snelheid, inlaat snelheid, waaier wringkrag en die waaier omwentelingspoed in. Die uitlaat snelheidsprofiel verskil vir die twee warmte-uitruilers, maar die totale volumetriese vloeitempo tussen die twee kante slegs met 3%. Die snelheidsprofiel bly naastenby dieselfde vir verskillende lemhoeke en verander slegs met ‘n konstante waarde regoor die profiel, Druklesings is ook geneem in die vier mure volgens ISO 5802 (2008), maar die resultate daarvan as nutteloos beskou weens dit heeltemal te lae resultate gegee het.

Deur gebruik te maak van die sisteem vloei vergelyking, vanaf Kröger (2004, 8.1.30), is die druk herwinningskoëffisiënt vir die B2-waaier in die A-raam opstelling bereken om 0.505, 0.685 en 0.412 vir die 28º, 31º and 34º lemhoeke respektiewelik te wees. Die herwinningskoëffisiënt vir die M-waaier is bereken om 0.143 en 0.322 vir die 34º en 35º lemhoeke respektiewelik te wees. Hierdie koëffisiënt word gebruik om die gedeelte kinetiese energie wat in druk omgeskakel word binne die plenum kamer te beskryf. Die sensitiwiteit van hierdie koëffisiënt vir verandering in die volumetriese vloeitempo en warmte uitruiler druk verlies koëffisiënt is ook bereken deur gebruik te maak van die Monte Carlo metode. Die belangrikheid van akkurate metings om die volumetriese vloeitempo te bereken word duidelik gemaak deur die normaal verspreiding van die herwinnings koëffisiënt deur gebruik te maak van die gemiddelde en standaardafwyking van die volumetriese vloeitempo. ‘n Funsionele A-raam toetsfasiliteit kan nou gebruik word om verskillende warmte uitruiler en waaier samestellings mee te toets. Deur die waaier, tipe warmte uitruiler of die area van die warmte uitruiler te verander, kan die A-raam opstelling getoets word vir verskillende warmte uitruiler en waaier opstelling senarios.

# Acknowledgements

I would like to acknowledge my friends and family who stood by me through the good and the not so good times. To my mom, Naomi van Eck, I would like to say thank you for always being there and for all your support. You are a winner and can do anything you set your mind to. My dad, Johannes Jacobus van Eck, I would like to thank for your inspiration and motivation. I always enjoy our long conversations about new patents and projects entering the global market. My sister Petro van Eck, thank you for the example you set for all of us. You are indeed a driven person who gets the job done! My brother, Jacobus van Eck, I would like to thank for your humour in almost every situation. You always find a way to make someone laugh with the strangest of stunts. Jana-Mari, I would like to say thank you for always being there to light up my day when I needed it the most. Also thank you for your time assisting me in performing the tests at the test facilities. Without you it would have taken much longer. To Jana-Mari's family I say thank you for your interest in the progress and all your support.

I would also like to thank Hein Joubert for his intellectual contributions when I got stuck and needed some good insight in design matters. I appreciate your friendship.

Many thanks to Dr. Jacques Muiyser and Dr. Danie Els for the opportunity to do this research project. I am very grateful for all your input and guidance throughout the whole project. The project wouldn't have been such a success without you.

Dr. Francois Louw, I would like to thank you and your colleagues at Kelvion for all your effort and time regarding the finned heat exchanger tubes. Also, many thanks to Kelvion for the sponsoring of the tubes at a discounted price.

I would like to thank the staff of the workshop for their contributions in the manufacturing process, our long conversations and especially to Maurisha who I could always bother for some more tools. Calvin Harmse and Jacobus Samuels, I enjoyed working together with you. Your humour is always there to cheer someone up. Many thanks also to Ferdie and Cobus Zietsman for their guidance regarding the design process. Nathi and Julian, thank you for always assisting when needed.

Finally I would like to thank my Lord and Saviour, Jesus Christ, for the opportunities we have. I am grateful even for the difficult times of growth.

# Table of contents

# List of figures

**Page**

# List of tables

**Page**

# Nomenclature

## Abbreviations

| | |
|---|---|
| ACC | Air Cooled Condenser |

## Variables

| | | |
|---|---|---|
| $A$ | Area | [$m^2$] |
| $C_D$ | Coefficient of drag | |
| $C_p$ | Specific heat at constant pressure | [J/kgK] |
| $C_v$ | Specific heat at constant volume | [J/kgK] |
| $D$ | Diameter | [m] |
| d | Diameter | [m] |
| $E$ | Voltage | [V] |
| $F$ | Force | [N] |
| G | Mass velocity | [$kg/m^2s$] |
| $L$ | Length | [m] |
| $\dot{m}$ | Mass flow rate | [kg/s] |
| $m$ | mass | [kg] |
| $N$ | Rotational velocity | [rpm] |
| $p$ | Pressure | [$N/m^2$] |
| $P$ | Power | [W] |
| $r$ | Radius | [m] |
| $T$ | Temperature | [ºC] |
| $T$ | Torque | [N.m] |
| $v$ | Velocity | [m/s] |
| $V$ | Volumetric flow rate | [$m^3/s$] |
| $V$ | Voltage | [V] |
| $W$ | Width | [m] |

## Greek Symbols

| | |
|---|---|
| $\beta$ | Thermal expansion coefficient |
| $\eta$ | Efficiency |
| $\mu$ | Viscosity |
| $\rho$ | Density |
| $\varepsilon$ | Effectiveness |

## Subscripts

| | |
|---|---|
| $a$ | Air |
| $abs$ | Absolute |
| $amb$ | Ambient |
| $app$ | Approach |
| $b$ | Bridge |
| $c$ | Fan cross sectional area/Casing |
| $cal$ | Calibrated |
| $b$ | Bundle |

| | |
|---|---|
| *D* | Drag |
| *do* | Downstream |
| *e* | Effective fan flow area |
| *F* | Fan |
| *f* | Fin |
| *fr* | Frontal |
| *h* | Hub |
| *he* | Heat exchanger |
| *l* | Lognitudinal |
| *meas* | Measured |
| *n* | Nozzle |
| *o* | Outer |
| *r* | Root |
| *rec* | Recovery |
| *s* | Static |
| *sc* | Settling chamber |
| *sh* | Shaft |
| *sup* | Support |
| *t* | Total/Transverse |
| tr | Tube rows |
| *up* | Upstream |

**Constant Values**

| | | | |
|---|---|---|---|
| R | Ideal gas constant | 8.314 | [J/mol.K] |

# 1 Introduction

## 1.1 Background

Fans are used in various industrial processes where cooling, mixing and ventilation is required. These fans may differ in shape and size depending on the particular application. Factors such as noise, cost and performance characteristics are considered when selecting the correct fan to be used for the specific application. For high flow rate at low pressure, axial flow fans are used. The volumetric flow rate of these fans at a specified rotational speed increases with an increase in the number of fan blades (Kröger, 2004: 6.0.1). Increasing the angle of attack or rotational speed also results in an increase in the volumetric flow rate.

In many industries cooling of a working fluid is required. Dry cooling is normally used where water is scarce. This requires a closed loop system where the working fluid is cooled and reused in the next cycle. Air-cooled condensers find application in many of these industries and are used in induced draft and forced draft configurations. Forced draft dry cooling normally consists of an axial flow fan which forces air flow through the heat exchanger bundles. The air-cooled condenser, ACC, may take on various shapes, but commonly used today is the A-frame plenum as shown in Figure 1.1.

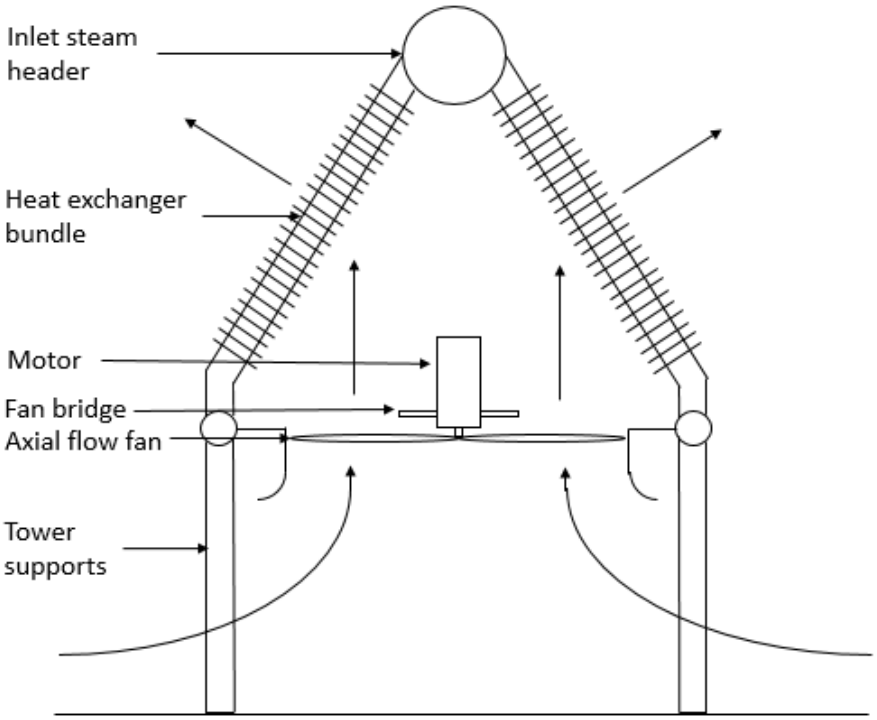


Figure 1.1: A-frame plenum ACC

For the induced draft air-cooled condenser, the fan sucks air through the heat exchanger with the fan blowing air from the plenum to the atmosphere. An advantage of such a system is the reduced recirculation of hot plume air due to a higher exit velocity. A disadvantage is that the fan is blowing hotter and thus thinner air than the forced draft ACC's.

The forced draft A-frame plenum assists with effective drainage of the condensate, minimizing the facility ground surface area and decreasing the length of the distribution steam ducts. Condenser tubes are angled downwards from the steam header to increase the area of condenser surface exposed to the airflow. The axial flow fans located below the plenum blows air into the plenum chamber which is then forced through the condenser.

## 1.2 Problem definition

Meyer and Kröger (1998) conducted tests on different fan and heat exchanger combinations in order to determine the influence that these combinations have on the losses inside of the plenum chamber. Tests were conducted at a BS 848 (1980) facility where the total flow rate and the outlet velocity profile was known. Heat exchangers were mounted so the flow would enter and exit normally. The recovery coefficient $K_{rec}$ introduced by Meyer and Kröger (1998), indicates that adding a plenum chamber with a heat exchanger to the fan outlet, results in a portion of the kinetic energy of the air being converted into pressure.

The value of the recovery coefficient is of importance as Meyer and Kröger (1998) indicates that the operating point of a fan installed in a plenum with a heat exchanger may not necessarily lie on the point where the fan pressure rise curve crosses the system pressure drop curve. Investigating if a difference in performance, for fans installed in a standardised fan test facility and fans installed in an A-frame ACC, can be quantified by a recovery coefficient can be of importance for the design of ACC systems. Meyer and Kröger (1998) found that there exists a critical minimum distance between the heat exchanger and the fan outlet. Should this distance be further decreased, it would result in the recovery value $K_{rec}$ decreasing radically. There thus exist certain design parameters which would should be considered to achieve a certain value for $K_{rec}$.

## 1.3 Aim and objectives of the study

The aim of this study is to determine if a difference in performance between a fan installed in a standardised fan testing facility as tested according to ISO 5801 (2007) and a fan installed in an A-frame ACC setup can be quantified by a recovery coefficient. Furthermore, the accuracy of recovery due to measurement accuracy should also be investigated.

The following objectives were identified to obtain the required data for an investigation on the fan performance results from a standard fan testing facility and an A-frame ACC setup:

1. The available 1:6 scale A-frame fan test facility had to be modified and commissioned for testing purposes to ensure that testing can be done safely without excessive vibration.

2. Measure the performance of a fan in a standardised fan test facility according to ISO 5801 (2007) and also in an A-frame test facility.

3. Investigate how the accuracy of measurements influences the accuracy to which a result can be represented.

# 2 Literature survey

A study of the available literature was needed to obtain the required knowledge of the working of ACC's and the current methods being used for testing the already installed fans. This chapter aims to provide the reader with a brief overview of the current literature available regarding the testing of already installed ACC fans.

## 2.1 Standardised fan performance testing

Fans are tested in standardised fan test facilities to determine the performance characteristics they have. For axial flow fans the BS 848 and even more recently updated ISO 5801 (2007) are used. Different installation types are recognized of which Type-A in Figure 2.1, which employs a free inlet and free outlet, is used and can be modified to perform type B, C and D installations.

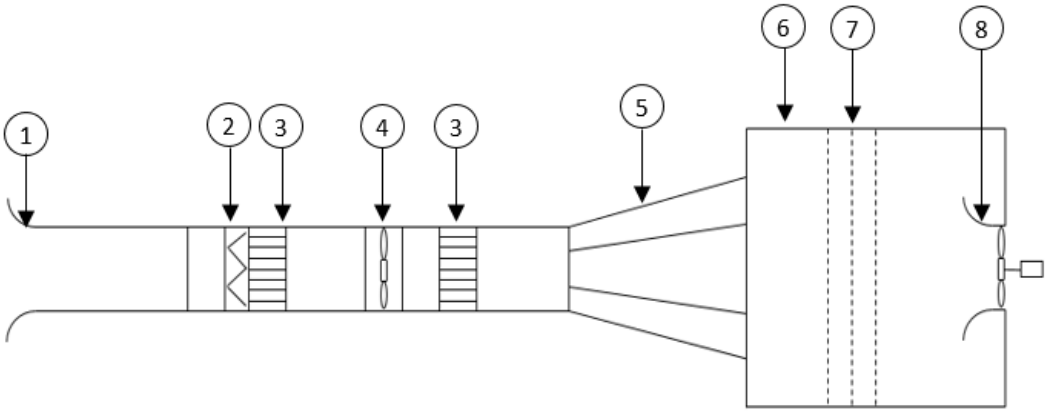


Figure 2.1: Schematic ISO 5801 (2007) fan testing facility

The inlet bell mouth is located at 1, followed by 2, which is a set of louvres acting as a flow resistance to change the system operating point. A set of flow straighteners at 3 follows the louvres to even out abnormalities in the flow velocity profile. An auxiliary fan at 4 overcomes frictional effects at higher flow rates after which another set of flow straighteners removes the swirl caused by the auxiliary fan. Guide vanes at 5 are used to more evenly distribute the flow into the settling chamber at 6 where wire mesh screens at 7 are used to improve the flow inside the chamber. The fan to be tested is located at 8 inside a bell mouth with a machined cylindrical section to achieve a constant fan blade tip clearance. The different installation types are listed below:

1. Type A – free inlet and free outlet.
2. Type B – free inlet and ducted outlet.
3. Type C – ducted inlet and free outlet.
4. Type D – ducted inlet and ducted outlet.

Le Roux (2010) investigated the method and accuracy of simulating axial flow fans with computational fluid dynamics. Tests were performed at the standard Type-A test facility and the results compared with the simulated model. When testing the B2-fan, designed by Bruneau (1994), Le Roux (2010) compared his fan performance curves to those of Stinnes (1998). Le Roux (2010) found similar results but, Stinnes (1998) measured better performance characteristics due to smaller tip clearances achieved. Stinnes (1998) managed the smaller tip clearances due to the shroud of the facility being fixed to the frame of the drive shaft, preventing them to move independently. Le Roux (2010) performed tests at a 3 mm tip clearance where Stinnes (1998) was able to test between 1 mm and 1.5 mm. Le Roux (2010) found that his final model over predicts the tested fan static pressure rise at the design flow rate of 16 $m^3/s$ by 1.4%.

Louw (2015) investigated the flow field in the vicinity of an axial flow fan operating at low flow rates. Tests were conducted on the B2-fan according to the BS 848 standard in a Type-A test facility. A new model was developed for the actuator-disk method. The new model gave a reasonable representation of the experimental results at the design flow rate, but still deviated from experimental results at low flow rates. It was however an improvement on the existing model.

Augustyn (2013) tested the performance of the L1-, L2- and N-fans, which are scale models of existing industrial fans, according to the BS 848 standards in a Type-A standardised test facility. These were scale fan tests of actual ACC fans. Augustyn (2013) found that at high flow rates the L1-fan and the L2-fan followed the trend of the full scale model. A noticeable difference between the L2-fan and the full scale model fan pressures could be the result of a difference in blade angles said Augustyn (2013). The N-fan also showed a comparable trend. It was however found that the L2-fan power correlated very well with the full scale L-fan. Furthermore a difference of 10-15% between the full scale and tested fan efficiencies was found. Augustyn (2013) also tested and demonstrated the validity of the scaling laws for the L2- and N-fan at different rotational speeds.

Wilkinson and Van der Spuy (2015) performed fan tests on the B2-fan to investigate the effect of fan tip clearance and fan tip modifications on the performance of the fan. These tests were also performed in the same facility as used by Le Roux (2010), Augustyn (2013) and Louw (2015). It was found that tip clearance contributes significantly to the fan performance. Their blade tip modifications also showed improvement of fan performance on larger tip clearances.

## 2.2 Performance of a fan in a plenum chamber

The performance of a fan inside of a plenum chamber may be influenced by various contributing factors such as geometry and system losses. Experiments completed regarding the performance of a fan in a plenum chamber is investigated to gain an understanding of the effect of the plenum chamber on the fan performance.

### 2.2.1 Plenum chamber and system losses

Experiments conducted by Meyer and Kröger (1998) indicated that the inlet geometry of the heat exchanger could significantly affect the performance characteristics of the plenum chamber. Obstacles located upstream and downstream from the fan are added as loss coeficients in the system by Kröger (2004, 8.1.30). These would include support, upstream, bridge, heat exchanger, downstream, jetting and outlet losses. Flow that apporaches the heat exchanger at an angle which is not perpendicular will add an additional loss term to the system. This is the case for A-frame plenums where the flow which also has a vertical component from the fan, is turned by the heat exchanger fins. Figure 2.2 shows a schematic representation of the flow through the heat exchangers of a section of an A-frame array. The jetting and outlet losses represent the losses due to the flow turning and exiting the array as a result of the symmetry plane where the adjacent heat exchanger bundles directs the flow towards each other at an angle.

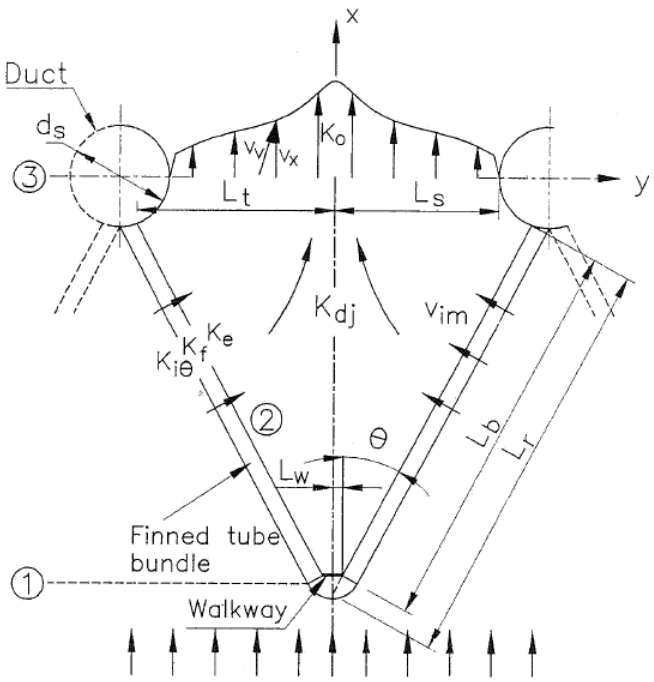


Figure 2.2: Section of an A-frame array (Kröger, 2004: 5.6.12)

Flow that approaches and exits a heat exchanger non-perpendicularly has higher losses due to separation of the flow as it meets the fins at an angle. This separation region acts as a flow constriction. Figure 2.3 shows how flow that approaches a finned heat exchanger at an angle separates upon entry as it is forced to turn suddenly and re-attaches to recover static pressure, thereby not dissipating the complete velocity component perpendicular to the fins as would be the case in a porous medium.

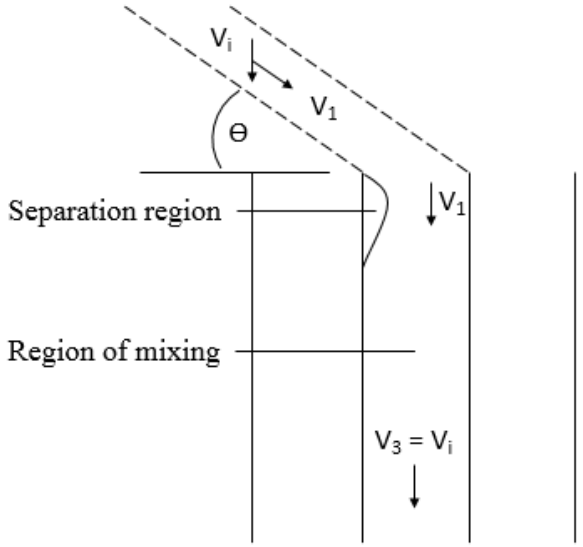


Figure 2.3 Entrance flow behaviour at a thin sheet bundle (Kröger, 2004: 5.6.2)

From Figure 2.4 it can be seen that flow that approaches and exits a finned heat exchanger bundle perpendicularly, or at 0º, has a lower pressure loss across the bundle than in the case of flow approaching the heat exchanger bundle at 30º and leaving perpendicularly, or at 0º. These tests were performed by placing a plate finned heat exchanger in wind tunnel and changing the approach- and exit angle of the flow with respect to the heat exchanger fins. A loss factor was then calculated at different volumetric flow rates through the bundle.

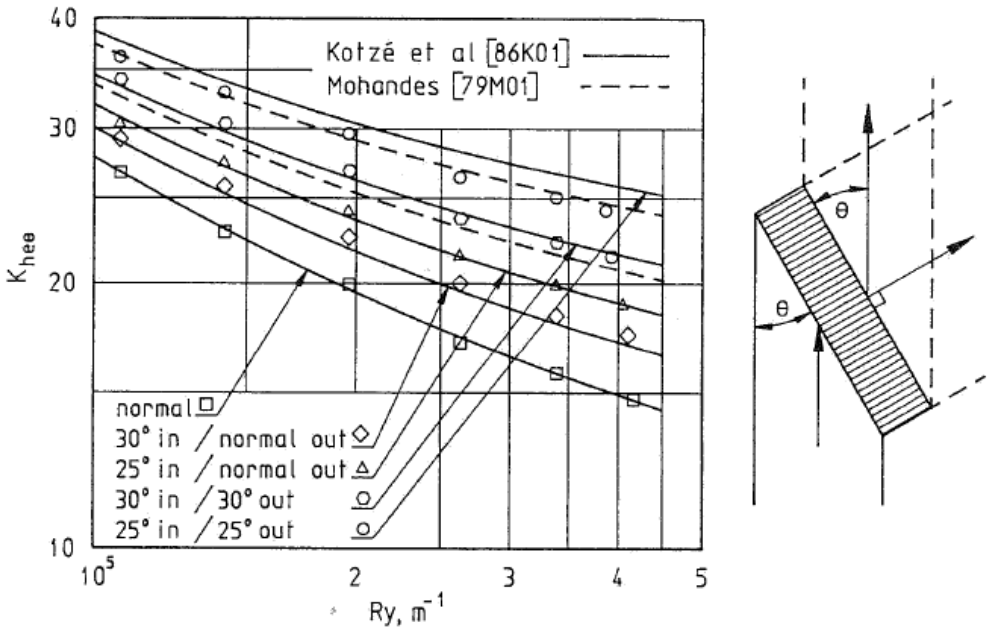


Figure 2.4: Two row plate finned heat exchanger loss factor(Kröger, 2004: 5.6.10)

### 2.2.2 Fan and plenum chamber tests

Meyer (1996) constructed a delta shaped ACC with a casing diameter of 1.542 m for use with the B-fan. An industrial type heat exchanger was used. The outlet velocity profile was measured at a plane, not parallel to the heat exchanger outlet surface, but rather at the outlet plane which would normally be above the top steam header. These measurements were possible due to symmetry planes added to the setup to represent a single A-frame ACC as if it was installed in an A-frame array.

Meyer and Kröger (1998) installed various different heat exchanger-plenum configurations over the outlet side of the Type-A standard fan test facility to test the effect that different heat exchanger and plenum chamber geometries have on the flow losses inside a plenum chamber. Figure 2.5 shows a schematic of the test setup.

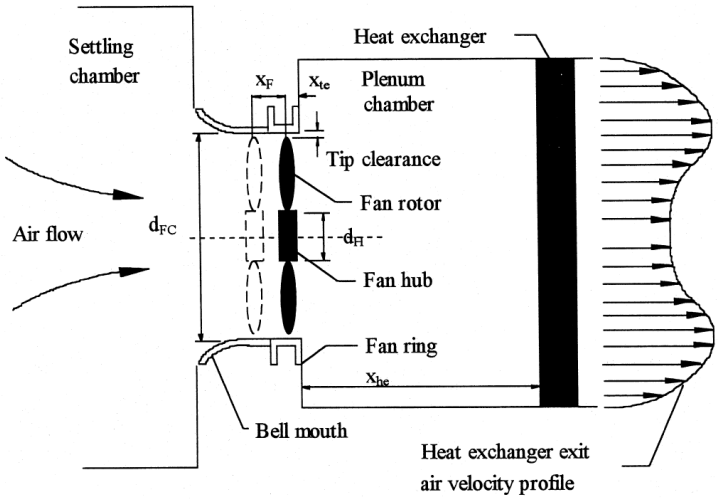


Figure 2.5: Fan and plenum chamber test setup (Meyer and Kröger, 1998)

Adding a plenum chamber with a heat exchanger to a fan, forces the flow to slow down and spread out across the heat exchanger area. The higher the flow resistance of the heat exchanger, the more evenly the flow will be distributed over the outlet surface. As the flow is slowed down the velocity component of the air is converted into pressure which is then recovered inside of the plenum chamber.

Testing at this standardised test facility allowed for the volumetric flow rate through the system to be accurately measured with the use of the calibrated bell mouth. The volumetric flow rate through the facility could also be changed with the use of a throttling device.

When using equation 2.1 from Kröger (2004, 6.4.4), it is assumed that all of the kinetic energy is lost inside of the plenum chamber. This is however not the case as shown by Meyer and Kröger (1998).

$$\Delta p_{Fs} = K_{he}\,\rho {v_{he}}^2/2 + \alpha_e\,\rho {v_{he}}^2/2 \tag{2.1}$$

Where $K_{he}$ and $\alpha_e$ represents the heat exchanger loss coefficient and velocity distribution correction factor respectively. The velocity through the heat exchanger $v_{he}$ is calculated with the use of the conservative volumetric flow rate at the point where the fan static pressure rise curve intersects the system pressure loss curve with the use of equation 2.2.

$$v_{he} = V/A_{fr} \tag{2.2}$$

The conservative volumetric flow rate V is divided by the frontal area of the heat exchanger $A_{fr}$ to calculate the velocity $v_{he}$ through the heat exchanger. Recovery introduced by Meyer and Kröger (1998), is a factor which describes the portion of kinetic energy of the air that is converted into pressure inside of the plenum chamber. This suggests that not all of the kinetic energy is lost inside of the plenum chamber. This results in the fans performing at a higher pressure in situ than in the standard fan test facilities at the same volumetric flow rate. The implication thereof is that the system operating point would not necessarily lie on the fan curve as determined by the standard fan testing procedures.

Meyer and Kröger (2004) found that the maximum $K_{rec}$ value does not necessarily coincide with the maximum fan static efficiency. This is an indication that the value for recovery is not necessarily constant for the fan at different operating points. Figure 2.6 shows how the operating point would differ from the point where the fan curve crosses the system pressure loss curve according to Meyer and Kröger (1998). It was also found that the value for $K_{rec}$ increased as the volume flow rate increased past the maximum fan static efficiency. From Kröger (2004, 6.4.4), equation 2.3 is used to calculate the value for $K_{rec}$ in a simplified forced draft heat exchanger where the only losses are that of the heat exchanger. The kinetic energy correction factor depicted by $\alpha_e$ accounts for the losses not accounted for when assuming a uniform outlet velocity profile.

$$\Delta p_{Fs} + K_{rec}\,\rho {v_F}^2/2 = K_{he}\,\rho {v_{he}}^2/2 + \alpha_e\,\rho {v_{he}}^2/2 \tag{2.3}$$

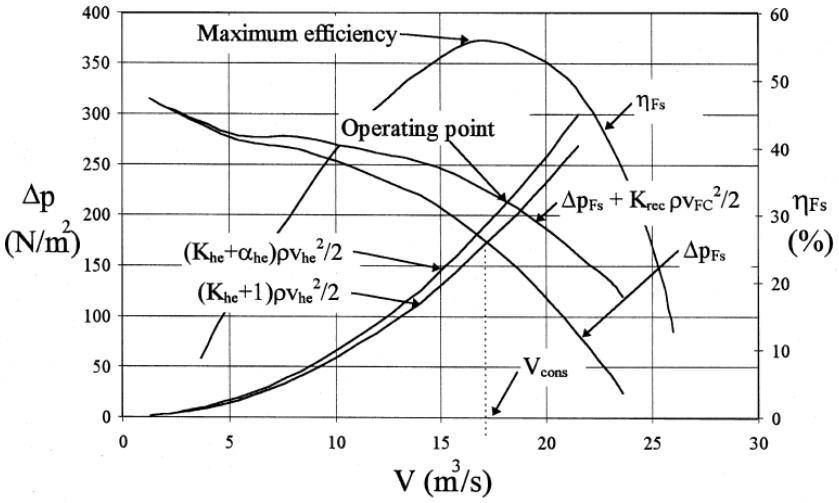


Figure 2.6: Operating point due to $K_{rec}$ (Meyer, 1998)

According to Kröger (2004, 6.4.4) recovery of the kinetic energy results in the volumetric flow rate being higher than the predicted value where the fan and system curves intersect. This can be an important aspect to consider when designing ACC systems. A higher volumetric flow rate than expected provides an additional safety factor with the increased cooling capability. Not taking this into account can result in over designing of an ACC system which leads to large, possibly unnecessary, extra manufacturing costs.

Meyer and Kröger (2004) performed a numerical investigation on the effect of the B-fan performance on the aerodynamic behaviour of the plenum chamber. Various different blade angles were tested and the results showed recovery values ranging from 0.4 to 0.8. Engelbrecht (2018) performed a numerical investigation of the performance of the B2a-fan in a forced draft ACC. A recovery coefficient of 0.527 was found through the numerical simulation. Engelbrecht (2018) validated his findings by comparing an experimental design with the numerically calculated recovery. A good correlation was found with the results form Meyer and Kröger (1998).

## 2.3 Effect of distorted inflow

The axial flow fans, as mentioned in section 1.1, are subject to operating conditions when installed on site, which differ from the ideal testing conditions for which they are designed and tested in the standard fan testing facilities. This can be a result of changes in ambient conditions such as temperature, humidity and wind. A small scale ACC fan installed indoors can be subject to distorted inflow over the fan due to structural components and spatial constraints negatively affecting the airflow towards the bell mouth. The effect of distorted inflow on fan performance is thus an important consideration due to the A-frame ACC being installed indoors with limited space and some obstructions that may negatively affect the flow. Salta and

Kröger (1995) investigated the effect of reducing the height of the fans from ground level. It was found that it reduced the efficiency of the edge fans due to a higher cross flow at the fan inlet. Fourie et al. (2015) investigated the effect of wind on an ACC by lowering the platform height in a small scale test facility. It was found that the volumetric effectiveness decreases with a decrease in platform height as the fans further away from the edge fan induces a flow across the edge fan inlet bell mouth. This leads to flow separation at the edge fan and a decrease in the volumetric effectiveness. Salta and Kröger (1995) found that reducing the platform height of a single or multiple fan row ACC reduces the volumetric efficiency exponentially.

Kröger (2004, 6.4.7) said that the absence of a bell inlet reduces the fan performance. This is due to separation at the edge of the inlet to the fan. Duvenhage et al. (1996) showed that replacing a well-rounded bell mouth inlet with a conical or cylindrical inlet will decrease the flow rate by about 3 and 5 percent respectively. Even if a well-rounded bell mouth is fitted, other factors such as the surrounding walls and the height of the fan to the floor surface can also adversely affect the fan performance. Monroe (1979) found that the horizontal approach velocity should not exceed one half of the axial flow velocity through the fan. Walls at different distances around the test facility can result in mal-distributed flow across the fan due to different approach velocities around the bell mouth circumference, resulting in an uneven load condition experienced by the fan blades (Muiyser et al., 2014).

Van Rooyen (2007) completed a study on the effect that wind has on the performance of an ACC. It was found that the fans situated on the perimeter of the ACC were affected the most and the fans inwards were mostly unaffected by the wind. It was also found that the static pressure at the edge fans was unequally distributed across the fan inlet. For this study wind would not have an influence on the test results as the facility is installed indoors.

Duvenhave and Kröger (1996) numerically investigated the influence of wind on the forced draft ACC performance and found that cross winds mainly lead to a reduction in upstream fan volumetric performance. Owen (2010) also performed a numerical investigation on the performance of an ACC under windy conditions with the use of data recorded at a full scale ACC. Wind velocity measurements at different elevations above ground level were used as input parameters to the numerical model. The ambient temperature measurements were used to determine the air temperature at the platform. Owen (2010) found that a good correlation was achieved between the numerical model and the test data. Discrepancies in the results obtained, although being small, can be described by the weather conditions and numerical inaccuracies from the numerical model used. Owen (2010) found that the wind screens appeared to have a positive effect on the fans that were located directly upstream of the screens. However, it seemed to be reducing the downstream fan performance.

## 2.4 Effect of fan tip clearance on performance

Venter and Kröger (1992) developed correlations for the V-type, eight bladed fan that showed the effect that increasing the fan tip clearance has on the flow rate and fan static pressure. It was shown that an increase in tip clearance results in a linear decrease in flow rate and static pressure respectively. This corresponds with Stinnes (1998) who achieved better performance characteristics with the B2-fan than Le Roux (2010) due to Stinnes (1998) being able to test as smaller tip clearances.

Wilkinson and Van der Spuy (2015) performed tip clearance tests on the B2-fan. The same type of linear relationship is seen for the B2-fan where an increase in tip clearance results in a linear decrease in flow rate and static pressure rise as seen in Figure 2.7.

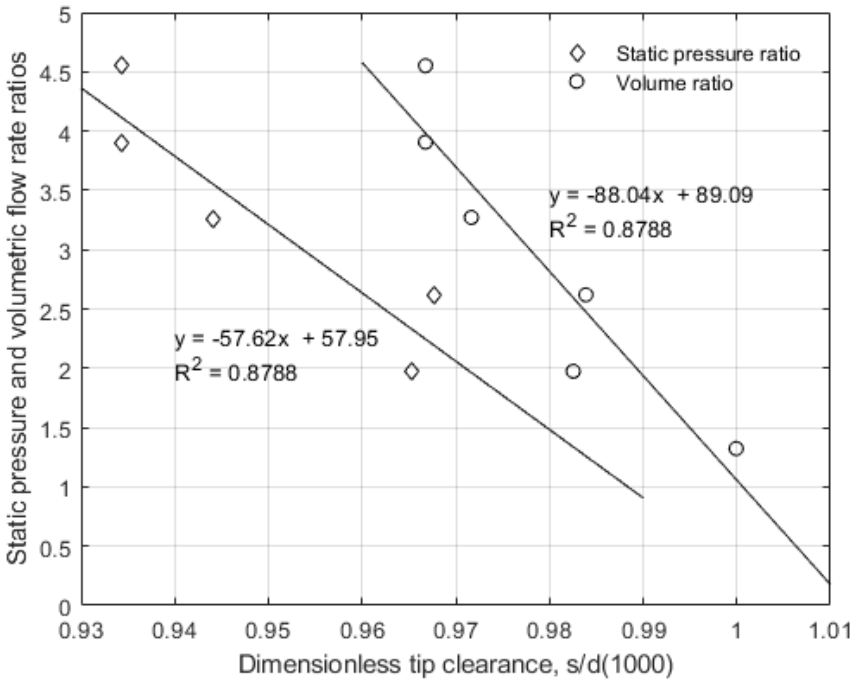


Figure 2.7: Effect of tip clearance on fan performance for flow rates above 6 $m^3/s$ (Wilkinson and Van der Spuy, 2015)

Tip modification tests were also done by Wilkinson and Van der Spuy (2015) to determine the effect on fan performance. The S20 end plate tip modification, which extended 20 mm from the centre of the leading edge to the pressure side with a 4 mm tip clearance, resulted in the same static efficiency as the 2 mm tip clearance. This can be of importance in full scale applications where it is difficult to achieve a constant and small tip clearance on the large diameter fans and fan casings.

## 2.5 In situ volumetric air flow measurements

According to ISO 5802 (2008) the volumetric flow rate in an airway may be determined by measuring the velocity at various points and calculating the mean velocity. By using the velocity area method the volumetric flow rate can then be calculated from the velocity profile. Another method is by using a pressure differential measurement device like an orifice plate, Venturi or a flow nozzle.

Muiyser (2012) investigated the use of different air flow sensors in order to establish the method for measuring the volumetric flow rate through the ACC cooling fans. The use of a propeller anemometer, pressure probe, and also a two axis ultrasonic anemometer was considered. Due to its slower response time and accurate measurement up to 40º off from its main axis Muiyser (2012) did not use pressure probes to measure the flow through the cowling. Muiyser (2012) used both propeller and ultrasonic anemometers to measure the inlet flow velocities. The ultrasonic anemometers were used to measure the inlet flow and the propeller anemometers used to measure the out of plane flow component inside the fan casing. Maulbetsch et al. (2011) suspended propeller anemometers under the fans to monitor the inlet velocity at selected fans. These measurements were made to determine the effect of wind on the ACC performance.

Venter (1990) made use of a five holed pressure probe to measure the velocity components, making use of a spherical coordinate system, at the fan inlet and fan outlet respectively. To measure the velocity profile at the heat exchanger outlet, Venter (1990) made use of a vane anemometer which was traversed at a distance of 25 mm from the outlet of the heat exchanger surface. The outlet velocity profile of the unit was measured between the apexes of the A-frames with the use of the same vane anemometer. Meyer and Kröger (1998) measured the outlet velocity profile of a heat exchanger by traversing a 1.9 m rod and eight anemometers that were evenly spaced. Zapke (1997) used an aluminium beam fitted with 10 anemometers to perform a full scale traverse of the outlet side an A-frame ACC. These anemometers were spaced 200 mm away from the outer side of the heat exchanger bundle.

## 2.6 In-situ fan performance measurements

When measuring the pressure rise across a fan a certain test length of the duct is required at which measurements shall be taken according to ISO 5802 (2008). For measurements upstream of the fan, the pressure measurement plane shall not be closer than 1.5 diameters $D_e$ and for downstream measurements no closer than 5 diameters $D_e$. Where $D_e$ is the equivalent diameter of a non-circular cross section. ISO 5802 (2008) stipulates that these distances may be shorter if the flow is already stable at a closer distance. Some fans are directly connected to the plenum chamber on either the inlet or outlet sides of the fan. When taking the pressure measurements it should be done in a plane as close as possible to the face of the plenum chamber to which the fan is connected. These points of pressure measurements should be located in areas with no significant air velocity. When the pressure measurements

between the pressure taps in the walls differs by less than 5%, they can be interconnected to achieve an average gauge pressure (ISO 5802, 2008).

## 2.7 A-frame test facility

Böck (2017) designed and constructed an A-frame test facility to investigate the performance of the B2-fan with a forced draft configuration. Bruneau (1994) designed two experimental fans, the B1- and B2-fan, which were tested according to the BS 848 Type A standards. The requirements of the design for Böck (2017) included the following:

1. A forced draft design with an A-frame plenum and apex angle of 60º.
2. Use of the existing B2-fan to compare results with standardised tests performed on the fan in a Type A fan testing facility.
3. Minimum flow distortion at the bell mouth inlet.

Figure 2.8 shows the constructed test facility. Böck (2017) had a few limitations to consider during the design which included the width and height of the facility. The width was limited to 3.5 m and the height to 5.2 m due to the service trenches and the maximum hook height of the crane respectively. The motor, which was a reconditioned 15 kW three phase motor, was too heavy and big to be put on the fan bridge and would have affected the flow inside of the plenum chamber negatively. It was thus mounted below the fan on the inlet side to the bell mouth.

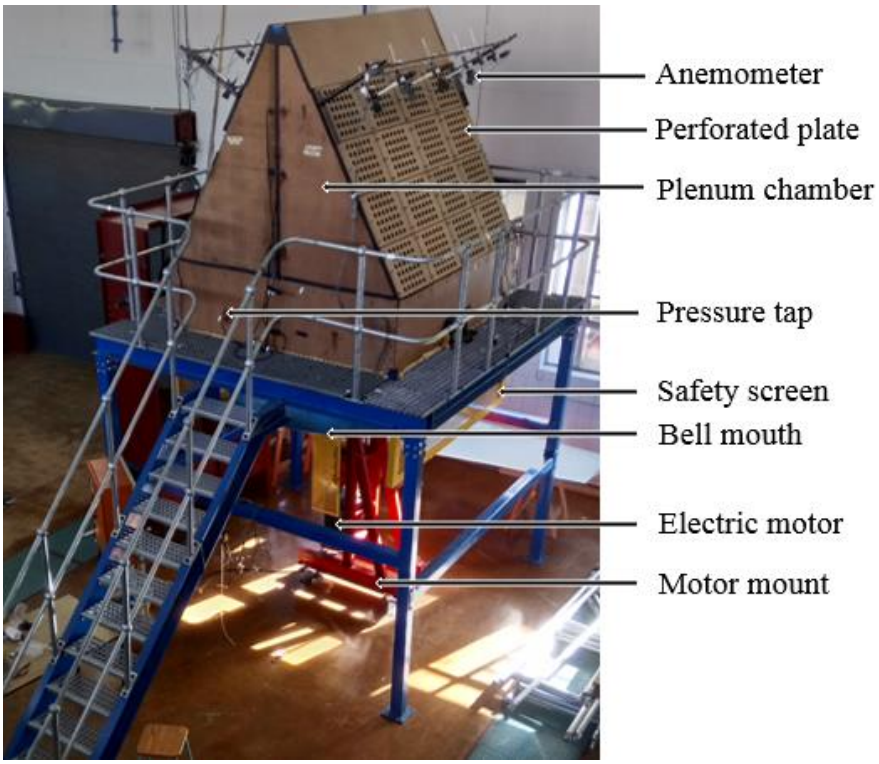


Figure 2.8: A-frame test facility constructed by Böck (2017)

The constructed facility was designed on a 1:6 scale. Perforated plates and guide fins were constructed and tested by Böck (2017). The purpose of these plates was to enable the system to be throttled and tested at different operating points. Guide fins on the inside of the perforated plates were supposed to direct the flow before exiting the plenum chamber. For safety during testing, safety screens were added below the inlet bell mouth. These were to protect the facility operator during testing. A variable speed drive was used by Böck (2017) to operate the fan at the calibrated rotational speed. A potentiometer and display allow the user to set the motor to the desired rotational speed.

## 2.8 Selected fans for testing

Two different fans were selected for testing in the A-frame ACC test facility. They were chosen to be different to each other with regards to the hub to tip ratio, static pressure rise and operating rotational speed. This would allow the outlet velocity profiles to be compared to establish to which degree the fan influences the outlet velocity profile of the A-frame ACC.

### 2.8.1 B2-fan

The B2-fan designed by Bruneau (1994) utilises the high lift characteristics of the NASA LS series profile with a free vortex design and can be seen in Figure 2.9. This fan has a hub diameter $D_h$ of 0.6 m and a total diameter $D_f$ of 1.53 m and is used inside a casing of 1.542 m diameter. The tip clearance can be decreased or increased for safe operation inside the particular bell mouth. Table 2.1 shows the B2-fan characteristics.

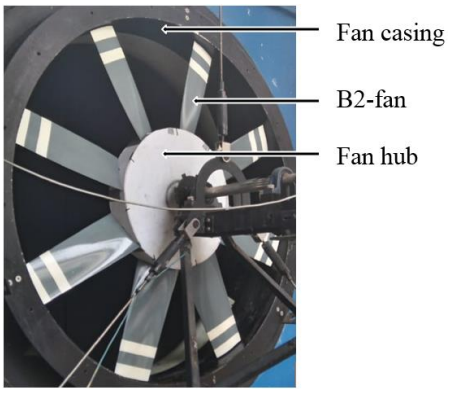


Figure 2.9: B2-fan

Table 2.1: B2-fan Characteristics

| | |
|---|---|
| Diameter | 1.542 m |
| Number of blades | 8 |
| Hub to tip ratio | 0.39 |
| Fan rotational speed | 750 rpm |

### 2.8.2 M-fan

The M-fan, designed by Wilkinson (2017), was designed to achieve a high total-to-static efficiency at a selected operating point. With the recent trends of using high volumetric flow rate at a low pressure rise, this fan was designed. Figure 2.10 shows a schematic representation of the M-fan and Table 2.2 shows the fan characteristics.

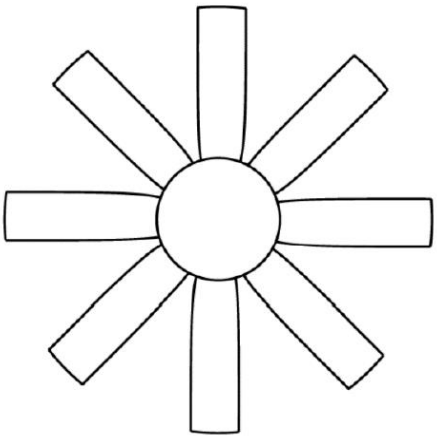

Figure 2.10: M-fan schematic (Wilkinson, 2017)

Table 2.2: M-fan characteristics

| | |
|---|---|
| Diameter | 1.542 m |
| Number of blades | 8 |
| Hub to tip ratio | 0.29 |
| Fan rotational speed | 722 rpm |

## 2.9 Summary of findings

From this literature it can be seen that adding a plenum chamber to a fan results in a portion of the kinetic energy to be converted into pressure. This recovery value has been measured by experiments by Meyer (1996) and Meyer and Kröger (1998), and more recently by Engelbrecht (2018) with the use of a numerical model. This indicates that a recovery value does exist explaining a portion of kinetic energy converted into pressure.

The tests performed by Meyer (1996) and Meyer and Kröger (1998) were however done with the use of a standardised fan testing facility allowing for accurate measurement of the volumetric flow rate through the fan which will not be the case for this experiment. Measuring of the volumetric flow rate through the A-frame test facility will be done with the use of outlet velocity measurements at the heat exchanger outlet surface. This will be the case as it is not possible to attatch a standardised fan testing facility to the inlet of a full scale ACC bell mouth inlet.

This project will develop a method to be used at full scale A-frame ACC's to measure the recovery at full scale setups. The results of the measurements performed can then be validated by a numerical model as the one presented by Engelbrecht in a subsequent study.

# 3 Facility modification and commissioning

As stipulated in section 1.3 it was identified that certain modifications to the ACC facility constructed by Böck (2017) had to be made in order for it to be used for testing purposes. This chapter aims to provide an overview of the identified areas of re-evaluation, redesign and also the manufacturing and installation procedures followed.

## 3.1 Fan drive system

When running the fan, excessive vibration limited the rotational speed at which the fan could safely be run. Vibration caused by the fan drive system had to be addressed as it was not possible to operate the facility at the required 750 rpm without excessive structural vibration. This was possibly caused by the misalignment of the motor and the bearings on the shafts of the torque transducer as a result of too many bearings that were placed in a single line.

The initial drive system had the motor mounted close to the floor as shown in Figure 3.1. Above the motor were three separate in-line shafts, each located by two bearings, which had to be aligned with each other and the motor shaft in order to have the drive running smoothly. This in itself would have proved difficult to achieve without reference surfaces to locate the bearings on to.

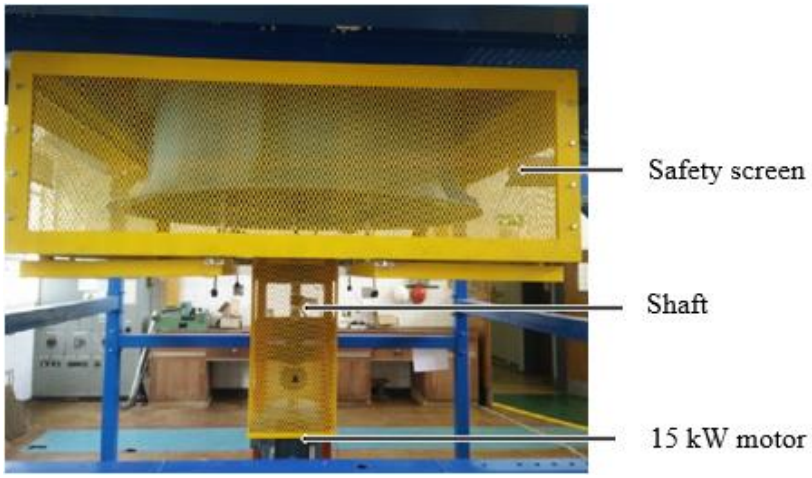


Figure 3.1: Initial fan drive system Böck (2017)

When the couplings between the shafts were removed, it could be seen that the shafts were not in proper alignment. As such, this was identified as one of the reasons for the vibration when running the facility. Marks on the inside of the fan casing indicated that the blades were scraping during testing. This had to be addressed as blades striking the casing wall can lead to damage of the fan and in worst case scenarios complete destruction of the test fan and possible injuries.

Having more than two bearings on a single shaft results in residual forces acting on the bearings if they are not properly aligned. It was found necessary to minimize the amount of bearings that were required in a straight line. Two different drive systems were considered to replace the existing one.

### 3.1.1 Bevel gearbox concept

A bevel gearbox was considered as it would allow the motor to be fixed outside of the plenum chamber, preventing it from obstructing the flow. The relative simple sealing between the shaft and the plenum chamber with the use of a radial lip seal was also considered. This would also allow for the hub of the fan to be bolted to the bevel gearbox output shaft. However, this would require inspection of the motor bearings and possible replacement due to the installed bearings having been made specifically for vertical mounting of the motor. Figure 3.2 shows the bevel gearbox concept.

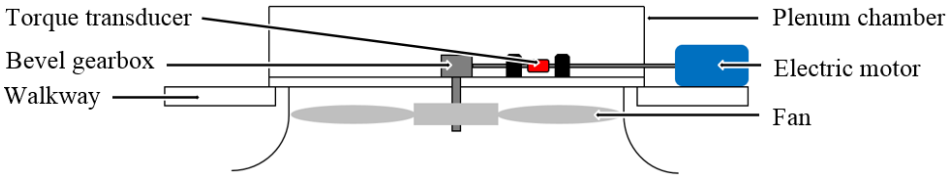


Figure 3.2: Bevel gearbox concept

### 3.1.2 Belt drive concept

A belt drive was also considered. It would involve the redesign of the fan bridge to accommodate the bearings for locating the shafts above and below the torque transducer. The bottom shaft would also be the shaft on which the fan would be mounted inside of the casing. With a 15 kW motor that had to be reused, it was important to install it in a location that would least adversely impact the flow inside of the plenum chamber. Mounting the motor inside the plenum was considered, but no suitable location could be identified that would not affect the air flow negatively. Due to its size, the motor would have to be mounted outside of the plenum chamber. This would lead to holes in the plenum chamber in order to accommodate the belts from the motor pulley to the pulley on the top shaft of the fan bridge. Long belts would allow for the motor to be at a fixed position outside of the plenum chamber as seen in Figure 3.3.

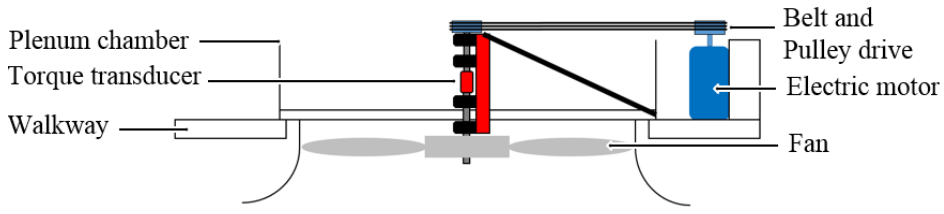


Figure 3.3: Belt drive concept

Three belts, two pulleys and taper lock bushings would be the main components required along with a belt cover. This was considered to be the more economic option than the bevel gearbox and also the chosen concept for the project.

In order to mount the motor on the outside of the plenum chamber, a mount had to be designed and manufactured for mounting onto the two I-beams passing on the Northern side below the plenum chamber. The original motor mount was modified and reused for this application as it would save on costs and time. Slots were made on the bottom of the motor mount to allow for belt tensioning by moving the motor mount relative to the I-beams in the Northerly direction. Diagonal supports were welded to the structure to withstand the moment acting on the mount due to the belts. Rubbers were inserted to act as absorbers of high frequency vibrations from the motor.

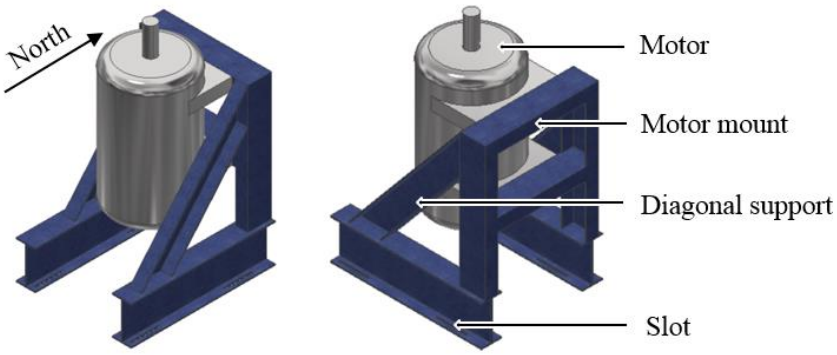


Figure 3.4: Motor mount welded assembly design

In order to prevent air from leaking from the plenum chamber where the belts exit and enter the plenum, a cover that seals on top of the motor and against the plenum chamber was designed. The manufactured and installed cover is shown in Figure 3.5.


Figure 3.5: Belt cover and motor mount

Adhesive sponge was placed on the perimeter top side of the motor and also where the cover is attached to the plenum. This achieved an air seal, preventing leakage from the plenum chamber.

## 3.2 Fan bridge

Redesigning the fan drive system to accommodate a belt and pulley drive required the redesign of the fan bridge. The fan bridge, which locates the fan within the bell mouth, had to be designed to be stiff enough to withstand the tension of the belts causing a moment on the bridge as seen in Figure 3.6. Rectangular tubing, 100 mm × 50 mm, which was initially oriented with its long side horizontally, was rotated through 90º to allow for a stiffer bridge in the vertical direction.

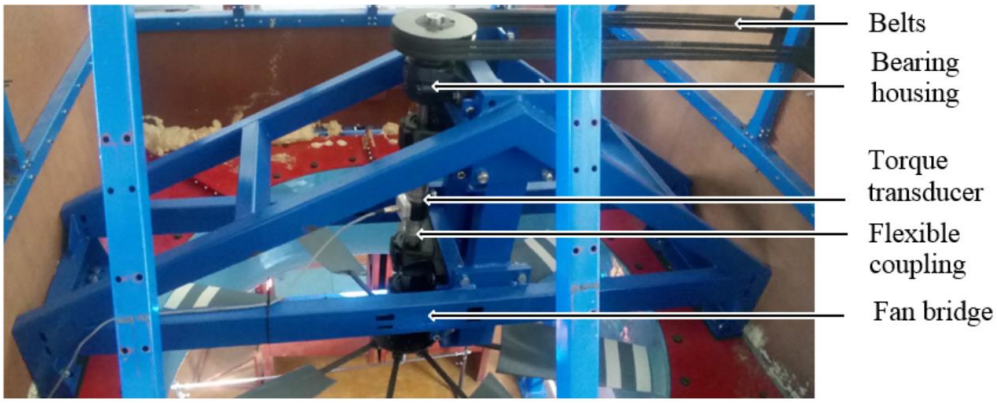


Figure 3.6: Manufactured and installed fan bridge

The surface, to which the bell mouth is bolted and which also makes up the bottom surface of the plenum chamber, is made up of eight sections which are bolted together. In order to firmly bolt the fan bridge to the structure and more accurately locate the bridge, it was decided that it would be better to cut out the sections where the fan bridge would support itself. These sections were removed two at a time, the necessary cuts made, and then replaced. This allowed the fan bridge to be bolted directly to the I-beams that provide the structural support.

In order to mark the exact locations for the drilling of the mounting holes it was decided to insert the whole fan bridge and centre it according to the bell mouth. The holes were then marked and drilled using a magnetic drill. The welded fan bridge was lowered into position with the overhead crane and bolted to the I-beams with rubbers to act as absorbers of high frequency vibrations. Slots in the bottom of the welded assembly allowed for adjustments to be made in the longitudinal direction of the bridge as shown in Figure 3.6.

The bearing mounting surface was placed in a milling machine to achieve a flat reference face. Self-aligning bearings locating the two shafts above and below the toque transducer were located on the surface by adjustment bolts located on either side of the bearing housings. With slots also in the bearing mounting surface, the bearings could be well aligned and the shafts also moved in the East-West direction as shown in Figure 3.7. On either side of each bearing housing a threaded hole with a bolt for adjusting the location of the bearings on the reference surface was also added. This ability to move the shaft in either of the four directions enabled the fan shaft to be centred inside of the bell mouth casing.

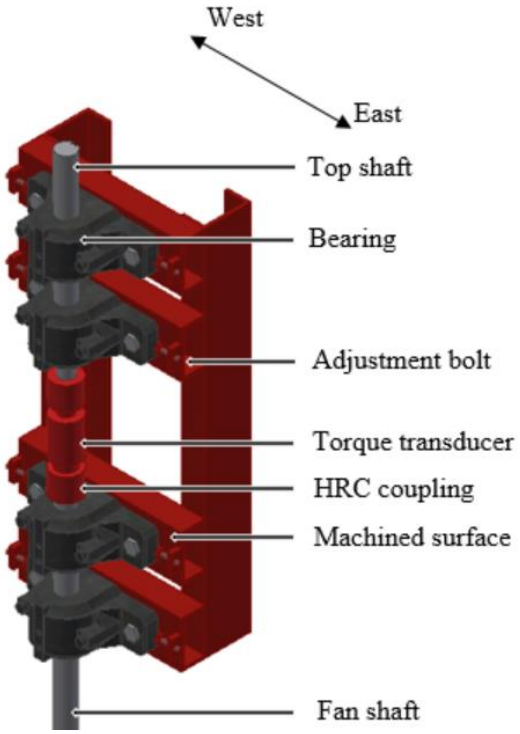


Figure 3.7: Machined bearing mounting surface

The original couplings, as seen in Figure 3.6, were flexible stainless steel couplings locating the torque transducer between the two shafts. These however resulted in excessive vibration to the torque transducer under higher toque. This was a result of the couplings acting like springs under torsion as the torque was increased. New couplings were ordered that would be more rigid whilst still allowing for some degree of misalignment. These couplings were fixed to the shafts using taper lock bushing.

The 40 mm diameter shafts were used as the bearings only allowed a shaft diameter of 40 mm as used by Böck (2017). This is only 2 mm less than that of the standardised Type-A fan test facility. The A-frame facility fan shaft also has an additional advantage of only torque and axial load being applied to it where the standardised fan test facility has a constant moment acting on the shaft due to the mass of the fan from being installed on a horizontal shaft. It was thus concluded

that the 40 mm shaft diameter will be more than sufficient for the setup. Appendix A.1 shows a sample calculation for the fan shaft strength.

The bridge total width equals 500 mm but is only comprised of two 50 mm wide beams. Engelbrecht (2018) modelled the bridge width as 2 m. With this model being a sixth scale of the full scale model, the total bridge width should equal 0.333 m. It was however decided that having wider bridge supports will result in a much more rigid setup as safety is of great importance when testing these fans at 750 rpm. This allows for a walkway of any width to be added to the bridge and the effect thereof tested for different scenarios.

The pulley diameters were selected to be a 1:1 ratio as the motor maximum rotational speed equalled 960 rpm where the required speed was 750 rpm. Selecting the belt and pulley sizes were done according to calculations that can be seen in Appendix A.2.

## 3.3 Heat exchanger bundles

Heat exchanger bundles are used to increase the air contact area to cool down the low pressure steam coming from the turbines. These heat exchanger bundles normally consists of finned surfaces increasing the heat transfer rate from the steam to the surrounding air.

### 3.3.1 Shortcomings of existing system

The perforated plates and guide vanes used by Böck (2017) as seen in Figure 3.8 were considered to be reused for the commissioning of the small scale A-frame ACC test facility.

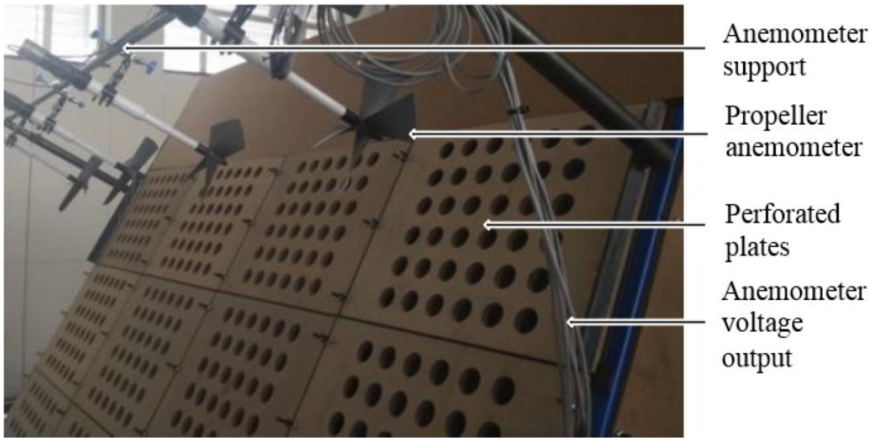


Figure 3.8: Perforated plates Böck (2017)

These perforated plates however only allowed for a total of 32 velocity measurement points, 16 on each side, due to each perforated plate only allowing for a single anemometer to measure the outflow of air. This was thought to be too

coarse a measurement of the flow exiting the plenum chamber. Böck (2017) suggested that the ability of the perforated plates and guide vanes to turn the flow also be investigated. It was decided that the existing perforated plates and guide vanes had to be replaced with an alternative which would better direct the flow with finer spaced guide vanes. The reason for redirecting the flow was to achieve a more accurate representation of a full scale A-frame ACC. Adding of a heat exchanger across the whole surface would also allow finer measurement capabilities of the outlet velocity profile due to no obstructed sections across the outlet surface.

### 3.3.2 Selection and theoretical analysis of heat exchanger tubes

Different heat exchanger tube types were considered for the application and are shown in Figure 3.9. An elliptical tube with a rectangular plate fin as shown in Figure 3.9(a) is used in ACC applications and is normally used with two or more rows. A round finned tube as shown in Figure 3.9(b) was also considered. These finned tubes are widely used today and were selected as an alternative as they are readily available. They are normally used with two or more tube rows. A wavy-finned flattened tube consists of a tube which is flattened to which wavy fins are bonded as shown in Figure 3.9(c). These heat exchanger tubes are particularly suited for ACC's as two or more rows of elliptically or round finned tubes may be replaced by a single row of wavy finned tubes (Kröger, 2004: 5.1.8).

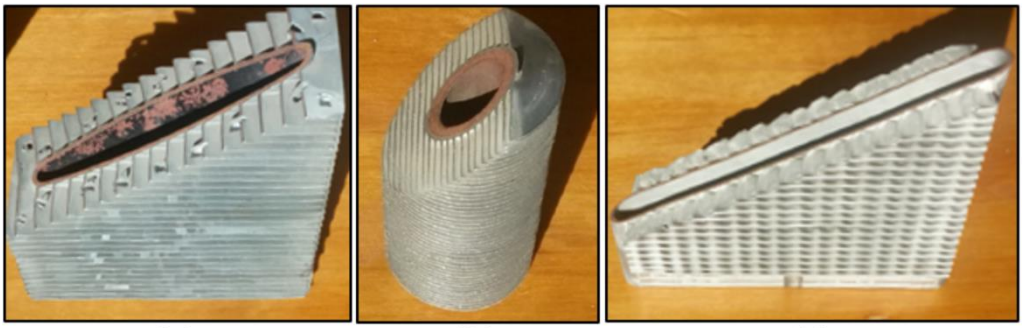


Figure 3.9: Heat exchanger tubes: (a) Rectangular plate fin; (b) Round finned; (c) Wavy finned flattened tube

After considering the availability, cost, delivery time and the required purpose of the heat different exchanger tubes, it was decided that the round finned heat exchanger tubes would be suitable to use for the heat exchanger bundles.

Böck (2017) designed the A-frame ACC with a bundle slope angle of 60º relative to the horizontal. Kröger (2004, 1.2.3) said that large ACC may have finned tube bundles which are sloped up to 60º. A staggered finned tube arrangement was selected as most of the literature in Kröger (2004, 5.4.17) utilises staggered finned tube arrangements for better mixing of the air. The required number of tube rows for the A-frame ACC is calculated from Kröger (2004, 5.5.11).

With a total width of 2 m and a total height of 1.5 m, the final design width and height for each heat exchanger came down to 1.8415 m and 1.4 m respectively. The parameters are listed:

| | |
|---|---|
| Fin diameter | $d_f$ = 0.0572 m |
| Fin root diameter | $d_r$ = 0.0276 m |
| Fin thickness | $t_f$ = 0.0005 m |
| Fin pitch | $P_f$ = 0.0028 m |
| Tube outer diameter | $d_o$ = 0.0254 m |
| Arrangement | Staggered |
| Tubes per row | $n_{tr}$ = 29 |
| Transverse tube pitch | $P_t$ = 0.0635 m |
| Longitudinal tube pitch | $P_l$ = 0.055 m |
| Finned tube length | $L_t$ = 1.400 m |
| Flow area width | $w$ = 1.8415 m |
| Flow area height | $h$ = 1.4 m |
| Frontal area | $A_{fr}$ = 5.1562 m$^2$ |
| Minimum flow area | $A_c$ = 2.4954 m$^2$ |
| Ambient temperature | $T_a$ = 20 ºC |
| Dynamic viscosity | $\mu_{T=20\,^{\circ}C}$ = 1.81454×10$^{-5}$ kg/m.s |

Equation 3.1 is used to calculate the minimum flow area through the finned tube heat exchanger bundle.

$$A_c = A_{fr} - n_{tr}L_t\left[d_f t_f + \left(P_f - t_f\right)d_r\right]/P_f \tag{3.1}$$

The total frontal area $A_{fr}$ would equal

$$A_{fr} = 2wh \tag{3.2}$$

The Reynolds number is

$$R_e = \frac{G_c d_r}{\mu} \tag{3.3}$$

Where the value for $G_c$ is

$$G_c = \frac{\dot{m}_a}{A_c} \tag{3.4}$$

Finally the pressure drop across the heat exchanger finned tube bundle is

$$\Delta p = \frac{{G_c}^2 \times 18.93 \times n_r \times {R_e}^{-0.316}}{\rho}\left(\frac{P_t}{d_r}\right)^{-0.927}\left(\frac{P_t}{P_d}\right)^{0.515} \tag{3.5}$$

Substituting different numbers of rows into $n_r$ gives different pressure loss values for the bundle at a constant volumetric flow rate. Figure 3.10 shows different pressure loss curves for two, four, and six row finned tube heat exchanger bundles.

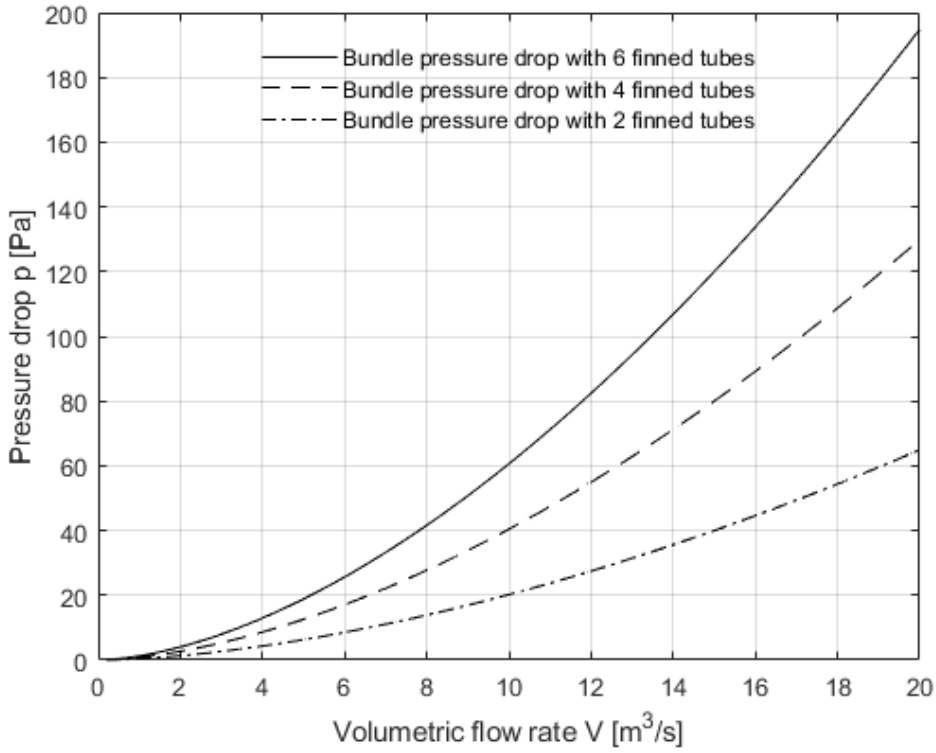


Figure 3.10: Analytical finned heat exchanger tube bundle pressure drop

These curves represent the analytical model for the heat exchanger bundles for flow entering and exiting the heat exchanger bundle perpendicularly. This is however not the case for the A-frame heat exchanger setup as the flow has to turn and then exit the heat exchanger bundle perpendicularly. Figure 2.4 showed how the turning of flow before entering the heat exchanger increases the total heat exchanger loss coefficient. It was however decided that the heat exchanger, being the biggest flow resistance of the A-frame ACC system, will give a reasonable indication of the number of finned tube rows required with the analytical normal flow calculations from Figure 3.10.

Wilkinson and Van der Spuy (2015) completed fan tests on the B2-fan. Tests were conducted at the design angle of 31º. From these tests the highest efficiency at a blade angle of 31º was 60.3% at a flow rate of 13.14 $m^3/s$. The fan static pressure rise at this flow rate equalled 230.9 Pa. For the system to operate close to the

maximum efficiency of the fan at the design blade angle, the point where the system resistance curve cross the fan static pressure rise curve should be at 13.14 $m^3/s$. From Figure 3.10 it was clear that not even 6 finned tube rows would provide enough flow resistance for this small scale ACC A-frame. Having more than two finned tube rows would be too heavy for the existing structure and an alternative design was required.

With the main function of the finned heat exchanger tubes being to turn the flow and provide a flow resistance, it was decided that an additional flow resistance should be placed between or in front of the heat exchanger tubes to provide the required pressure drop. Various woven steel meshes were explored as additional flow resistances. However, the pressure loss across the steel meshes were analytically calculated and it was found that it would not provide the required flow resistance.

Shade netting, which was readily available and inexpensive, was also an alternative solution as an additional flow resistance. Various shade netting ranging from 40%-up to 60% covered area were explored as a possible additional flow resistances.

### 3.3.3 Experimental verification of heat exchanger bundle selection

An induced draft wind tunnel shown in Figure 3.11 and described by Kröger (2004, 5.2.1) was used to measure the volumetric flow rate through and the pressure drop across the heat exchanger bundle designed for the test section as shown in Figure 3.12. A sample calculation on the working of the wind tunnel is shown in Appendix B.1.

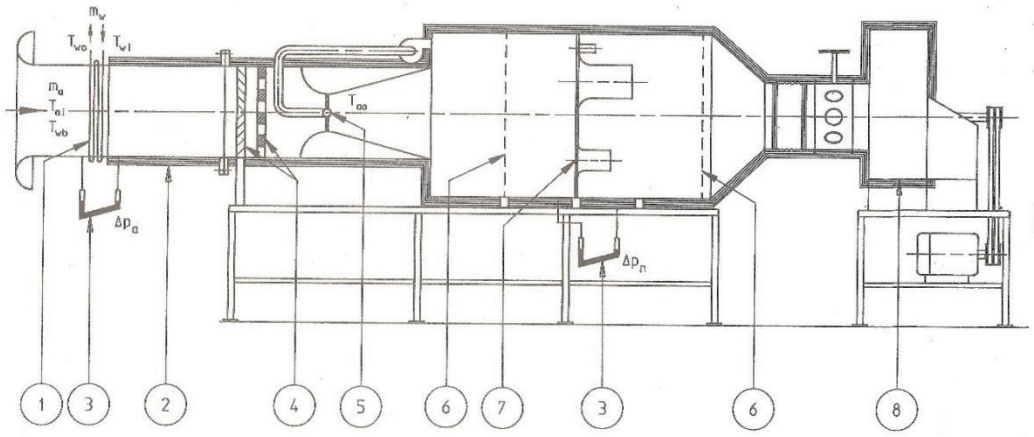


Figure 3.11: Induced draft wind tunnel from Kröger (2004, 5.2.2)

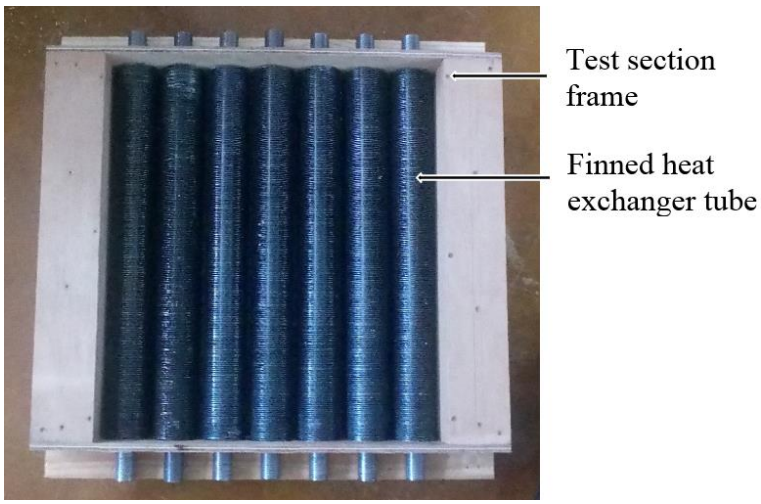


Figure 3.12: Finned tube heat exchanger test section

An additional pressure transducer which was calibrated according to the same procedure as described in 4.2.1, was used for measuring the static to static pressure drop across the heat exchanger bundle. The other two pressure transducers used in calculating the flow rate through the test section were also calibrated again. The calibration procedure of the pressure transducers is listed in Appendix B.2. In Figure 3.13 the pressure drop across the finned heat exchanger bundle test section is shown at various flow rates.

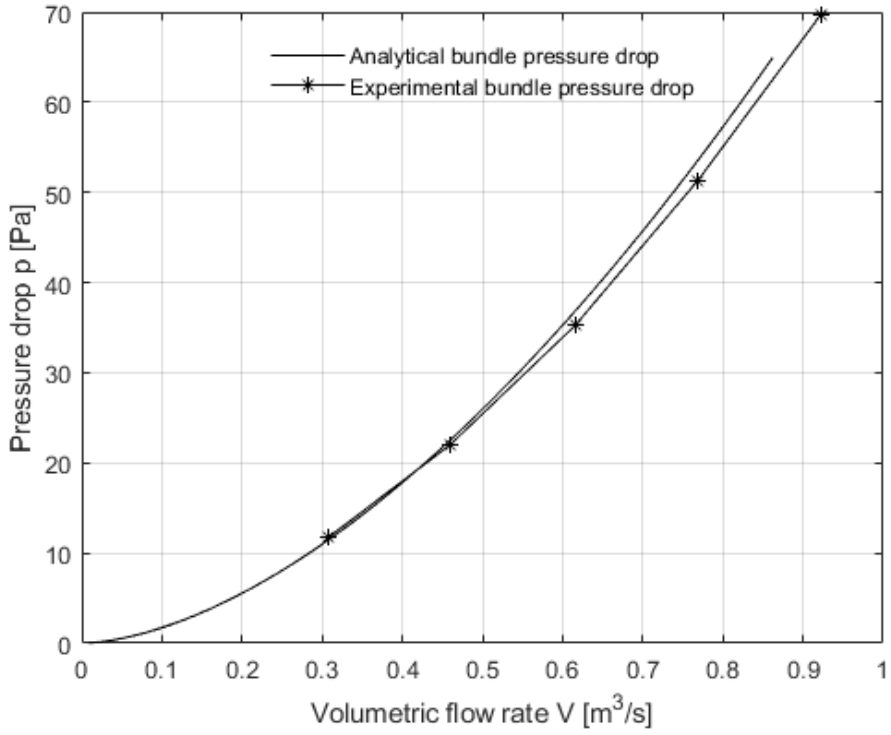


Figure 3.13: Analytical and experimental bundle pressure drop

It can be seen that the analytical model predicts the experimental results at low flow rates well and slightly over predicts the experimental results at higher volumetric flow rates. This can be due to tolerances in the manufactured design or fin surface finish leading to different frictional losses.

After multiplying the flow rate by the area ratio between the wind tunnel test section and the outlet area of the ACC, the prediction was confirmed that the pressure loss over the two row finned tube heat exchanger was much too low for the B2-fan to operate close to its highest static efficiency at a 31º blade angle. Different netting and netting configurations were tested to achieve different pressure loss curves for the heat exchanger bundle. The results from the different configurations are shown in Figure 3.14.

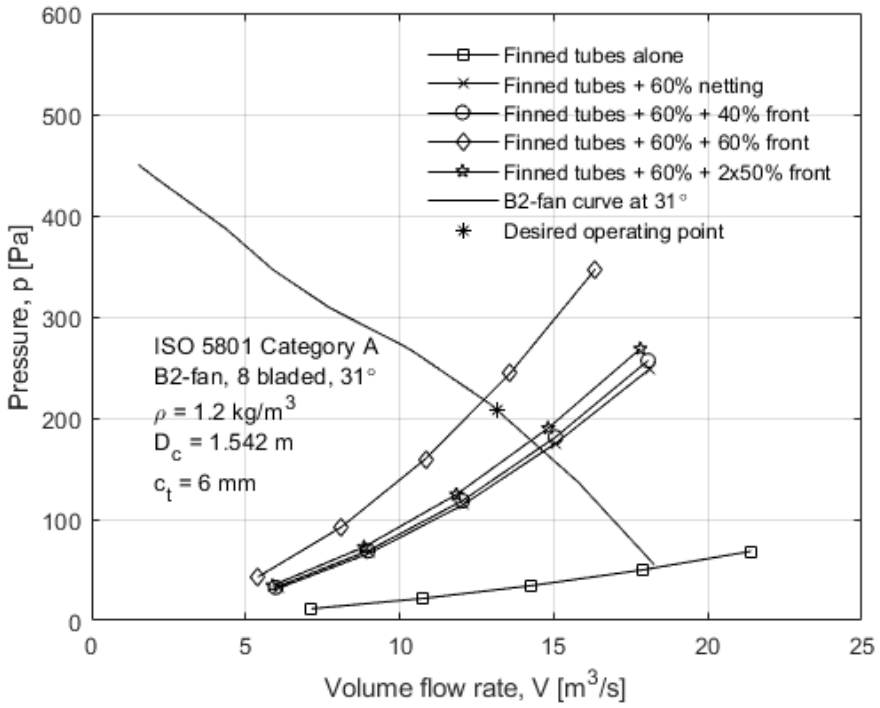


Figure 3.14: Heat exchanger calibration with multiple netting configurations

It can be seen that adding a 60% shade netting between the two finned tube rows resulted in a considerable increase in the bundle pressure drop over the heat exchanger bundle. Adding another 40% or two times 50% shade netting in front, on the inlet side to the heat exchanger, only resulted in a marginal increase in the total pressure drop. The 60% shade netting in front with a 60% netting between the tubes however resulted in an excessively large pressure drop.

It can be seen, from Table 3.1 that the expected operating point for the finned tubes with the added 60% shade netting will be at a static pressure and volumetric flow rate of 167.03 Pa and 14.67 $m^3/s$ respectively. Additional pressure losses due to the flow turning, bridge- and support losses will result in the pressure loss curve to

intersect the fan static pressure curve at a higher pressure and lower volumetric flow rate. This will lead to the fan performing closer to its maximum static efficiency of 60.3% at a volumetric flow rate of 13.14 $m^3/s$ as tested by Wilkinson and Van der Spuy (2015).

Table 3.1: Expected operating points

| Heat exchanger configuration | Volumetric flow rate V [$m^3/s$] | Static pressure $p_s$ [Pa] |
|---|---|---|
| Tubes alone | 18.33 | 52.42 |
| Tubes + 60% netting | 14.67 | 167.03 |
| Tubes + 60% + 40% front | 14.54 | 170.39 |
| Tubes + 60% + 2×50% front | 14.27 | 177.83 |
| Tubes + 60% + 60% front | 12.73 | 217.98 |

### 3.3.4 Finned heat exchanger bundle design

It was necessary to locate the 59 finned heat exchanger tubes with the tube pitch and arrangement as described in section 3.3.2. A simple design for locating all of the tubes was manufactured for ease of assembly and can be seen in Figure 3.15. This design consists of three main parts which includes the tube locator, side support and finned tubes.

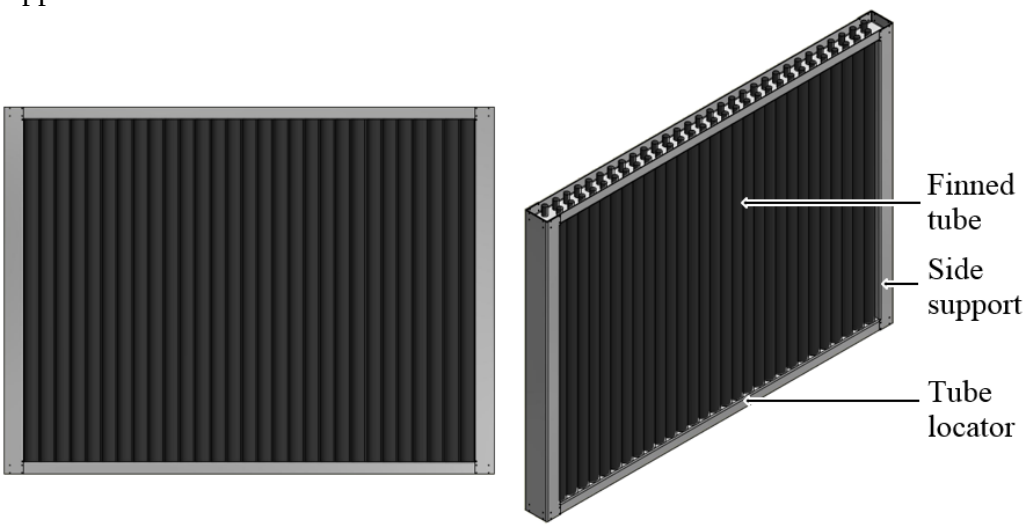


Figure 3.15: Heat exchanger assembly design

With the available structure of the A-frame, the heat exchanger bundles could be bolted directly to the open areas where the perforated plates were located. To all of the surfaces where sealing was required, between the heat exchanger bundle frame and the A-frame structure, adhesive sponge tape was added before fastening. The installed finned heat exchanger tube assembly can be seen in Figure 3.16.

Figure 3.16: Installed heat exchanger bundles with anemometer traverse rod

This anemometer traverse allows for a much finer grid than achieved by Böck (2017). Figure 3.17 shows the velocity measurement grid possible with the new heat exchanger outlet and anemometer traverse rod.

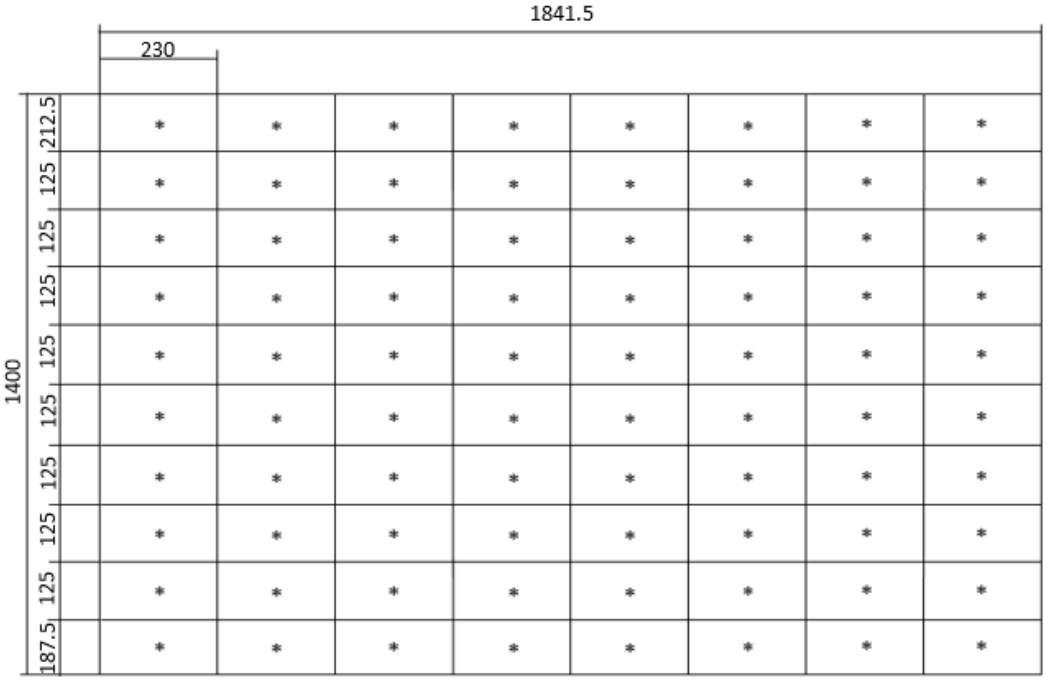


Figure 3.17: Velocity traverse measurement grid (dimensions in mm)

A total of 80 velocity measurement locations per heat exchanger outlet surface is achieved for the redesigned A-frame heat exchanger setup. This will give a better representation of the volumetric flow rate exiting the heat exchanger outlet surface.

## 3.4 Measuring equipment installation and calibration

All sensors used were tested before installation on the A-frame ACC unit. The detail regarding the calibration of the sensors is provided in Appendix B.

### 3.4.1 Torque transducer

Muiyser (2012) attached strain gauges to the shaft which connects the fan to the gearbox. The placement of the strain gauges was done in a manner so that the bending of the shaft could be measured in two directions orthogonally angled. Strain gauges were also installed to measure the torsional strain on the shaft.

A HBM T22/200 torque transducer was installed at the small scale A-frame ACC test facility for measuring the torque applied to the fan at various blade angle settings. The applied torque is used to calculate the power consumed by the fan. Located between two shafts, connecting the output of the motor to the fan, the torque transducer uses contactless transmission for measuring the torque. A linear output voltage, with a tolerance of 0.2%, is documented to determine the applied torque. Appendix B.3 shows the calibration procedure followed during the calibration process. The torque transducer torque is given by equation 3.6.

$$T_F = 39.893V - 0.178 \text{ N.m} \tag{3.6}$$

The rotation of the bearings between the torque transducer and the fan would result in a frictional torque. This frictional torque cannot be accounted for by only the calibration of the transducer through application of a static torque. Removal of the fan from the bottom shaft and running the shaft up to testing speed showed the bearing frictional torque. This value is subtracted from the measured total torque during testing to determine the torque used by the fan. The bearing frictional torque at between the operating rotational speed of 722 rpm and 750 rpm equalled 1.093 N.m.

### 3.4.2 Propeller anemometers

Eight Young Model 27106 propeller anemometers were used to measure the outlet velocity profile for the finned tube heat exchanger. They were spaced 230 mm apart horizontally to achieve a fine spread of data points across the outlet of the finned heat exchanger tubes. The horizontal bar on which they were mounted was designed to be moved from the top to the bottom of the finned heat exchanger tubes in increments of 125 mm, giving a total of 80 velocity measurements on each side of the A-frame ACC outlet. A voltage output is generated for each anemometer which is proportional to the air velocity. The propeller which rotates the tacho-generator measures airflow parallel to the axis. The calibration results for the eight propeller anemometers can be seen in Appendix B.4.

## 3.5 Facility commissioning

This section aims to provide the reader with the information regarding the commissioning of the indoor small scale A-frame ACC test facility. After the required changes were made, commissioning of the facility ensured that testing could be performed safely. The effect of distorted inflow as discussed in 2.3 had to be considered as the facility is installed indoors with walls at different distances from the bell mouth inlet. The bell mouth is also mounted not too far from the floor surface which might result in the approach velocity exceeding one half of the velocity through the fan.

### 3.5.1 Vertical inflow velocity

It was decided to record vertical inlet velocity measurements to determine if the fan is subject to a distorted inlet velocity profile. A round bar with two clamps mounting it to the perimeter of the bell mouth was used as a support for mounting anemometers to measure the vertical inlet velocity. The anemometers were thus mounted in a fashion which would least obstruct the flow and alter the inlet velocity profile. They were mounted on selected radii of 0.436 m and 0.657 m and can be seen in Figure 3.18. The measurement results are shown in Figure 3.19 and the tabulated vertical inflow velocities can be seen in Appendix D.2.

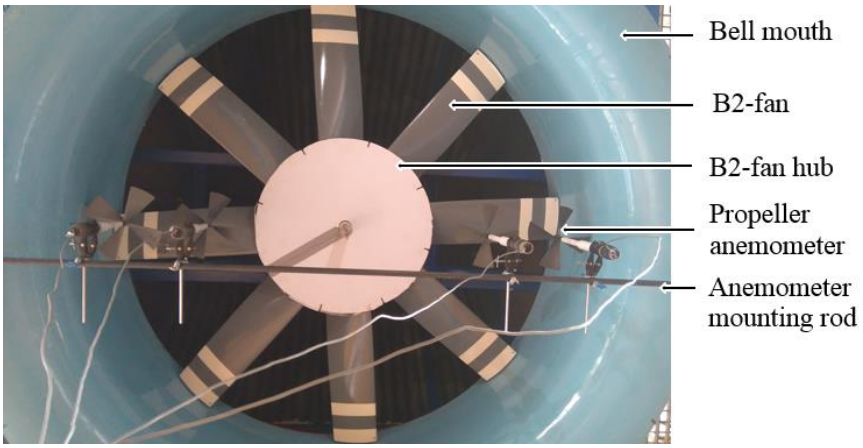


Figure 3.18: Vertical inflow velocity measurement

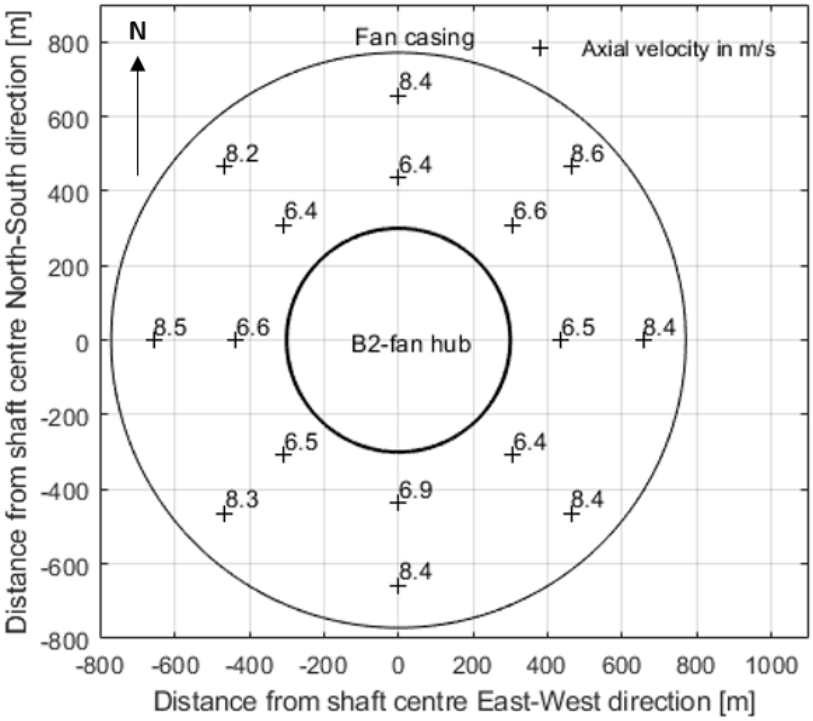


Figure 3.19: Vertical inflow velocity measurement results

From these measurements it can be seen that the highest vertical inflow velocity on the outer measurement radius is 8.6 m/s at the North-East side of the casing. The highest velocities is also measured on the outer diameter. The lowest vertical inflow velocity was measured at the North-West side to be 8.2 m/s. With an average of 8.4 m/s on the outer measurements, the maximum and minimum velocities were found to be only 2.4 % above and below the average measured velocity respectively.

On the inner radius the maximum and minimum inflow velocities equalled 6.9 m/s and 6.4 m/s respectively. With an average inflow of 6.54 m/s the maximum velocity was found to be 5.5 % above the average. This point was located at the South end of the fan hub. These results were considered as acceptable as the vertical inflow velocities measured showed a fairly evenly distributed axial inflow towards the fan.

### 3.5.2 Horizontal approach velocity

An anemometer stand, consisting of 8 anemometers was placed vertically to measure the velocity around a vertical cylindrical section below the bell mouth as seen in Figure 3.20. The anemometers were evenly spaced on the stand, each at a further distance below the bell mouth. It was found that only the data of the top anemometer, closest to the bell mouth, was usable as is gave the most constant velocity during testing.


Figure 3.20: Horizontal approach velocity measurements

Measurements were taken at eight points around the perimeter of the bell mouth in increments of 45º measured clockwise from North. Figure 3.21 shows the averaged approach velocities around the bell mouth perimeter. The exact values for each test can be seen in Appendix B.2.

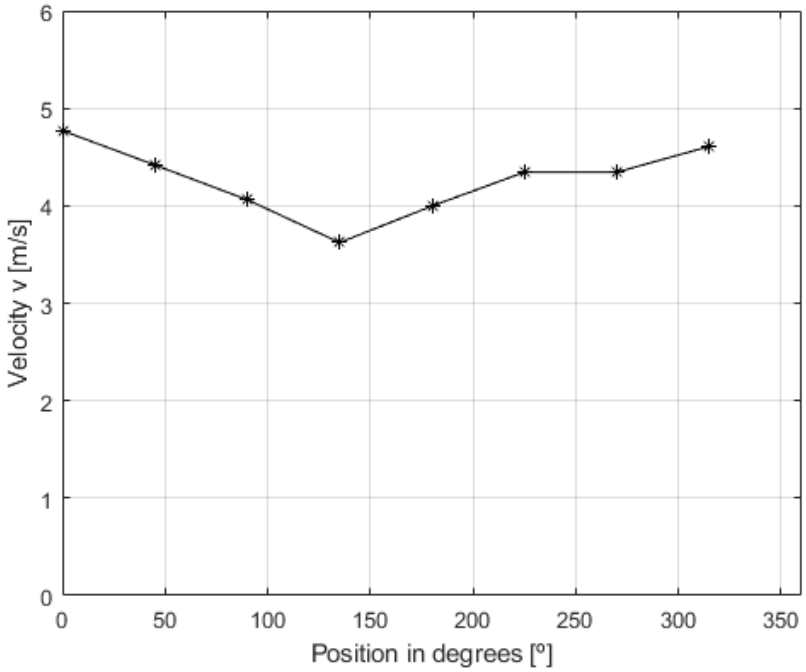


Figure 3.21: Horizontal approach velocity around bell mouth perimeter

From these velocity measurements it was found that the approach velocity at 0º, and at 135º were the maximum and minimum approach velocities respectively. With an average of 4.27 m/s the horizontal approach velocity was decided to be acceptable as it is roughly one half of the axial velocity through the fan (Monroe, 1979).

### 3.5.3 Effect of heat exchanger end plates

Before adding end plates to the heat exchanger outlet surface, a test was conducted on the A-frame ACC to measure the heat exchanger outlet velocity profile. This was to investigate if end plates were needed on the sides of the heat exchanger outlet to prevent edge effects. Figure 3.22 shows the outlet velocity profiles of the test conducted without end plates.

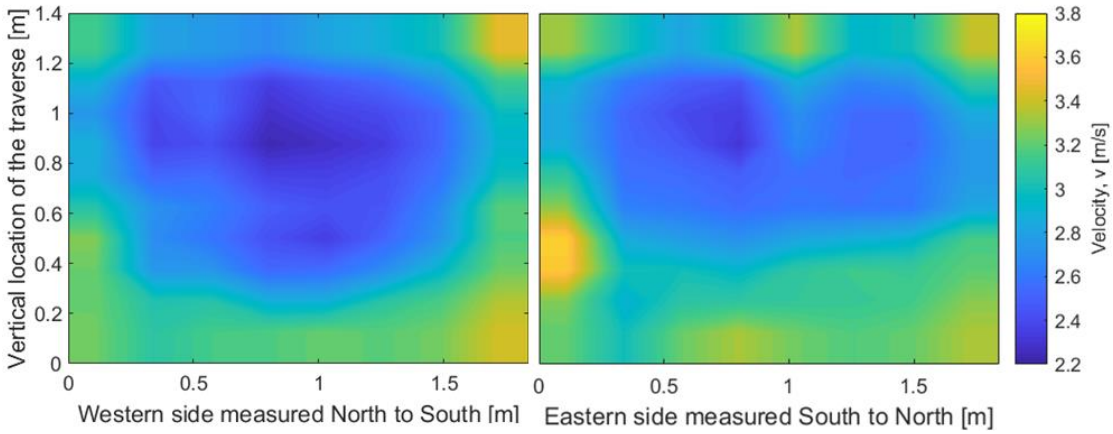


Figure 3.22: Outlet velocity profiles in at 31º blade angle without end plates

After the tests were conducted without the end plates fitted to the sides of the heat exchanger outlet, end plates were added and the tests repeated. These end plates were simple L-shaped pieces of sheet metal to simulate a symmetry plane between two adjacent fan cells. With only one cell being tested, this would prevent end effects from the sides altering the results to miss represent the outlet velocity profile. Figure 3.23 shows the resulting outlet velocity profiles with the added end plates.

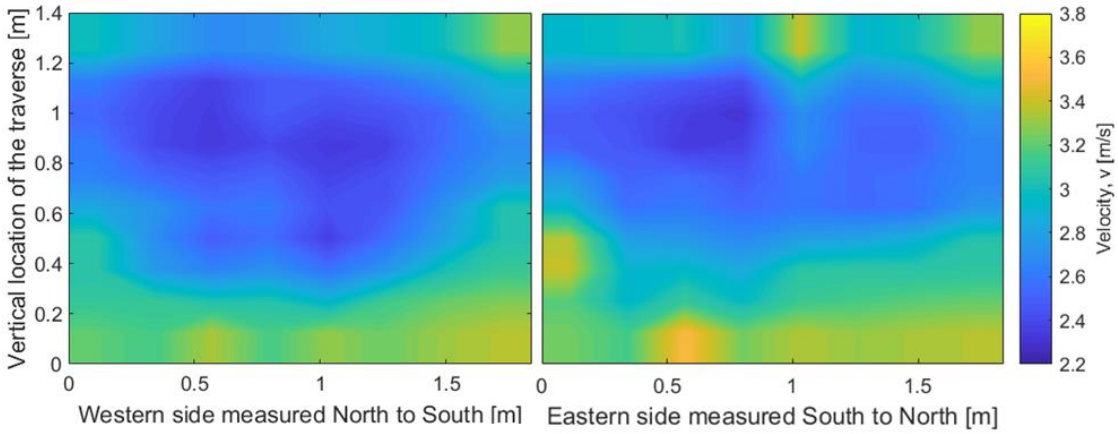


Figure 3.23: Outlet velocity profiles in at 31º blade angle with end plates

Investigating the colour of the plots, particularly in the vertical regions for both the Eastern and Western heat exchanger outlets, shows that a lower velocity is

measured at the sides with the added end plates than without them. This might be the result of end effects caused by the exiting airflow without the end plates. The lower velocity area is also a bit wider spread out over the surface with the added end plates.

It is however noted that, with the endplates lowering the velocity measurements at the sides, certain areas near the bottom and top parts of the heat exchanger experiences slightly higher velocities than without the end plates at the sides. This can be a result of the reduced side end effects reducing the airflow in those areas and leading to slightly higher velocities in others. From these measurement results it can be concluded that end plates should be added when performing tests on this single fan A-frame ACC setup.

### 3.5.4 Plenum chamber pressure measurements

In order to determine if the pressure rise over the fan installed in the A-frame ACC can be measured, pressure measurements were performed according to ISO 5802 (2008) by placing pressure taps in the walls of the plenum chamber as show in Figure 3.24. Pressure measurements were performed with the B2-fan at its design angle of 31º and rotational speed of 750 rpm whilst measuring the volumetric flow rate at the outlet of the heat exchanger bundles as shown in section 3.5.3. The measured pressures around the plenum chamber are documented in Table 3.2.


Figure 3.24: Pressure measurement points

Table 3.2: Plenum chamber pressure measurements

| Point | 1 | 2 | 3 | 4 | 5 | 6 | 7 | 8 |
|---|---|---|---|---|---|---|---|---|
| Pressure p [Pa] | 120.8 | 125.3 | 126.7 | 121.5 | 125.4 | 129.3 | 127.1 | 128.2 |

With a volumetric flow rate of 14.615 $m^3/s$ it is noted from the fan static pressure rise curve for the B2-fan at 31º blade angle, that the pressure rise over the fan should be in the vicinity of 168.4 Pa. This leads to conclude that the pressure measurements

performed on the plenum chamber walls according to ISO 5802 (2008) could not be used to determine the pressure rise over the fan in this particular case as the measured pressures were considerably lower than the expected pressure rise over the fan. This was however only for this specific case and further pressure measurement techniques should be investigated for this setup.

# 4 ISO 8501 and ACC facility testing

With the use of the ISO 5801 (2007) fan test results and the results from the fan tested inside the A-frame ACC, an investigation can be done on whether the plenum chamber results in a portion of the kinetic energy of the air to be recovered into a pressure inside of the plenum chamber.

## 4.1 ISO 5801 (2007) fan tests

In order to obtain fan curves for the B2-fan with its hub configuration and blade angles, fan tests were performed at the standardised fan test facility of the Mechanical and Mechatronic Engineering Department of Stellenbosch University according to ISO 5801 (2007) as discussed in section 2.1.

Calculating the mass flow rate through the fan is generally done by using equation 4.1 from Kröger (2004, 6.1.1).

$$\dot{m} = C_n \epsilon_n A_n (2\rho_n \Delta p_n)^{0.5} \tag{4.1}$$

$C_n$ is the flow coefficient of the nozzle and $\epsilon_n$ the expansibility factor. Calculating the density inside of the settling chamber can be done using the ideal gas relation. The static pressure difference between the inside and the outside of the settling chamber is measured and used as $\Delta p_{sc}$.

$$\rho_T = \frac{(p_{amb} + \Delta p_{sc})}{R T_{amb}} \tag{4.2}$$

The volumetric flow rate and dynamic pressure are shown in equation 4.3 and equation 4.4 respectively.

$$V_F = \frac{m}{\rho_F} \tag{4.3}$$

$$p_{dF} = \frac{0.5(m/A_{sc})^2}{\rho_F} \tag{4.4}$$

The fan power can be calculated by

$$P_F = \frac{2\pi T N_F}{60} \tag{4.5}$$

Calculating static pressure rise over the fan is done by subtracting the dynamic pressure from the pressure inside of the settling chamber and can be done by

$$\Delta p_{FS} = -\Delta p_{sc} - p_{dF} \tag{4.6}$$

Finally, calculating the fan static efficiency can be done by

$$\eta_{Fs} = V_F \Delta p_{Fs} / p_F \tag{4.7}$$

### 4.1.1 Torque measurements

Measuring the torque applied to the fan shaft is done with a HBM T22/100 torque transducer. Appendix B.6 shows the calibration process for the torque transducer, pressure transducers and rotational speed. The calibrated equation for the torque transducer is given by equation 4.8.

$$T = -0.0568V^2 + 20.477V - 1.6871 \tag{4.8}$$

### 4.1.2 Bearing frictional torque

The frictional torque from the bearings would need to be deducted from the measured torque. This frictional torque was determined by running the shaft without the fan at 750 rpm for the B2-fan. The torque value was recorded to be 3.64 N.m. This value was subtracted from all torque measurements to obtain the correct torque applied to the fan.

### 4.1.3 Fan testing procedure and results

After completion of the calibration and blade angle setting, the fan was fitted onto the shaft. A hub, consisting of a cylindrical section and two circular sides, as shown in section 2.8, was fitted to the fan to prevent reverse flow at the centre of the fan. The rotational speed of the fan was set to 750 rpm with the louvres initially set to a closed setting. Changing the flow rate to obtain different operating points is achieved by opening the louvres stepwise. When the flow rate is increased by opening the louvres, the losses inside of the system increase due to frictional effects at the higher volumetric flow rates. To overcome the frictional effects, the auxiliary fan at 4 is switched on, the previous measurement repeated, and the louvres are opened further until fully open. From Figure 4.1 and Figure 4.2 it can be seen that a greater angle of attack results in a higher static pressure rise and also greater power consumption respectively.

Figure 4.3 shows that a low blade angle results in higher peak efficiencies at lower flow rates. For repeatability the tests were completed three times at each different blade angle as can be seen in Appendix D.1.

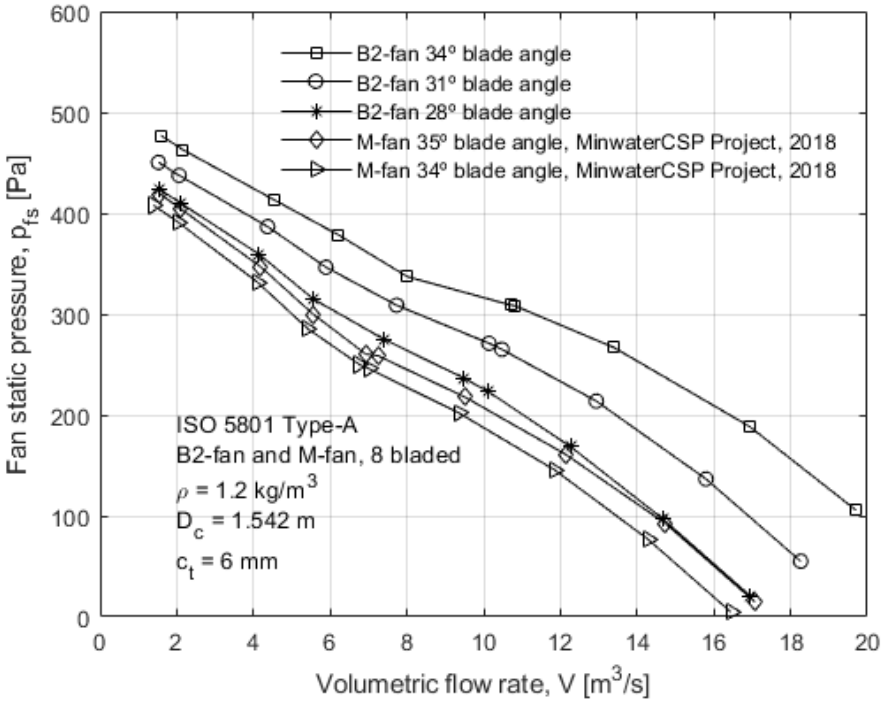


Figure 4.1: Fan static pressure rise at different blade angle settings

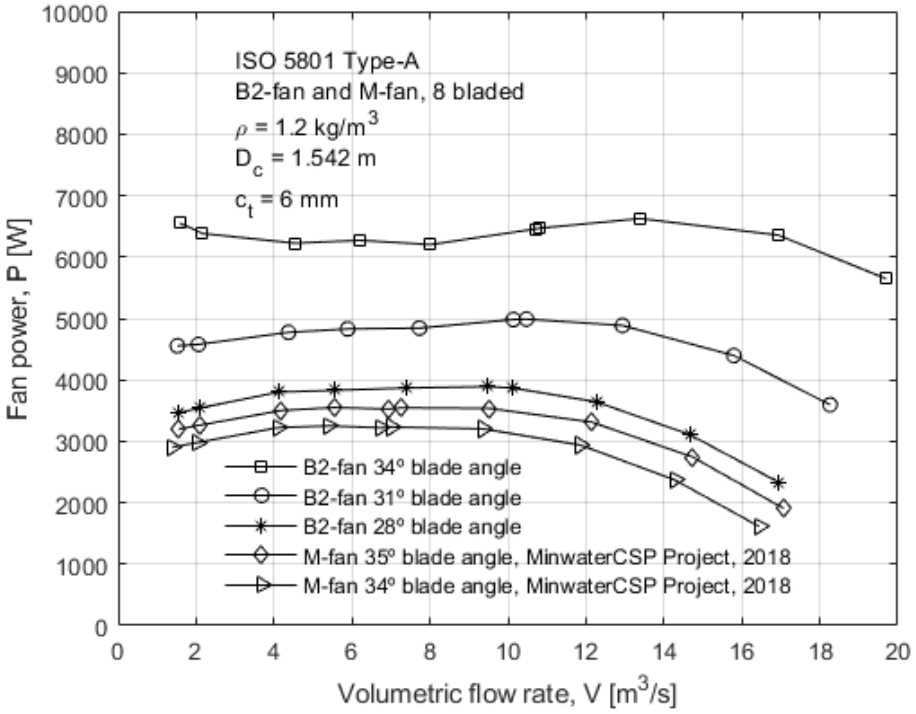


Figure 4.2: Fan power consumption at different blade angle settings

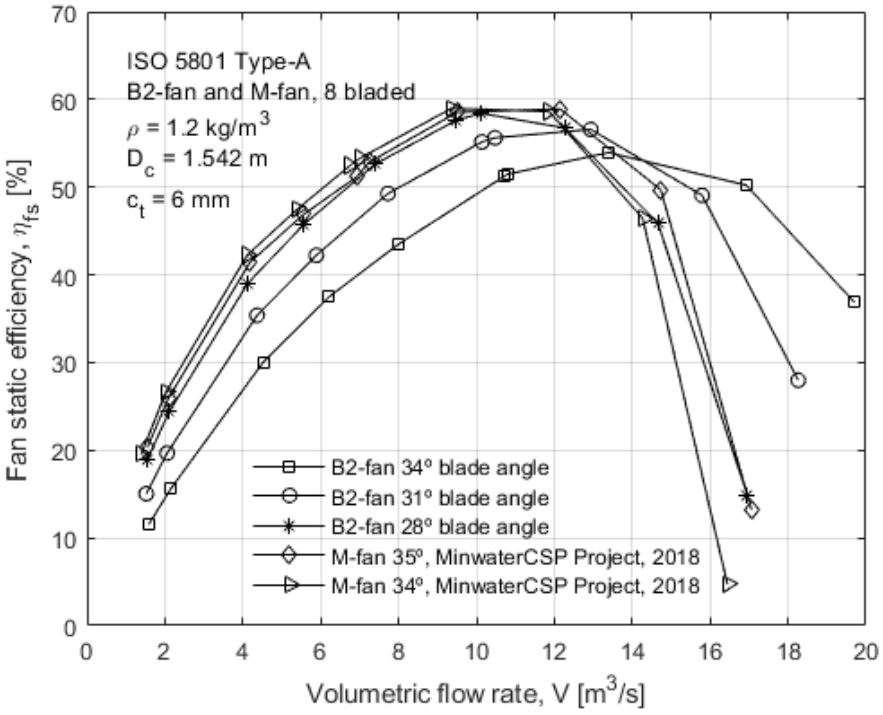


Figure 4.3: Fan static efficiency at different blade angle settings

Although the same type of hub was used, it seemed as if the thickness of the hub used by Wilkinson and Van der Spuy (2015) was thinner in the axial direction. For the fan static pressure rise curve, a higher pressure rise was achieved at the lower volumetric flow rate. This might have resulted to more leakage at lower volumetric flow rates and high pressures for Wilkinson and Van der Spuy (2015).

Comparing the power consumption by the fan at the 31° blade angle shows that more power was consumed than in the tests that Wilkinson and Van der Spuy (2015) performed. This can be due small differences in blade angle setting or during the calibration of the torque transducer. The fan static efficiency curves at a 31° blade angle can be well compared up until the 16 $m^3/s$ point after which Wilkinson and Van der Spuy (2015) achieved a slightly higher fan static efficiency. This is a result of the higher static pressure rise achieved after the 16 $m^3/s$ volumetric flow rate. It is concluded that the obtained characteristic fan curves are sufficient for the purpose of comparing the performance of the fan to that of the same fan installed in a plenum chamber. The differences between the tested values can be as a result of slight differences in blade angle setting. It is however important to note that the same fan, hub, blade angle setting and calibration procedures are used in both the standardised fan testing procedures and the constructed A-frame test facility.

## 4.2 A-frame ACC facility fan performance testing

The measurements conducted in measuring the performance of the B2- and M-fans in the A-frame ACC included the measurement of the heat exchanger outlet velocity profile and the torque applied to the fan.

### 4.2.1 Volumetric flow rate measurements

Measuring the air velocity on the outlet side of the small scale ACC test facility was done with eight anemometers spaced as described in section 3.4.2. With a vertical traverse of 10 locations, a total of 80 velocities were measured on each outlet side giving a total of 160 velocity measurement points for the outlet surfaces of the heat exchanger. For each velocity, a small area as shown in Figure 3.17, is assumed to have the same velocity, as measured by the anemometer, across its entire area. Equation 4.9 shows the total volumetric flow rate for one side of the A-frame ACC.

$$V = \sum_{j=1}^{10} \sum_{i=1}^{8} v_{ij} A_{ij} \tag{4.9}$$

Where 'i' represents the horizontal number of the anemometers from left to right and 'j' the vertical position of the traverse, measured from the top to the bottom of the outlet surface. The average power consumption and flow rate measured at the ACC facility with different blade angle settings is shown in Table 4.1.

Table 4.1: Fan power consumption and average volumetric flow rate

| Fan tested | Blade angle [°] | Power consumption P [W] | Average volumetric flow rate V [$m^3/s$] |
|---|---|---|---|
| B2-fan | 28 | 3079.37 | 13.117 |
| | 31 | 4411.16 | 14.615 |
| | 34 | 5799.58 | 15.929 |
| M-fan | 34 | 2365.96 | 12.234 |
| | 35 | 2791.54 | 12.824 |
| | 36 | 3255.02 | 13.547 |

Figure 4.4, Figure 4.5 and Figure 4.6 show the outlet velocity measurements as a colour plots on the East side and West side of the A-frame for the B2-fan at blade angle settings of 28°, 31° and 34° respectively. A colour bar on the right hand side of the colour plots indicates the magnitude of velocity and the colour associated with it.

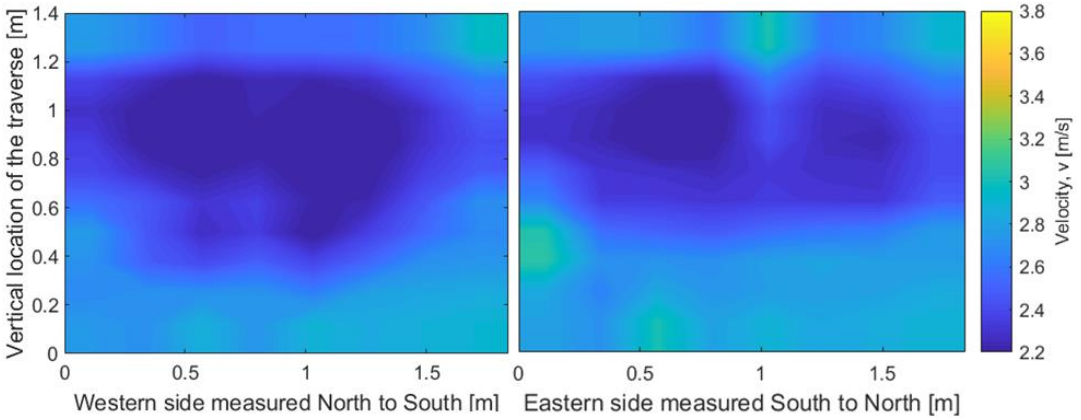


Figure 4.4: B2-fan outlet velocity profiles in at 28º blade angle

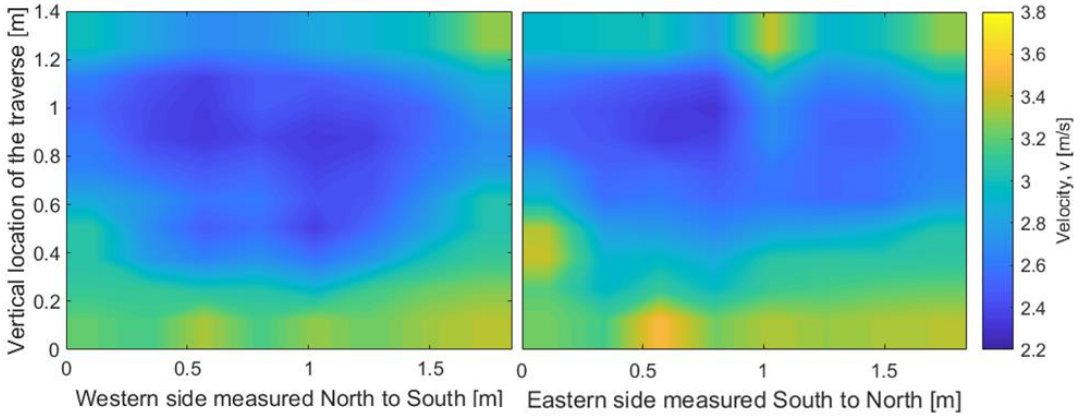


Figure 4.5: B2-fan outlet velocity profiles in at 31º blade angle

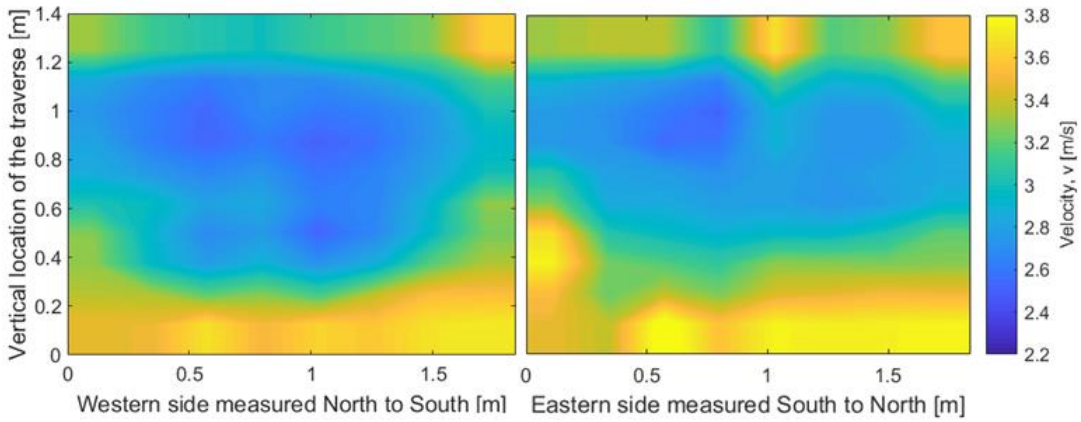


Figure 4.6: B2-fan outlet velocity profiles in at 34º blade angle

Figure 4.7, Figure 4.8 and Figure 4.9 show the outlet velocity measurements as a colour plots on the East side and West side of the A-frame for the M-fan at blade angle settings of 34º, 35º and 36º respectively. A colour bar on the right hand side of the colour plots indicates the magnitude of velocity and the colour associated with it.

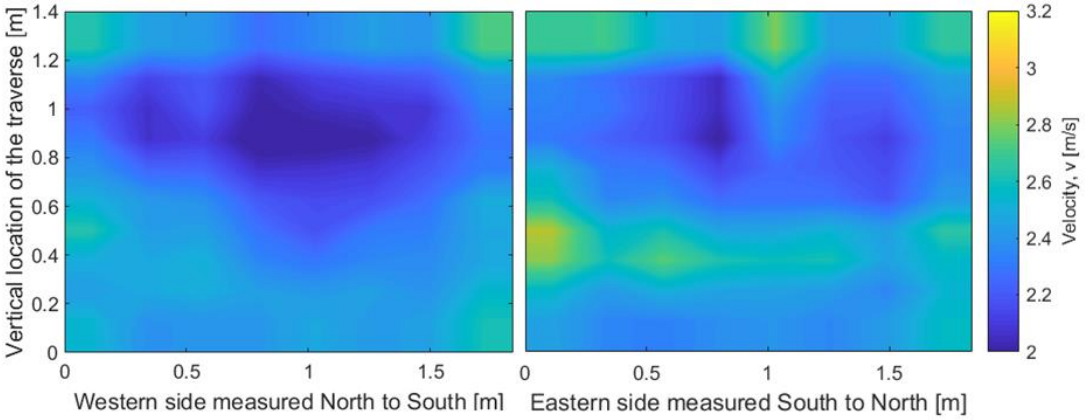


Figure 4.7: M-fan outlet velocity profiles in at 34º blade angle

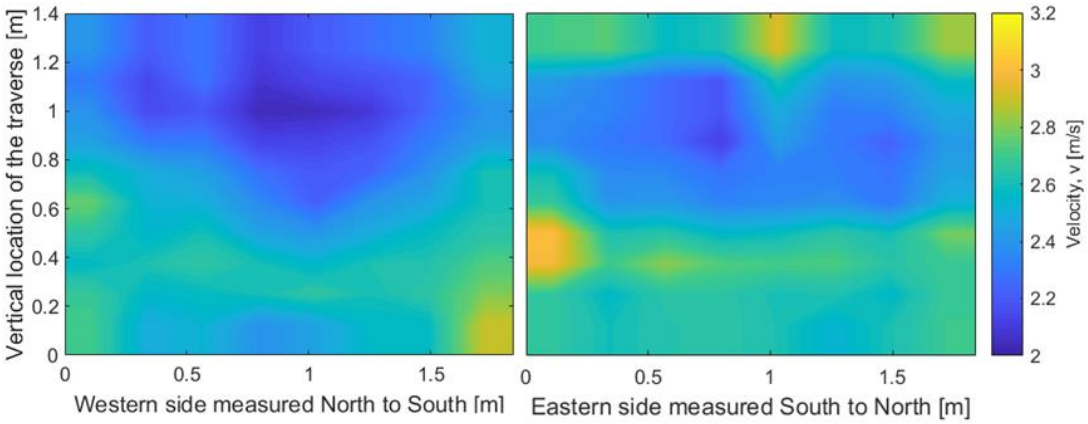


Figure 4.8: M-fan outlet velocity profiles in at 34º blade angle

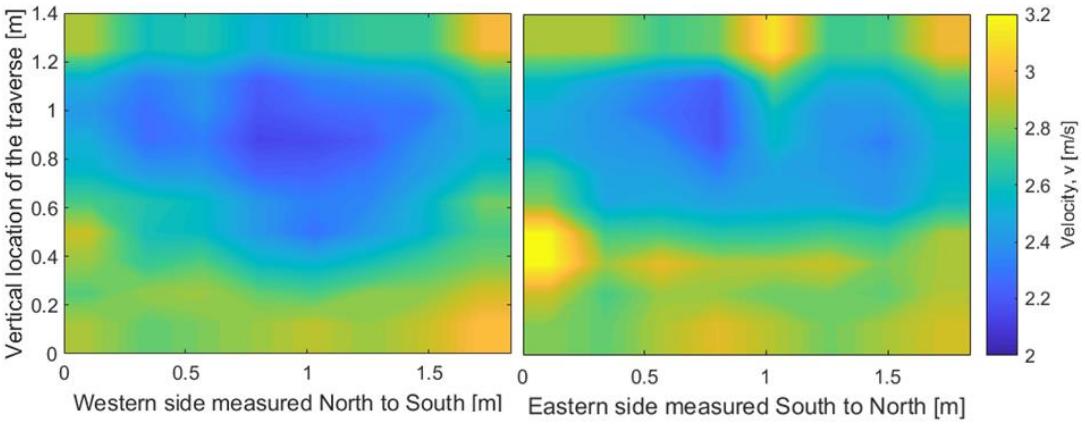


Figure 4.9: M-fan outlet velocity profiles in at 34º blade angle

From these measurements it can be seen that the outlet velocity profile for the Eastern side is similar for the different blade angle settings for the B2-fan and only differ in magnitude. The same can be said for the M-fan. Although the Western differs from the Eastern velocity profile, it shows a similar profile for the different blade angles which again only differs in magnitude. It is also seen from the profiles that the lower part of the heat exchanger on the Eastern and Western sides experiences a considerably higher exit velocity than the rest of the heat exchanger surface. This is observed for all of the blade angle settings for both of the fans tested. The outlet velocity profiles of the M-fan however, shows at the Eastern side that a higher velocity region is measured at a vertical position of 0.4 m, where for the B2-fan the higher outlet velocity region was at the bottom of the heat exchanger outlet. This difference in outlet velocity profile can be as a result of the dynamic component of the air inside of the plenum chamber due to the difference in fan blade geometry. Furthermore, it is noted that the volumetric flow rate on the Western side is about 3% less than on the Eastern side. From the vertical inflow measurements in section 3.5.1 it can be seen that the inlet velocity at the East side is slightly higher at the outer most part of the fan casing. This might be an indication that the higher inlet velocity on the East perimeter of the bell mouth resulted in the slightly higher volumetric flow rate at the East side heat exchanger outlet. The heat exchanger outlet volumetric flow rate for each fan at the different blade angle settings is given in Table 4.2.

Table 4.2: Heat exchanger volumetric flow rates

| Fan tested | Blade angle [º] | East Side Volumetric flow rate V [$m^3/s$] | West Side Volumetric flow rate V [$m^3/s$] | Percentage difference [%] |
|---|---|---|---|---|
| B2-fan | 28 | 6.661 | 6.456 | 3.1% |
| | 31 | 7.409 | 7.206 | 2.7% |
| | 34 | 8.094 | 7.835 | 3.2% |
| M-fan | 34 | 6.225 | 6.009 | 3.6% |
| | 35 | 6.549 | 6.275 | 4.4% |
| | 36 | 6.886 | 6.66 | 3.4% |

These outlet velocity profiles correlate qualitatively well with results from Engelbrecht (2018) who numerically investigated the performance of the B2a-fan in a forced draft ACC. The numerical model predicts higher axial velocities inside of the plenum chamber near the bottom of the heat exchanger than higher up to the top part of the heat exchanger.

### 4.2.2 Fan power consumption

With the torque transducer, as described in 4.1, the torque is measured to determine the power delivered to the fan. Figure 4.10 shows the power consumption curves as tested in 4.1 for the B2-fan with the power consumption and flow rate of the small scale A-frame ACC test facility at the three different blade angle settings. Figure 4.11 shows the M-fan power consumption curves and the power consumption as tested in the A-frame ACC facility at two different blade angle settings.

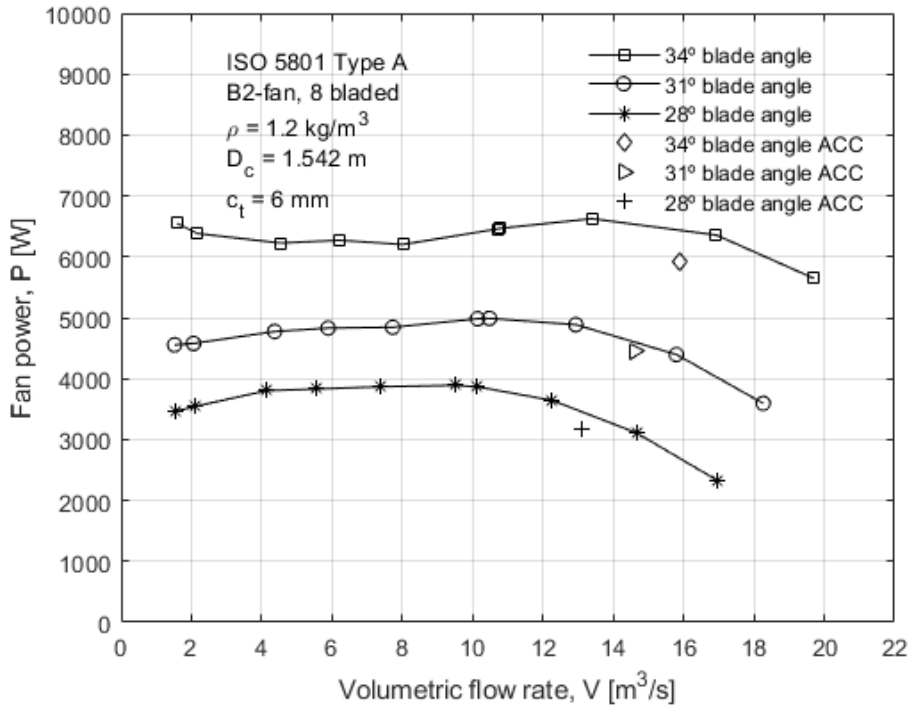


Figure 4.10: A-frame ACC and ISO 5801 (2007) B2-fan power consumption

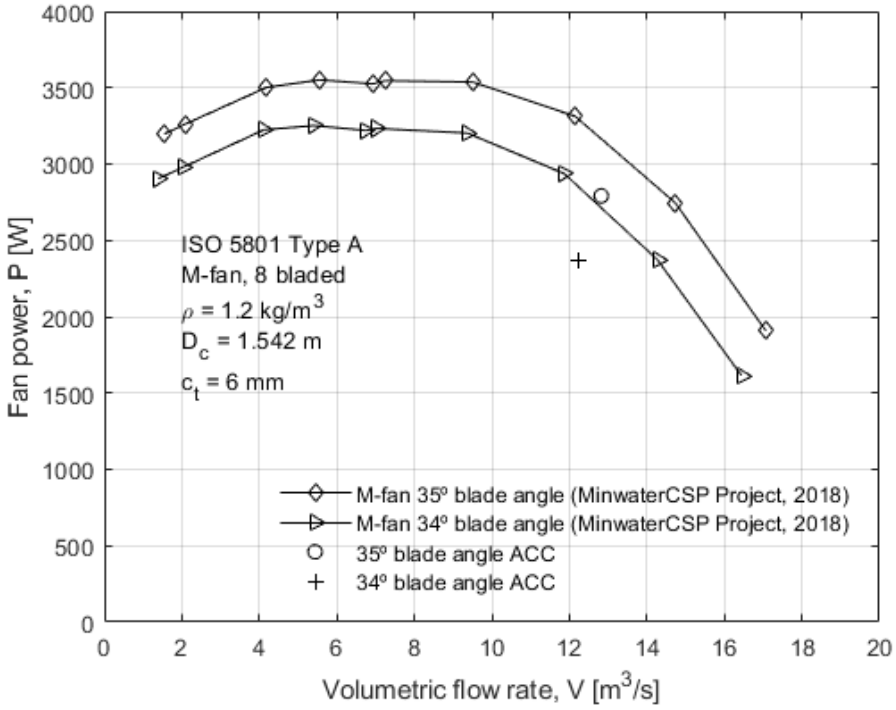


Figure 4.11: A-frame ACC and ISO 5801 (2007) M-fan power consumption

Comparing the power consumed by the B2- and the M-fan installed in an A-frame test facility with the fan power curves from the ISO 5801 (2007) Type-A fan tests, shows that the fans consumed less power at the same volumetric flow rate inside the A-frame plenum chamber. This might be a result of recovery affecting the performance of the fan inside the plenum chamber. It is seen that the decrease in power usage for the M-fan is even more significant than that of the B2-fan.

# 5 System draft equation

In order to compare results from the standardized fan tests, in the Type-A test facility, with the tests performed at the A-frame ACC facility, the system draft equation from Kröger (2004, 8.1.30) for an A-frame ACC is used. This chapter provides the draft equation for the ACC setup by calculating the K-loss and gain factors for the A-frame facility. The sensitivity of the system to change in selected parameters is also investigated analytically with the use of the draft equation from Kröger (2004, 8.1.30).

## 5.1 System draft equation

Kröger (2004, 8.1.30) used a draft equation that adds the loss and gain coefficients of the ACC to determine the recovery value as discussed in 2.2. This equation takes into account the support, bell mouth, fan bridge and heat exchanger loss coefficients factor and the fan static pressure rise coefficient. Equation 5.1 shows the system draft equation.

$$0 = K_{ts}\frac{\left(\frac{m_a}{A_2}\right)^2}{2p_{a1}} + K_{Fsi}\frac{\left(\frac{m_a}{A_c}\right)^2}{2p_{a3}} + K_{up}\frac{\left(\frac{m_a}{A_e}\right)^2}{2p_{a3}} - (K_{Fs} + K_{rec})\frac{\left(\frac{m_a}{A_c}\right)^2}{2p_{a3}} + K_b\frac{\left(\frac{m_a}{A_e}\right)^2}{2p_{a7}} + K_{he\theta}\frac{\left(\frac{m_a}{A_{fr}}\right)^2}{2p_{a567}} \quad (5.1)$$

With no steam in the heat exchanger tubes, the assumption is made that the temperature of the air is constant throughout the system. Having a small scale A-frame ACC system, the height difference from the inlet to the outlet of the ACC is assumed small enough to not affect the air density. Due to this small scale A-frame setup being a single unit with no turning of the flow at the outlet surface, the jetting and outlet losses, as described by Kröger (2004, 5.6.12), is equal to zero. Furthermore the value for $K_{Fsi}$ for a well-rounded bell mouth according to Kröger (2004, 6.4.7) is equal to zero. This is a bell mouth with the outer bell diameter equal to 1.25 the casing diameter. There is also no obstructions upstream of the fan resulting in the value for $K_{up}$ to equal zero. These assumptions simplify equation 5.1 to equation 5.2.

$$0 = K_{ts}\left(\frac{m_a}{A_2}\right)^2 - (K_{Fs} + K_{rec})\left(\frac{m_a}{A_c}\right)^2 + K_b\left(\frac{m_a}{A_e}\right)^2 + K_{he\theta}\left(\frac{m_a}{A_{fr}}\right)^2 \quad (5.2)$$

## 5.2 ACC supports loss coefficient

The supports elevating the intake of the bell mouth from the floor surface, located between 1 and 2 in Figure 5.1, are taken into account as a flow obstruction to the airflow upstream of the fan bell mouth. The calculation for this can be seen in Appendix C.1.

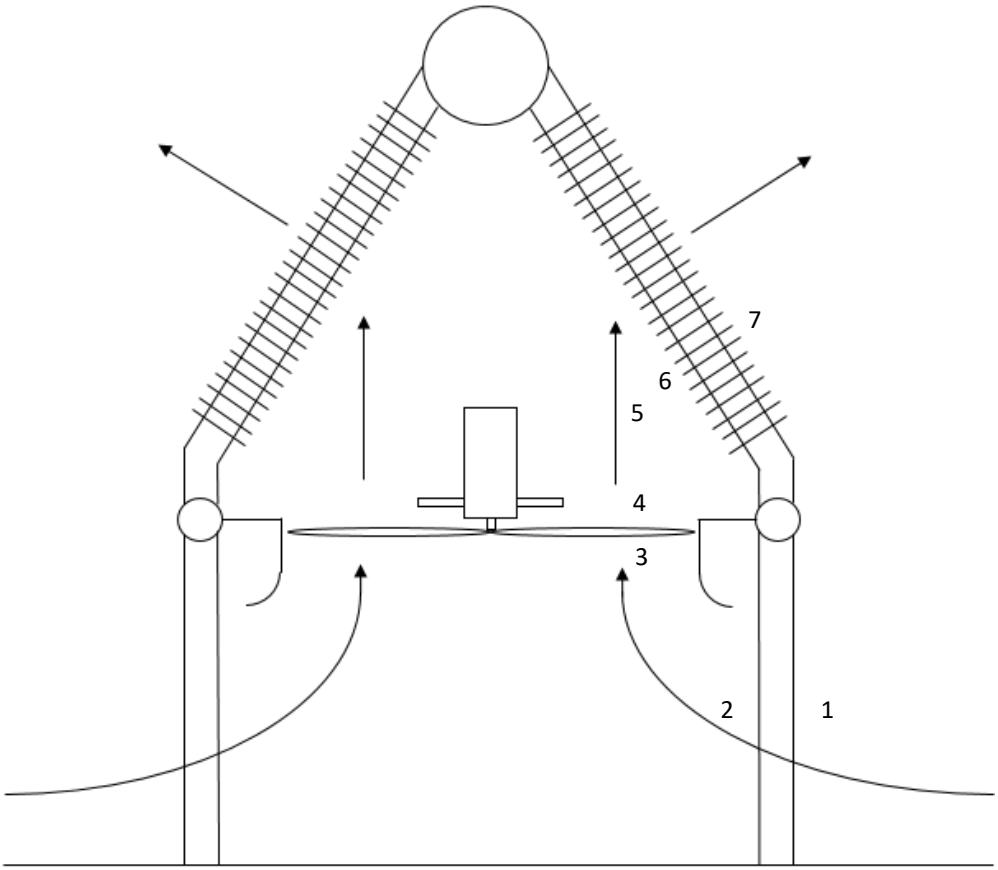


Figure 5.1: A-frame ACC schematic representation

The assumption was made that the airflow is uniform from all directions around the perimeter of the bell mouth for simplification of the loss coefficient calculation. Although the horizontal approach velocities were not exactly the same as shown in Figure 3.21, the assumption was considered to be reasonable. The area for the cylindrical region which intersects all four of the supports was calculated to determine the average approach velocity $v_s$ at the supports. From this $Re_s$ was calculated which is used to determine the drag coefficient $C_D$ of the supports.

The parameters are listed below:

| | |
|---|---|
| Vertical support length | $L_s = 2$ m |
| Support width | $a = 0.1$ m |
| Diagonal support width | $d_s = \sqrt{a^2 + a^2}$ |
| Distance between supports | $b = 3\ m$ |
| Number of supports | $n_s = 4$ |

The cylindrical area through which the flow will approach the bell mouth and flow past the vertical supports as shown in Figure 5.2 is calculated using equation 5.3

$$A_2 = \sqrt{b^2 + b^2} \times \pi L_s \tag{5.3}$$

Dividing the volume flow rate $V$ by the flow area $A_2$ gives the approach velocity at the vertical supports as shown in equation 5.4

$$v_s = V/A_2 \tag{5.4}$$

With $v_s$ known, the Reynolds number for the flow at the support is calculated using equation 5.5

$$Re_s = \rho v_s\, d_s/\mu \tag{5.5}$$

The drag coefficient $C_{d,s}$ is then calculated by equation 5.6 from Figure 5.3.

$$C_{d,s} = -6.813 \times 10^{-6} Re_s + 1.841 \tag{5.6}$$

With the drag coefficient known it is possible to calculate $K_s$, the support K-loss factor, using equation 5.7 for the four supports.

$$K_s = C_{d,s} L_s d_s\, n_s/A_2 \tag{5.7}$$

Equation 5.8 shows the support loss coefficient as a function of volumetric flow rate.

$$K_s = -0.000101V + 0.0781 \tag{5.8}$$

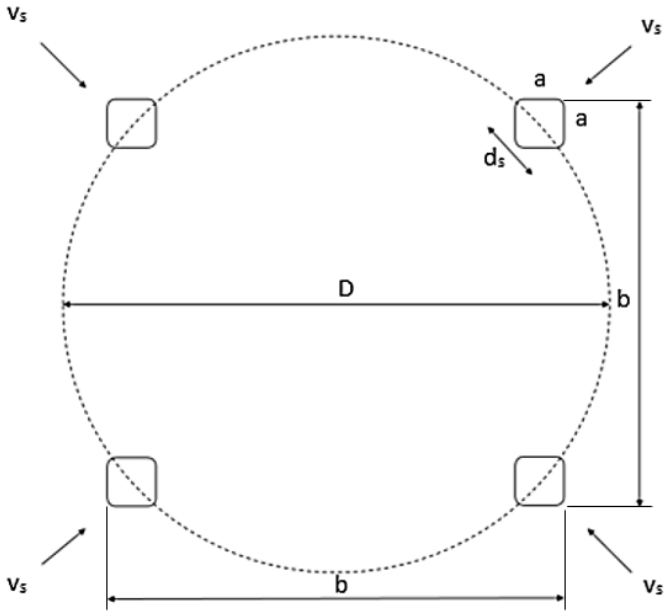


Figure 5.2: ACC supports and cylindrical flow area

## 5.3 Fan bridge loss coefficient

The fan bridge consists of two rectangular beams oriented with the short edge facing the oncoming flow. The two beams cross the outlet side of the fan shroud where it acts as a flow obstruction and results in a pressure loss factor $K_b$. From Figure 5.3 and equation 5.13 the drag coefficient of the beams can be calculated.

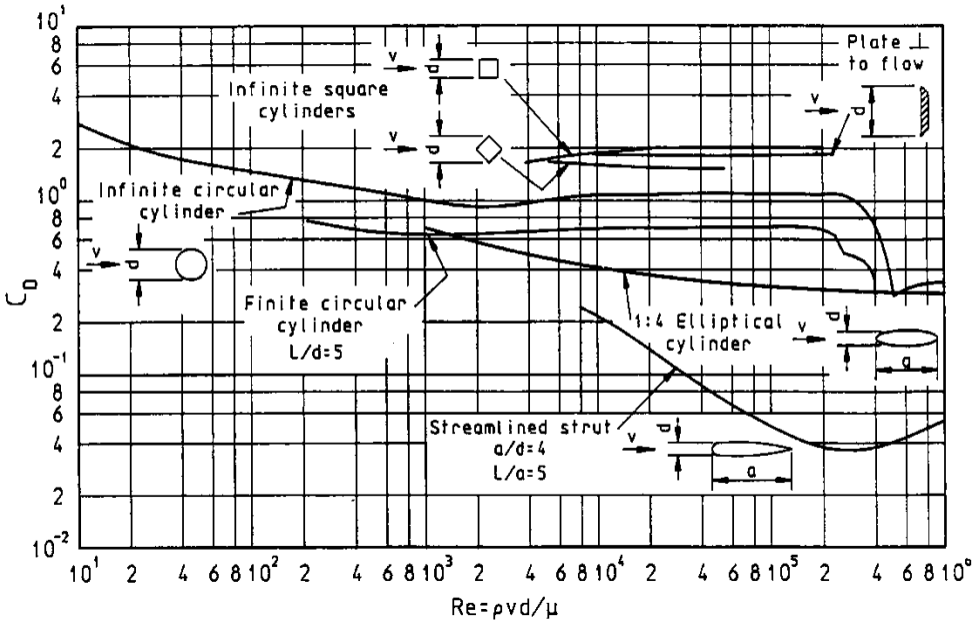


Figure 5.3: Coefficient of drag for two dimensional bodies (Kröger: 2004, 2.5.1)

Only the length of the bridge crossing the flow directly above the outlet of the fan was considered for calculating the pressure loss over the bridge. The assumption was made that the flow velocity in line and above the hub will be negligible as the flow is created by the fan from the root to the tip of the fan blades. The pulleys, shafts and bearings above the bridge will not be added as flow losses as they are above the fan in line with the hub where the velocity is considered negligible. The bridge loss coefficient calculation can be seen below:

Parameters:

$d_b = 0.05$ m
$D_c = 1.542$ m
$L_b = 2.55$ m

$$Re_b = \rho \left(\frac{V}{A_e}\right) \frac{d_b}{\mu} \tag{5.9}$$

The circular area through which the flow will approach the fan bridge is calculated using equation 5.10 by subtracting the hub area from the casing area.

$$A_e = \pi \left( \left(\frac{D_F}{2}\right)^2 - \left(\frac{D_h}{2}\right)^2 \right) \tag{5.10}$$

Dividing the volume flow rate $V$ by the flow area $A_e$ gives the approach velocity at the fan bridge as shown in equation 5.11

$$v_b = V/A_e \tag{5.11}$$

With $v_b$ known, the Reynolds number for the flow at the bridge is calculated using equation 5.12

$$Re_b = \rho v_b \, d_b/\mu \tag{5.12}$$

The drag coefficient $C_{d,b}$ is then calculated using Figure 5.3 and equation 5.13

$$C_{d,b} = 2.365 \times 10^{-5} Re_b + 1.496 \tag{5.13}$$

With the drag coefficient known it is possible to calculate $K_b$, the bridge K-loss factor, using equation 5.14 for the bridge.

$$K_b = C_{d,b} L_b d_b \, n_b / A_e \tag{5.14}$$

Equation 5.15 shows the $K_b$ value as a function of volumetric flow rate.

$$K_b = 0.00792V + 0.241 \tag{5.15}$$

## 5.4 Heat exchanger loss coefficient

The heat exchanger used is as described in section 3.3 with two rows of finned tubes in a staggered arrangement and an added netting between the two tube rows. It is however necessary to add additional losses to the heat exchanger as it is angled at 30º relative to the approaching flow direction.

Meyer and Kröger (2001) showed, through experiments, that if flow does not approach the heat exchanger bundle perpendicularly, an additional factor should be added to account for the sudden turn the flow encounters. This is due to separation at the leading edge of the finned heat exchanger tubes. This separation results in a jet forming, according to Kröger (2004, 5.6.2). The loss factor as tested by Meyer and Kröger (2001) for a two row heat exchanger bundle is shown in equation 5.16.

$$K_{he\theta} = \left(0.86 + \frac{0.98}{sin(\theta)}\right)\left(\frac{1}{sin(\theta)} - 1\right) + K_{\theta=90^\circ} \tag{5.16}$$

For the configuration of the test facility with $\theta = 30°$ the equation simplifies to equation 5.17

$$K_{he\theta} = 2.82 + K_{\theta=90^\circ} \tag{5.17}$$

Kröger (2004, 5.6.4) suggested equation 5.18 for calculating $K_{he\Theta}$

$$K_{he\theta} = K_{\theta=90^\circ} + \left(\frac{1}{sin(\theta)} - 1\right)\left[\left(\frac{1}{sin(\theta)} - 1\right) + 2{K_{ci}}^{0.5}\right] \tag{5.18}$$

Where the value of $K_{ci}$ is calculated using equation 5.19

$$K_{ci} = K_c/{\sigma_{21}}^2 \tag{5.19}$$

$K_c$ can be found using equation 5.20

$$K_c = \left(1 - \frac{1}{\sigma_c}\right)^2 \tag{5.20}$$

The contraction ratio $\sigma_c$ is calculated by using the area ratios. Where $A_1$ and $A_2$ is the total frontal area of the heat exchanger bundle and the minimum open area of the heat exchanger respectively. Equations 5.21 and 5.22 are used to calculate $A_1$ and $A_2$ respectively. The parameters for calculating $A_2$ are listed in Table 5.1.

$$A_1 = 2L_tW \tag{5.21}$$

$$A_2 = 2\left(n_{tr}L_t/P_f\right)\left(P_tP_f - \left(d_f - d_r\right)t_f - P_fd_r\right) \tag{5.22}$$

Table 5.1: Heat exchanger parameters

| Parameter | Symbol | Value |
|---|---|---|
| Tubes per row | $n_{tr}$ | 29 |
| Tube length | $L_t$ | 1400 mm |
| Fin pitch | $P_f$ | 2.8 mm |
| Tube pitch | $P_t$ | 63.5 mm |
| Outer fin diameter | $d_f$ | 57.2 mm |
| Fin root diameter | $d_r$ | 25.4 mm |
| Fin thickness | $t_f$ | 0.5 mm |
| Outlet width | $W$ | 1841.5 mm |
| Outlet height | $H$ | 1400 mm |

Equation 5.23 gives the value of $\sigma_{21}$ which is used in Figure 5.4 to calculate $\sigma_c$ to be 0.65.

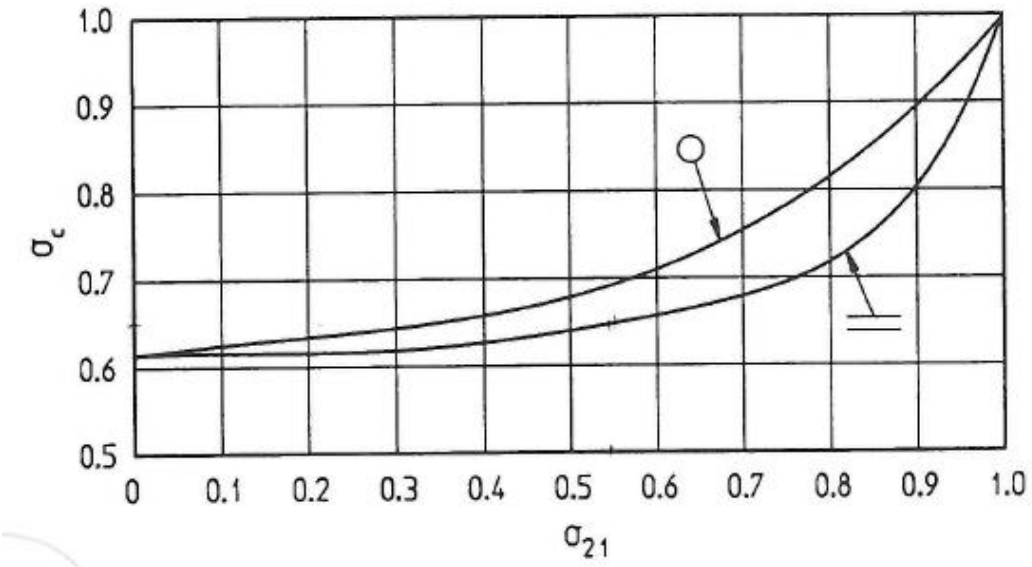


Figure 5.4 Contraction ratio for round tubes and parallel plates
(Kröger: 2004, 2.3.6)

$$\sigma_{21} = \frac{A_2}{A_1} \tag{5.23}$$

From this the value of $K_{he\theta}$ according to Kröger (2004, 5.6.8) can be calculated to be

$$K_{he\theta} = 3.11 + K_{\theta=90^\circ} \tag{5.24}$$

From this it can be seen that the constant value of 3.11 is slightly higher than the experimentally determined value of 2.82 from Meyer and Kröger (2001). The analytically determined value from Kröger (2004, 5.6.4) will be used in all further calculations due to it being more recent data. In section 3.3.3 it was showed that the wind tunnel calibration results for the pressure drop across the heat exchanger bundle, with two rows of finned tubes, correlates well with the analytically calculated values. From the heat exchanger calibration results in section 3.3.3 it was decided to use a single 60% netting between the two finned tube rows to achieve the desired flow resistance. The resulting $K_{he}$ loss factor for normal flow through the heat exchanger is given by equation 5.25 and shown in Figure 5.5.

$$K_{he} = 0.0299V^2 - 1.112V + 43.913 \tag{5.25}$$

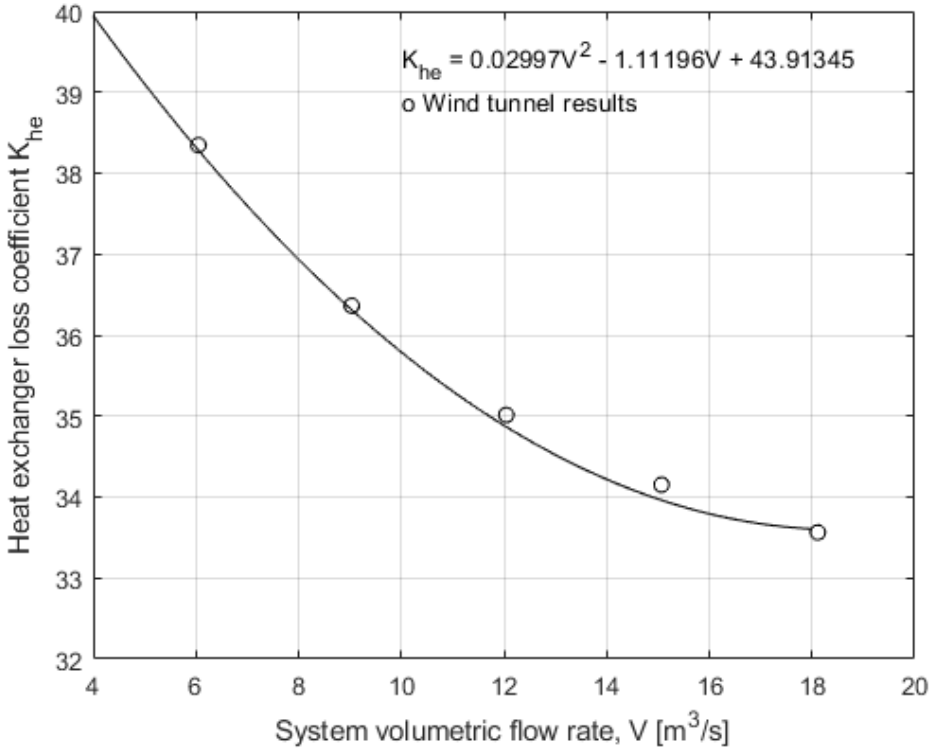


Figure 5.5: Heat exchanger loss coefficient for normal flow $K_{he}$

## 5.5 Fan static pressure rise coefficient

The fan static pressure rise at the selected flow rate can be calculated from the fan curves in Figure 4.1. Calculating the fan static pressure rise coefficient can be done using equation 5.26.

$$K_{Fs} = 2p_{fs}\rho/(V/A_c)^2 \tag{5.26}$$

Where $A_c$ is the fan casing cross sectional area. The value $K_{Fs}$ is a gain coefficient rather than a loss coefficient as in the case of the heat exchanger, supports and fan bridge. Figure 5.6 shows the $K_{Fs}$ curves for the selected blade angle setting settings of the B2-fan. Equations 5.27, 5.28 and 5.29 gives the $K_{Fs}$ values at blade setting angles of 28º, 31º, and 34º respectively.

$$K_{Fs28} = 0.003945V^4 - 0.231V^3 + 5.198V^2 - 54.393V + 228.916 \tag{5.27}$$

$$K_{Fs31} = 0.003105V^4 - 0.193V^3 + 4.592V^2 - 50.645V + 225.256 \tag{5.28}$$

$$\mathrm{K_{Fs34}} = 0.002128\mathrm{V}^4 - 0.142\mathrm{V}^3 + 3.613\mathrm{V}^2 - 42.720\mathrm{V} + 205.054 \tag{5.29}$$

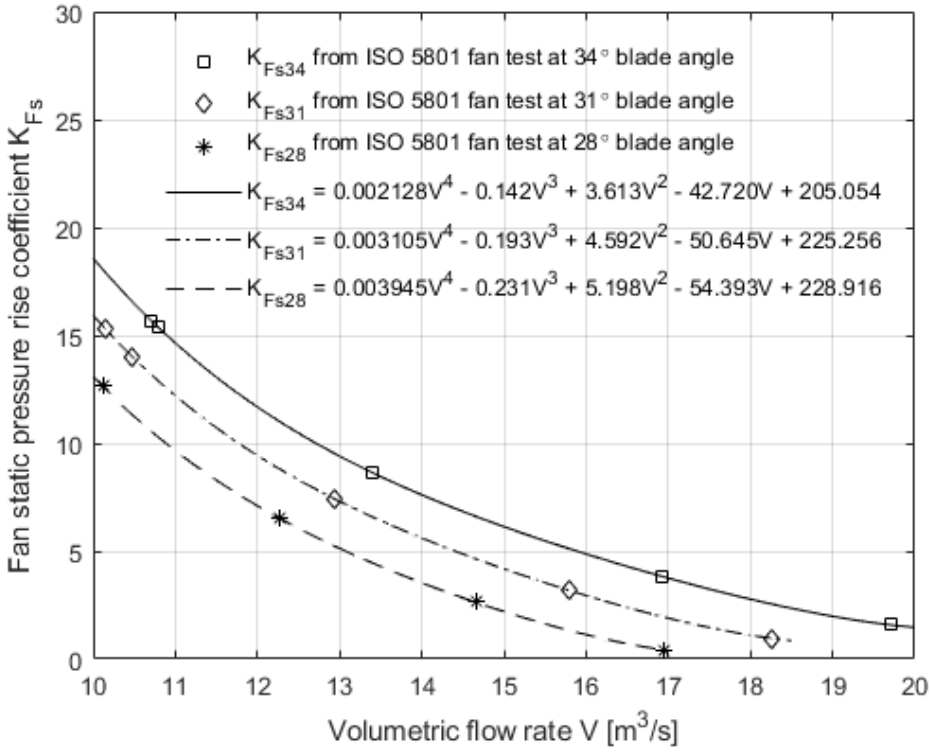


Figure 5.6: Fan static pressure rise coefficient $K_{Fs}$ for B2-fan

From equations 5.27 – 5.29 the fan static pressure rise coefficients were calculated for the different blade angle settings of the B2-fan. Table 5.2 shows the calculated $K_{Fs}$ values.

Table 5.2: B2-fan static pressure rise coefficient

| Parameter | 28º Blade angle setting | 31º Blade angle setting | 34º Blade angle setting |
|---|---|---|---|
| Average volumetric flow rate $V$ [m$^3$/s] | 13.117 | 14.615 | 15.929 |
| $K_{Fs}$ | 4.923 | 4.702 | 4.951 |

From these values it can be seen that the static pressure rise coefficient of the B2-fan at the A-frame facility doesn't change by much between the 28º, 31º and 34º blade settings. This might be due to the system resistance not changing by much with a change in the volumetric flow rate as seen in Figure 5.5. The data for the M-fan provided the fan static pressure rise curves shown in Figure 5.7.

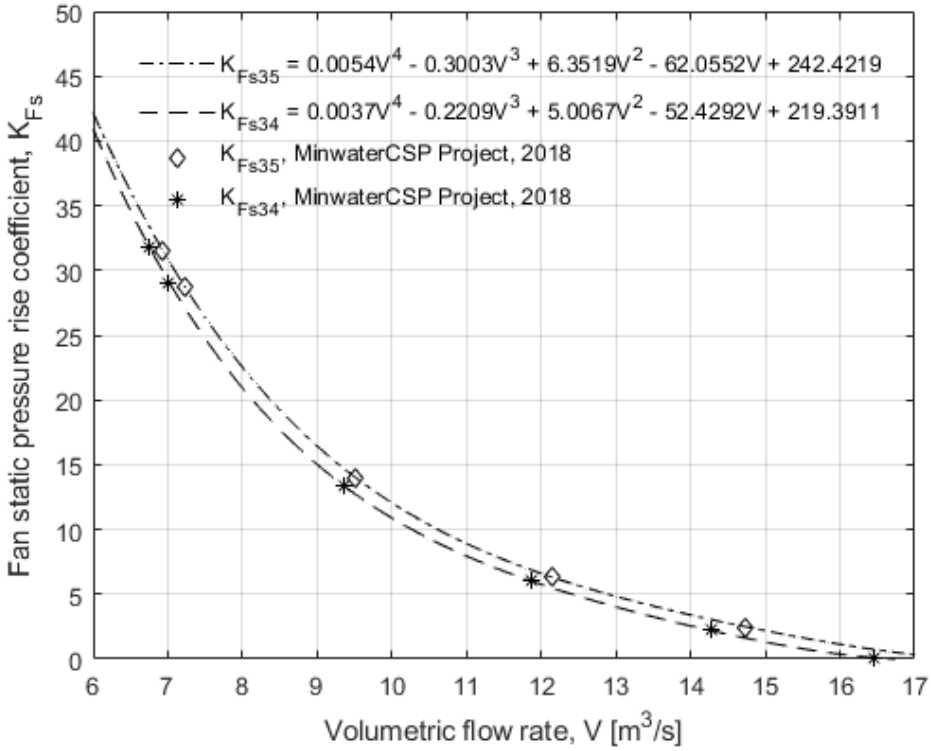


Figure 5.7: Fan static pressure rise coefficient $K_{Fs}$ for M-fan

Equations 5.30 and 5.31 shows the fan static pressure rise coefficient for the M-fan for the 34º and 35º blade angles respectively. Table 5.3 provides the fan static pressure rise coefficients at the 34º and 35º blade angle settings for the M-fan operating in the A-frame ACC.

$$K_{Fs34} = 0.0037V^4 - 0.2209V^3 + 5.0067V^2 - 52.4292V + 219.391 \quad (5.30)$$

$$K_{Fs35} = 0.0054V^4 - 0.3003V^3 + 6.3519V^2 - 62.0552V + 242.422 \quad (5.31)$$

Table 5.3: M-fan static pressure rise coefficient

| Parameter | 34º Blade angle setting | 35º Blade angle setting |
|---|---|---|
| Average volumetric flow rate $V$ [m$^3$/s] | 12.234 | 12.824 |
| $K_{Fs}$ | 5.317 | 5.116 |

From these results it is seen that the 34º blade angle had a slightly higher static pressure rise coefficient than that of the 35º blade angle. This might be as a result of the fitted curve for the M-fan at 34º over predicting the value.

## 5.6 Analytical system sensitivity to changes

The draft equation of the commissioned ACC facility is used to predict how sensitive the system would be to certain changes made to the facility. It is also used to determine the influence of measurement inaccuracies on the accuracy of the final system results.

Tests conducted by Meyer and Kröger (1998) included bundle loss factors ranging from 7 to 24. The area ratio between the fan casing and the frontal area of the heat exchanger varied within the range $0.34 \leq A_c/A_{fr} \leq 0.599$. The recovery coefficients for the performed tests were in the range $0.2 \leq K_{rec} \leq 0.6$. Kröger (2004, 6.4.6) recommends a conservative value of 0.3 for most designs.

The parameters analysed for sensitivity included the frontal area of the heat exchanger, heat exchanger loss coefficient, and volumetric flow rate. By changing a parameter incrementally and analysing the percentage change in the value of the $K_{rec}$ coefficient, a prediction on the sensitivity of the value of recovery to a small change in the parameter chosen was provided. Equation 5.2 was rewritten to equation 5.32 for calculating the value of recovery.

$$K_{rec} = \left[K_{ts}\left(\frac{m_a}{A_2}\right)^2 - K_{Fs}\left(\frac{m_a}{A_c}\right)^2 + K_b\left(\frac{m_a}{A_e}\right)^2 + K_{he\theta}\left(\frac{m_a}{A_{fr}}\right)^2\right] \Big/ \left[\left(\frac{m_a}{A_c}\right)^2\right] \quad (5.32)$$

This equation is simplified to:

$$K_{rec} = K_{ts}\left(\frac{A_c}{A_2}\right)^2 - K_{Fs} + K_b\left(\frac{A_c}{A_e}\right)^2 + K_{he\theta}\left(\frac{A_c}{A_{fr}}\right)^2 \quad (5.33)$$

Taking the partial derivative of $K_{rec}$ with respect to the volumetric flow rate gives the sensitivity of recovery to change in volumetric flow rate. It is known that the fan static pressure rise coefficient $K_{Fs}$ and the heat exchanger loss coefficient $K_{he\theta}$ are both functions of the volumetric flow rate. Inserting these coefficients into equation 5.33 and taking the partial derivative with respect to volumetric flow rate gives equations 5.34 to 5.36 for the three different blade angle settings of the B2-fan. Similarly equations 5.37 and 5.38 can be calculated for the M-fan at its different blade angles.

$$\frac{\partial K_{rec28}}{\partial V} = -0.0158V^3 + 0.693V^2 - 10.39V + 54.247 \quad (5.34)$$

$$\frac{\partial K_{rec31}}{\partial V} = -0.0124V^3 + 0.579V^2 - 9.18V + 50.637 \quad (5.35)$$

$$\frac{\partial K_{rec34}}{\partial V} = -0.0085V^3 + 0.426V^2 - 7.22V + 42.712 \quad (5.36)$$

$$\frac{\partial K_{rec34}}{\partial V} = -0.0148V^3 + 0.663V^2 - 10.01V + 52.283 \quad (5.37)$$

$$\frac{\partial K_{rec35}}{\partial V} = -0.0216V^3 + 0.901V^2 - 12.69V + 61.909 \quad (5.38)$$

Taking the partial derivative of recovery with respect to the heat exchanger loss coefficient gives equation 5.39 for the different blade angle settings at the A-frame test facility.

$$\frac{\partial K_{rec}}{\partial K_{he\theta}} = 0.00777V + 0.144 \quad (5.39)$$

Taking the partial derivative of recovery with respect to the heat exchanger frontal area gives equation 5.40 for the different blade angle settings at the A-frame test facility.

$$\frac{\partial K_{rec}}{\partial A_{fr}} = -0.00151V^2 + 0.0559V - 2.432 \quad (5.40)$$

Equations 5.34 – 5.40 gives the sensitivity of the recovery value to change in certain chosen parameters. It was realised that these equations are only applicable to this particular A-frame setup. The value used for the volumetric flow rate in each case can only be that of the total flow rate at each blade angle setting. Changing of the volumetric flow rate can for example only be done by varying a selected parameter like the blade angle, heat exchanger loss coefficient, or the heat exchanger frontal area. The implication thereof is that, changing the blade angle changes the fan static pressure rise curve, leading to a new equation for the partial derivative of the

recovery value with respect to volumetric flow rate. The same can be said for changing the heat exchanger loss coefficient or the heat exchanger frontal area.

The volumetric flow rate obtained from the outlet velocity measurements on the ACC facility was used to calculate the value of the partial derivatives at the different blade angles. Table 5.4 lists the calculated values for recovery at the measured flow rates and also the analytically calculated partial derivatives.

Table 5.4: $K_{rec}$ change as a result selected parameters

| Fan | Blade angle [º] | Volumetric flow rate $V$ [m$^3$/s] | $K_{rec}$ | Partial derivatives with respect to selected parameters | | |
|---|---|---|---|---|---|---|
| | | | | $\frac{\partial K_{rec}}{\partial V}$ | $\frac{\partial K_{rec}}{\partial K_{he\theta}}$ | $\frac{\partial K_{rec}}{\partial A_{fr}}$ |
| B2-fan | 28 | 13.117 | 0.505 | 1.538 | 0.246 | -1.959 |
| | 31 | 14.615 | 0.685 | 1.435 | 0.258 | -1.938 |
| | 34 | 15.929 | 0.412 | 1.44 | 0.268 | -1.925 |
| M-fan | 34 | 12.234 | 0.143 | 1.952 | 0.239 | -1.522 |
| | 35 | 12.824 | 0.322 | 1.793 | 0.244 | -1.963 |

From these results it is seen that a small deviation in the volumetric flow rate has a substantial influence in the calculated recovery value. This emphasizes the importance of accurately measuring the volumetric flow rate through the system in order to be able to calculate the recovery value to a good degree of accuracy.

It can be seen that an increase in the volumetric flow rate would have a greater effect on the value of recovery than an increase in the heat exchanger loss coefficient. Increasing either the flow rate or the heat exchanger loss coefficient increases the expected recovery value. However, an increase in the total frontal area of the heat exchanger leads to a decrease in recovery.

## 5.7 Effect of measurement variability on $K_{rec}$

Analysis of performance results with the use of instrumentation introduces a certain degree of uncertainty to the measured results. Presenting the results with a correct tolerance is important for future tests and for improvement of the methods used. When analysing a large amount of data values captured, the mean and the standard deviation can be used to describe the normal distribution of possible outcomes of the measurement.

### 5.7.1 Monte Carlo simulation

A useful tool for modelling measurements with variability is the Monte Carlo simulation (O'Connor and Kleyner, 2012). Lombard (2017) made use of the Monte Carlo simulation to investigate the effect of strain gauge misalignment on the stress experienced by the strain gauge when measuring stresses in large gearbox shafts.

Lombard (2017) also investigated the effect of variability in shaft material properties on the outcome of the measured strain by the strain gauges. The Monte Carlo mathematical procedure uses a random set of input parameters to produce and record different possibilities of output parameters. The random set of input parameters are produced using probability distributions which simulates sampling from an actual population of data points. The probability density function from Mahadehaven (1997) of the Gaussian or normal distribution is given by

$$f(x) = \frac{1}{\sigma_x\sqrt{2\pi}} exp\left[-\frac{1}{2}\left(\frac{x-u_x}{\sigma_x}\right)^2\right] \tag{5.41}$$

Where $\sigma_x$ and $\mu_x$ represents the standard deviation and the mean of the data respectively. The value for $x$ is the position along the $x$-axis of the standard deviation curve. It can be seen from equation 5.41 that when the value of $x$ is set to the mean of the data, the maximum point of the normal distribution curve will be

$$f(x) = \frac{1}{\sigma_x\sqrt{2\pi}} \tag{5.42}$$

Knowing that the area under the normally distributed curve is equal to unity, the percentage area falling between two selected points on the curve indicates the percentage of data values that can be expected to fall within the selected region. A tall and thin distribution would have a small standard deviation and a wider and not so tall distribution will have a bigger standard deviation. Having a small standard deviation of data points will thus yield more accurate end results.

Dunn and Shultis (2011) uses the probability density function in equation 5.41 to estimate a new random variable with the use of equation 5.43. If the function z($x$) was a random value, the mean could be expected to equal

$$(z) = \int_a^b z(x)f(x)dx \tag{5.43}$$

The standard deviation of this random value can be described by equation 5.44

$$\sigma^2(z) = [z(x) - (z)\,]^2 = \int_a^b [z(x) - (z)]f(x)dx \tag{5.44}$$

An estimation is made with the use of equation 4.45

$$\bar{z} = \frac{1}{N}\sum_{i=1}^{N} z(x_i) \tag{5.45}$$

Where N represents the number of estimates and $x_i$ sampled from f($x$). According to Dunn and Shultis (2011) the law of large numbers states that

$$\lim_{N\to\infty} \bar{z} = (z) \tag{5.46}$$

Taking the above into account each measurement can be approached with the use of the Monte Carlo simulation in order to generate a normal distribution curve for

each measurement. This will allow uncertainty in measurements to be used as a guide to establish with what certainty there can be spoken about a measured or calculated result. With each random input value an output can be generated for each case. Increasing the number of different random input cases produces a large number of random output cases. These different outputs are then displayed as a normal distribution curve which may be used as an indicator to which degree of certainty a result may be used in further research.

### 5.7.2 Anemometer velocity measurements

Each anemometer calibrated for testing purposes had its own standard deviation for the calibration output $\sigma_{cal}$. For each anemometer the standard deviation was documented. This standard deviation of the instrument measurement is then combined with the measured outlet velocity standard deviation $\sigma_{meas}$ by using equation 5.47 from Budynas and Nisbett (2008):

$$\sigma_x = (\sigma_{meas}{}^2 + \sigma_{cal}{}^2)^{\frac{1}{2}} \tag{5.47}$$

Making use of the mean and calculated standard deviation, a random sample of outlet velocities can be calculated for each anemometer at each measurement location on the traverse. From these outlet velocities a total system volumetric flow rate was calculated and the whole process repeated to generate $10^6$ different outlet velocity possibilities. The different possibilities for volumetric flow rate and its frequency of occurrence was then used to generate a mean and standard deviation for the volumetric flow rate. Figure 5.8 shows the normal distribution curves for the different volumetric flow rates of the B2-fan.

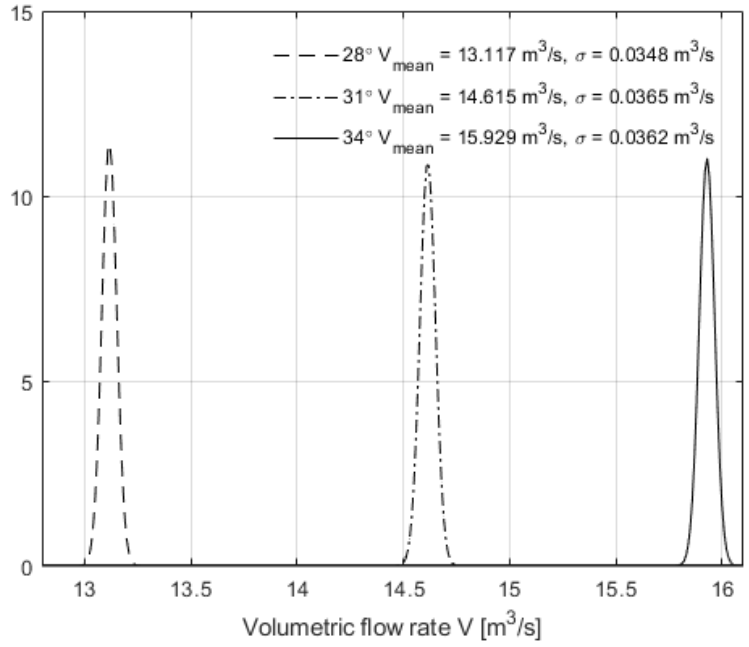


Figure 5.8: Volumetric flow rate normal distribution curve for B2-fan

It can be seen that the different blade angle settings gives very similar standard deviations in volumetric flow rate with the lowest standard deviation for the 28º blade angle setting.

The supports and bridge loss coefficient normal distributions are both also calculated using the normal distribution curves of the volumetric flow rate. Table C.1 and Table C.2 in Appendix C shows the mean and standard deviation for the support and bridge loss coefficients at the different volumetric flow rates respectively.

### 5.7.3 Heat exchanger loss coefficient

From the calibration of the heat exchanger an average value and also a standard deviation can be determined for the $K_{he}$ value. Table 5.5 shows the average and also the standard deviation of the heat exchanger loss coefficient at the different volumetric flow rates calibrated during calibration testing.

Table 5.5: Average and standard deviation of $K_{he}$ during calibration

| Volumetric flow rate $V$ [$m^3/s$] | Mean $K_{he}$ value | Standard deviation in $K_{he}$ value σ |
|---|---|---|
| 6.049 | 38.347 | 0.3979 |
| 9.033 | 36.364 | 0.2413 |
| 12.043 | 35.014 | 0.1616 |
| 15.066 | 34.152 | 0.0826 |
| 18.108 | 33.562 | 0.0802 |

It should be however noted that the standard deviation in the volumetric flow rate results directly affects the heat exchanger loss coefficient. Each value calculated for the heat exchanger loss coefficient with the normal distribution values of the volumetric flow rate is recalculated with the standard deviation of the heat exchanger calibration results. This way both of the volumetric flow rate and the heat exchanger loss coefficient standard deviations are accounted for in the resulting heat exchanger normal distribution curve. The mean and standard deviation of the heat exchanger results are listed in Table C.3 Appendix C.

### 5.7.4 Fan static pressure rise coefficient

Performing tests on the fan at the different blade angle settings provided the data for calculating the fan static pressure rise coefficient. Repeating each test three times however only provided three different average values at each operating point. These were too little of an amount of data points to accurately calculate a standard deviation for the data in the region the fan would operate in. It was decided to make use of a 95% confidence interval around the measured data points to get a good estimate of the possible value of the fan static pressure rise coefficient. The 95% confidence interval is an interval which contains 95% of the population distribution. There is a 95% certainty that the interval contains the population mean. Subtracting the predicted mean curve from the upper limit of the confidence interval gave the

value to be used, in calculating the possible variability in the fan static pressure rise values, rather than the standard deviation of the data. Figure 5.9 shows the confidence intervals for the fan static pressure rise coefficient at the different blade angle settings.

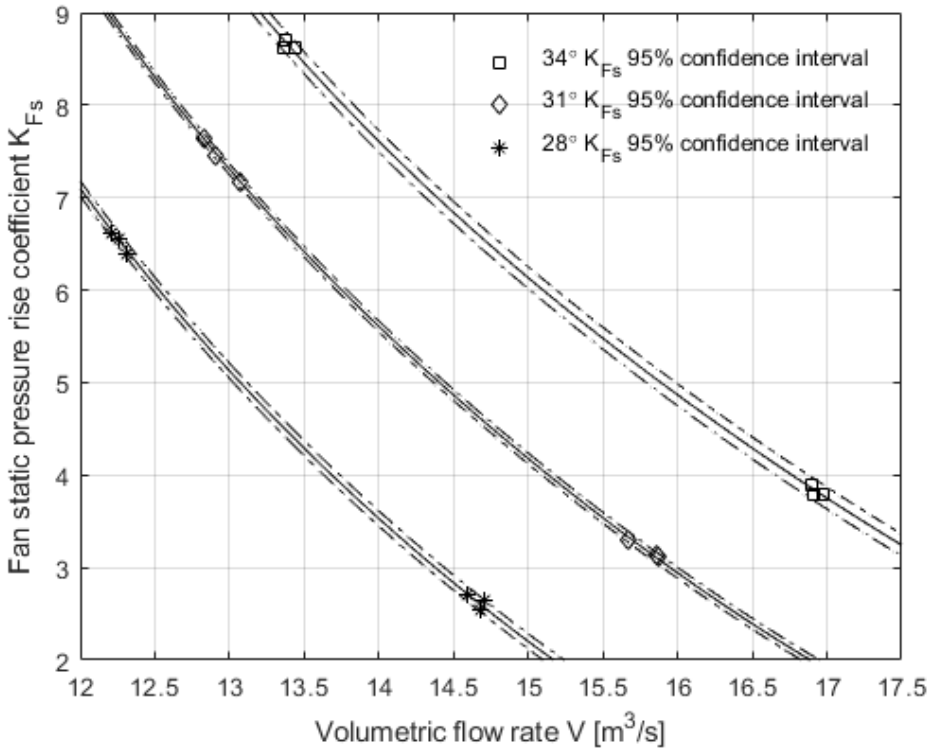


Figure 5.9: Fan static pressure rise coefficient 95% confidence intervals for the B2-fan

It can be seen that the 31º blade angle has the best fitted 95% confidence interval during the fan tests as the interval lines are the closest together with an interval of 0.0588. The 31º and 34º blade angle settings have values of 0.0818 and 0.1184 respectively.

### 5.7.5 System specific sensitivity

In order to test the sensitivity of the system to variability certain parameters were isolated and allowed to be the only one with variability. The selected system parameters included the volumetric flow rate, heat exchanger loss coefficient and fan static pressure rise coefficient. Setting all of the system variabilities to zero and keeping the volumetric flow rate variability resulted in the normal distribution curves for recovery shown in Figure 5.10.

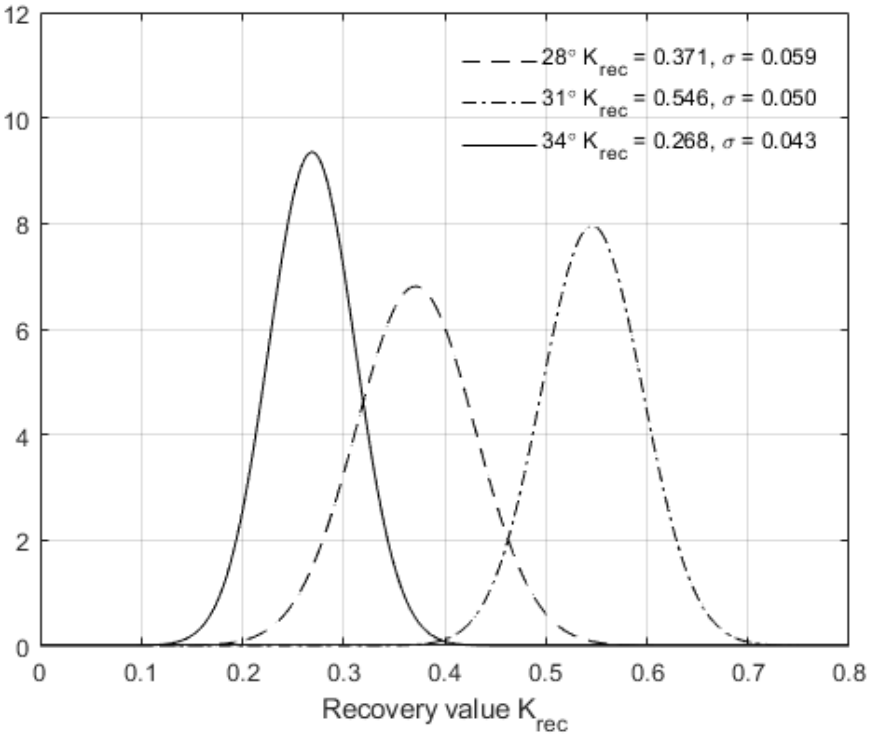


Figure 5.10: Normal distribution of $K_{rec}$ from variability in volumetric flow rate for the B2-fan

From these distributions it becomes clear that the accuracy of volumetric flow rate plays a considerable role in the confidence interval in which the value of recovery may fall. It can here be seen that at the higher blade angle of 34º, and thus higher volumetric flow rate, the standard deviation of the data is considerably lower than at the 28º and 31º blade angle settings. This gives an indication that using the same measurement equipment at higher volumetric flow rates will yield more accurate results at the same test facility under the same environmental operating conditions.

Investigating the effect of the heat exchanger loss coefficient variability on the final calculated recovery value was done by setting the standard deviations of all of the other system losses equal to zero while keeping the standard deviation of the heat exchanger loss coefficient as determined through calibration testing. Figure 5.11 shows the normal distributions of the recovery value due to the heat exchanger loss coefficient variability.

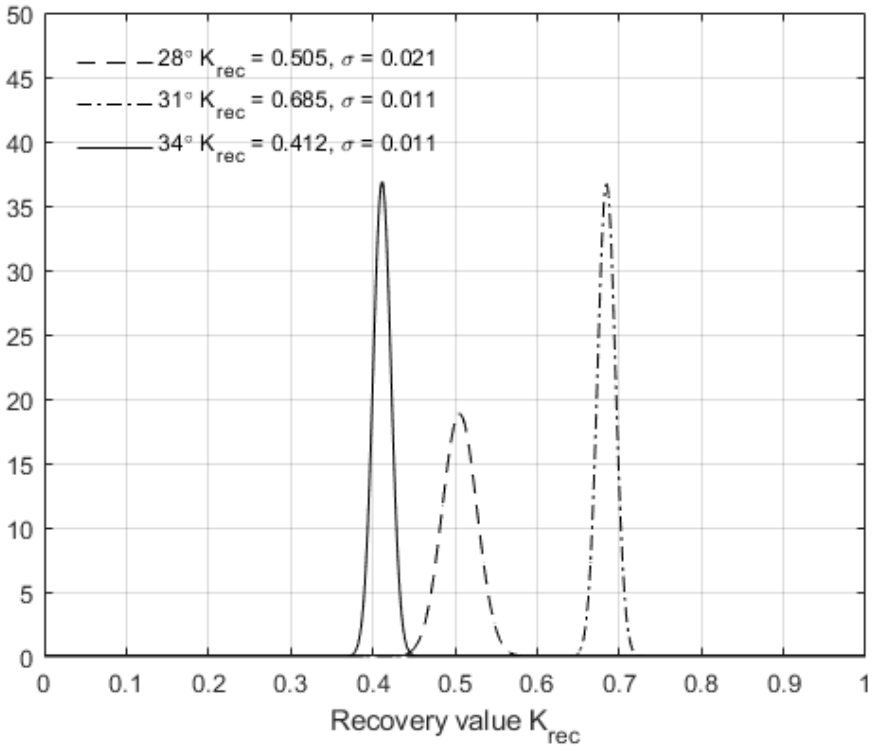


Figure 5.11: Normal distribution of $K_{rec}$ from variability in $K_{he}$ for B2-fan

From these results it is clear that the effect of the heat exchanger standard deviation on the standard deviation of the recovery value is considerably less than that of the volumetric flow rate. This makes sense as the volumetric flow rate affects every single loss or gain factor seen in equation 6.33 where the heat exchanger loss coefficient $K_{he}$ is only one of the loss coefficients in the equation.

Finally by removing all variability from the system losses and only keeping that of the fan static pressure rise coefficient, the influence of the latter on the normal distribution curve of recovery can be investigated. Figure 5.12 shows the normal distribution curves due to variability in the fan static pressure rise coefficient.

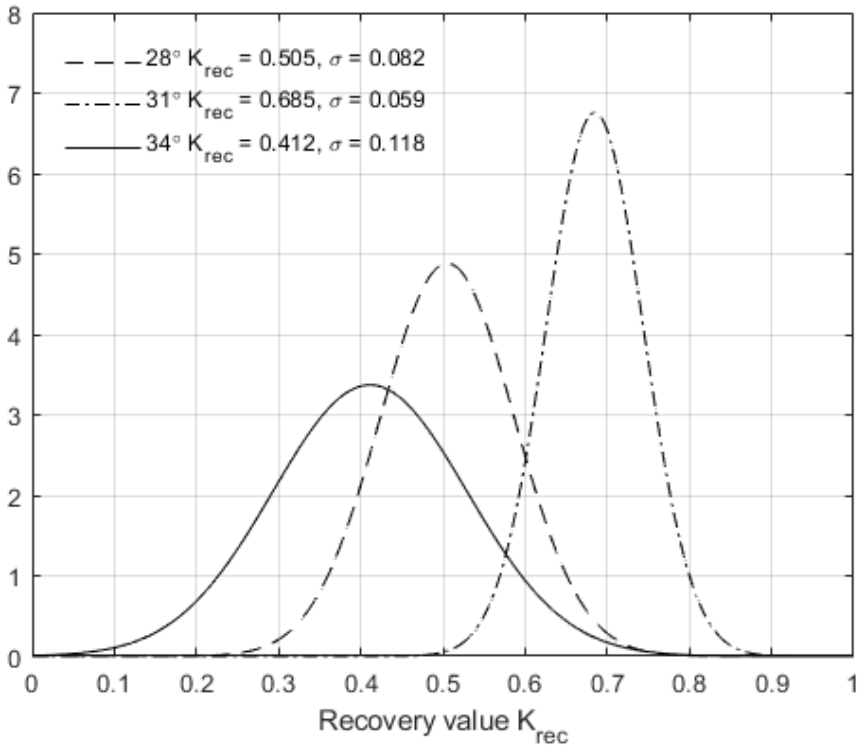


Figure 5.12: Normal distribution of $K_{rec}$ from variability in $K_{Fs}$ for the B2-fan

From these results it can be seen that the variability in the fan static pressure rise coefficient can have an even more significant effect on the recovery normal distribution curve than the variability in volumetric flow rate. This makes sense due to $K_{Fs}$ being the only term in equation 6.33 which is not multiplied by the square of a small area ratio. From this is concluded the importance of knowing the fan static pressure rise coefficient of the fan being tested to a great accuracy within the region of testing. This can be achieved by taking multiple averaged measurements above and below the volumetric operating point. With the use of these points a standard deviation in the data can be calculated and used to a higher degree of accuracy than by using the 95% confidence interval as a greater sample size will provide a more accurate representation of the population of data points.

The accuracy of measuring the volumetric flow rate out at the outlet surface of the heat exchanger is also of great importance as it influences every term in the draft equation as all of the loss- and gain coefficients are dependent on the volumetric flow rate through the system.

### 5.7.6 Recovery normal distribution curve

The results obtained from 5.1 – 5.5 were used to calculate $10^6$ different values for the recovery coefficient $K_{rec}$. With the use of the mean and standard deviation of the recovery values, the resulting normal distribution curves were produced.

Figure 5.13 and Figure 5.14 shows the normal distributions for the different blade angle settings of the B2-fan and the M-fan respectively.

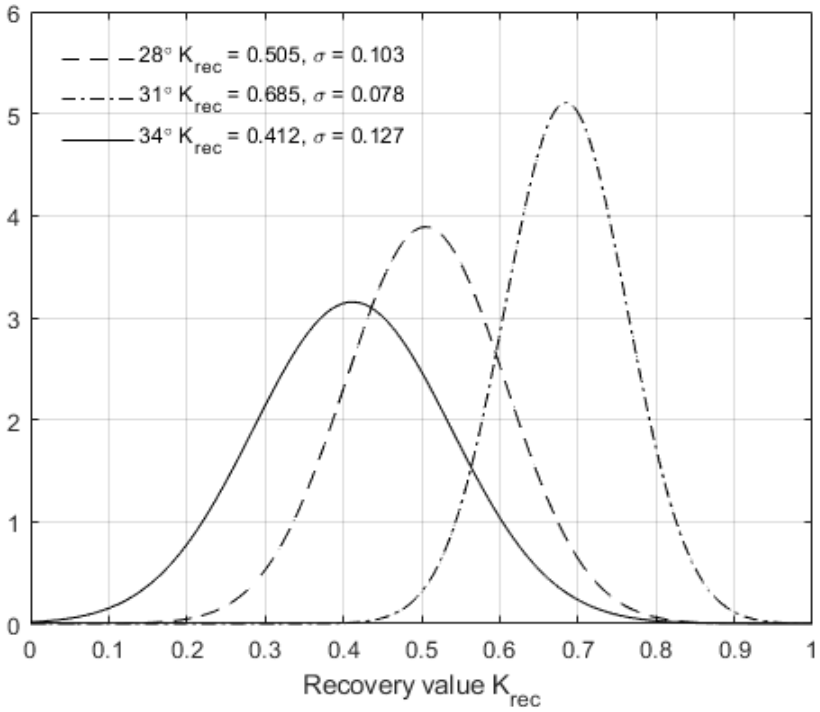


Figure 5.13: Recovery normal distribution curve for B2-fan

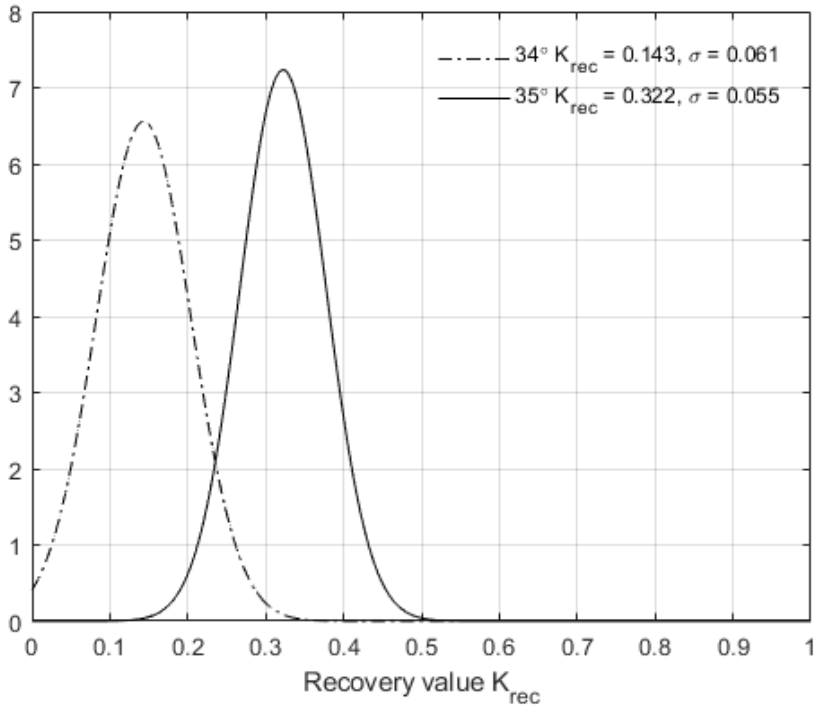


Figure 5.14: Recovery normal distribution curve for M-fan

From this it was seen that the 31º blade angle setting, taking into account all of the standard deviations from the volumetric flow rate measurements, heat exchanger calibration and fan static pressure rise tests, had the lowest standard deviation between the different blade angle settings for the B2-fan. It should however be noted that these normal distributions are dependent on the fan performance tests and the accuracy of the repeated tests with each other. This is thus a factor that individually affects the end result of recovery for each blade angle setting and which is not included for the M-fan recovery normal distribution curves. The reason being that the available test data for the M-fan was averaged values and did not have a standard deviation or confidence interval value which could be used for the overall recovery distribution. Thus it resulted in a more concentrated normal distribution than that of the B2-fan. It is also noted that all of the averaged recovery values fell between 0.14 and 0.69.

From Figure 5.13 and Figure 5.14 it can be seen that the M-fan had lower recovery of 0.143 and 0.322 for the 34º and 35º degree blade angles respectively, than that of the B2-fan installed in the same A-frame ACC having recovery coefficients of 0.505, 0.685 and 0.412 for the 28º, 31º and 34º blade angles respectively. These results seem to be contradicting the power consumption shown in Figure 4.10 and Figure 4.11 for the B2-fan and the M-fans showing a greater reduction in power consumption for the M-fan than that of the B2-fan. It is recommended that this be further investigated to determine the relationship between $K_{rec}$ and the power consumed by the fan installed in an A-frame ACC.

# 6 Conclusions and recommendations

The aim of the study was to test the performance of an axial flow fan in an A-frame test facility. In order to perform the required testing, the available A-frame test facility was modified and commissioned before testing. Modifications to the facility mainly consisted of the redesign and manufacture of a new fan drive system, fan bridge, heat exchanger bundles and improving of the overall structural rigidity. Commissioning of the facility included measurements such as the horizontal approach- and the vertical inflow velocity. These measurements showed a fairly evenly distributed approach velocity and vertical inflow. Structurally the facility was found to be much more rigid and had less noise and vibration during tests.

Performance tests conducted on the selected B2-fan according to ISO 5801 (2007) in a Type-A fan test facility provided fan performance curves to which results obtained from the A-frame facility tests were compared. Furthermore with the use of the standardised fan test results the fan static pressure rise coefficient was calculated for the B2-fan and M-fan at the A-frame measured volumetric flow rate. This was necessary for calculating the recovery value with the use of the system draft equation. Velocity measurements on the A-frame test facility heat exchanger outlet were used to calculate the volumetric flow rate through the facility. It was only possible to directly compare the power consumption of the fan in the different facilities as both the power and volumetric flow rate was known. It was found that the fans consumed less power installed in the A-frame test facility than when installed in the standardised Type-A fan test facility.

Outlet velocity profiles of the A-frame test facility showed the velocity distribution across the heat exchanger outlet. The minimum exit velocities occurred at the centre of the heat exchanger where the maximum velocities were observed near the bottom of the heat exchanger outlet on both the Western and Eastern sides. This can be as a result of the velocity distribution on the inside of the A-frame test facility leading to a higher dynamic pressure component in the lower part of the heat exchanger. This higher dynamic component might be a result of the tangential component of the air as it leaves the fan and is thrown into the bottom part of the heat exchanger. These results are comparable to results obtained by Engelbrecht (2018) who performed a numerical investigation the B2a-fan performance in a forced draft A-frame ACC. With the B2a-fan being a redesigned version of the B2-fan, the results obtained can be expected to be similar to a certain degree. The numerically calculated results for the A-fan in the same A-frame setup showed a more evenly distributed axial velocity than that of the B2a-fan. This indicates that testing of various fans at the commissioned A-frame ACC test facility will provide actual data showing the effect of different fan types on the outlet velocity profile. The effect of these outlet velocity profiles on the heat transfer from such a facility should be further investigated to determine the effect thereof on the total ACC system performance.

Pressure measurements were made according to ISO 5802 (2007) in the walls of the plenum chamber to determine if these measurements could give an indication on the pressure rise over the fan. These measurements however showed pressures far below the expected pressure rise at the measured volumetric flow rate. It is recommended that pressure measurements inside the plenum chamber be further investigated for future data capturing.

The system draft equation is used to calculate the recovery value for the different blade angles of the B2-fan tested. These were found to be 0.505, 0.685 and 0.412 for the 28º, 31º and 34º blade angles respectively. This is higher than the recommended design value of 0.3 by Meyer and Kröger (1998) at heat exchanger loss coefficients between 15 and 25. It should however be noted that the heat exchanger loss coefficient ranged between 36 and 38 depending on the volumetric flow rate. The recovery calculated for the M-fan in the A-frame ACC test facility was 0.143 and 0.322 for the 34º and 35º blade angles respectively. These values for the M-fan fell closer to the recommended $K_{rec}$ value of 0.3. It is however noted that this high difference in recovery with a small change in blade angle for the M-fan is exactly the difference in the $K_{Fs}$ value between the two blade angles. The importance of accurately measuring and calculating the value for $K_{Fs}$ is critical for calculating the value for $K_{rec}$.

Calculating the fan static pressure rise coefficient for the different blade angle settings at the measured volumetric flow rate of the A-frame test facility showed that the fan static pressure rise coefficient for the B2-fan lies within the range of 4.923, 4.702 and 4.951 for the 28º, 31º and 34º blade angles respectively. The fan static pressure rise coefficient for the M-fan was 5.32 and 5.11 for the 34º and 35º blade angles respectively. It is recommended that a variety of blade angles be tested in which the fan static pressure rise coefficients can be compared to determine if there is a similarity when operating at different blade angle settings with the same fan.

The system sensitivity to change and accuracy of measurements was also investigated. It was found that the accuracy of the volumetric flow rate measurements in calculating the recovery is of great importance and had a substantial influence on the standard deviation of the calculated recovery value. The volumetric flow rate normal distribution curve was used to calculate a normal distribution for the calculated recovery. This showed that the accuracy of the instruments and also the standard deviation of data points during measurements greatly affects the range in which the recovery value may fall. The standard deviation of the recovery value due to volumetric flow rate data was greater at lower volumetric flow rates. This can be the result of small flow disturbances inside the lab due to air flow entering and exiting through the hallways having a higher percentage influence at lower flow rates than at higher flow rates.

It is therefore important that instruments used for measuring the volumetric flow rate through an A-frame ACC facility are calibrated thoroughly and tests performed in steady state conditions to prevent a wide normal distribution for the recovery

coefficient. In some tests a variety of environmental conditions may be experienced during the recording period. It is recommended that data be analysed keeping the prevailing atmospheric conditions in mind.

For future research it is recommended that a variety of different fans be tested at the commissioned facility and the results compared to that of the standardised fan testing facility. This will provide an indication of the effect that different fans with the same heat exchanger A-frame configuration have on the value of recovery. For the fan tests performed at the standardised fan testing facility it is recommended that all the possible operating points be selected for the A-frame testing region to generate higher resolution fan characteristic curves. This will enable more accurate values to be calculated for the fan static pressure rise coefficient in equation 5.26.

A variety of heat exchanger configurations can be mounted and tested on the outlet of the A-frame ACC facility. These tests can be conducted with various fan and heat exchanger area ratios to investigate the effect thereof on recovery. This would provide results usable for the design of A-frame ACC configurations.

In order to change the operating point of the A-frame facility a set of louvres can be designed and manufactured to be installed on the inside of the A-frame next to the heat exchanger bundles. Different density shade cloth can also be used to achieve different pressure losses across the bundle. This would allow tests to be performed at different volumetric flow rates and pressures.

For ease of use and higher resolution in the outlet velocity profile measurements a traverse powered by stepper motors with anemometers on both of the heat exchanger outlets can be used which will shorten the time required for performing tests. This will allow the user to be at a workbench and control the position of the anemometer traverse through an interface. It will not only protect the anemometers from handling damage but also decrease flow disturbances in the lab due to a decrease in the required movement around the facility.

Symmetry planes can be added to resemble an array of A-frame heat exchangers. Care should however be taken to not extend the symmetry planes too high above the A-frame ACC due to vertical spatial constraints that could also negatively affect the system performance by adding additional unwanted flow losses.

Further tests should be conducted regarding the use of pressure taps and pressure measurements inside the A-frame plenum chamber as the pressure measurements done were regarded as unusable due to it being noticeably lower than the expected pressure rise across the fan at the specific volumetric flow rate. Pressure measurements along the vertical and along the sides leading up to the heat exchangers should be further investigated.

# References

Augustyn, O.P.H. (2013). *Experimental and numerical analysis of axial flow fans*. Master's thesis, University of Stellenbosch, South Africa.

Böck, R.D, and Van der Spuy, S. (2017). *The performance of an axial flow fan in a small scale A-frame test facility*. Master's thesis, University of Stellenbosch. South Africa.

British Standard 848 (1997). Fans for general purposes: Part1. performance tesing using standardised airways.

Bruneau, P.R.P. (1994). *The design of a single rotor axial flow fan for cooling tower application.* Master's thesis, University of Stellenbosch. South Africa.

Budynas, R.G. and Nisbett, J.K. (2008). *Shigley'sMechanical Engineering Design*. 8th edn. McGraw-Hill, New York.

Dunn and Shultis (2011). *Exploring Monte Carlo Methods*. 1st edn. Elsevier. pp. 21-46.

Duvenhage, K. et al. (1996). Flow distortions at the fan inlet of forced draft air-cooled heat exchangers, *Applied Thermal Engineering*, 16(95), pp. 741-752.

Duvenhage, K. and Kröger, D. (1996). The influence of wind on the performance of forced draught air-cooled heat exchangers. *Journal of Wind Engineering and Industrial Aerodynamics,* vol. 62, pp. 259-277.

Engelbrecht, R. A. (2018). *Numerical Investigation of Fan Performance in a Forced Draft Air-Cooled Condenser*. Ph.D. thesis, University of Stellenbosch. South Africa.

Fourie, N., van der Spuy, S. and von Backström, T. (2015). Simulating the effect of wind on the performance of axial flow fans in air-cooled steam condenser systems. *Journal of Thermal Science and Engineering Applications*, vol. 7, pp. 1-12.

ISO 5801 (2007). Industrial fans – performance testing using standardised airways.

ISO 5802 (2008). Industrial fans – performance testing in situ.

Kröger, D.G. (2004). *Air-cooled Heat Exchangers and Cooling Towers*. Penwell Corp., Tulsa.

Le Roux, N., 2010. *The CFD simulation of an axial flow fan*. University of Stellenbosch. Master's thesis. Stellenbosch University. South Africa.

Lombard, C.H.O. (2017). *Analysis of gearbox loads in large air cooled condensers.* Department of Mechanical and Mechatronic Engineering, University of Stellenbosch, South Africa.

Louw, F.G. (2015). *Investigation of the flow field in the vicinity of an axial flow fan during low flow rates*. Department of Mechanical and Mechatronic Engineering, University of Stellenbosch, South Africa.

Mahadevan, S. (1997). *Reliability-Based Mechanical Design*. Marcel Dekker, Inc.

Maulbetsch, J., DiFilippo M.N., and O'Hagan J. (2011). Effect of wind on air-cooled condenser performance. *Proceedings of the ASME 2011: International Mechanical Engineering Congress & Exposition.*

Meyer, C. (1996). *Plenum Losses in Forced Draught Air-Cooled Heat Exchangers*. Master's thesis, University of Stellenbosch.

Meyer, C. J. and Kröger, D. G. (1998) Plenum chamber flow losses in forced draught air-cooled heat exchangers, *Applied Thermal Engineering*, 18, pp. 875-893.

Meyer, C. J. and Kröger, D. G. (2001) Air-cooled heat exchanger inlet flow losses, *Applied Thermal Engineering*, 21, pp. 771-786.

Meyer, C. J. and Kröger, D. G. (2004) Numerical investigation of the effect of fan performance on forced draught air-cooled heat exchanger plenum chamber aerodynamic behaviour, *Applied Thermal Engineering*, 24(2–3), pp. 359-371.

MinwaterCSP Project, (2018). Scaled CSP Cooling Fan Performance Testing, Confidential Project Report,https://www.minwatercsp.eu/.

Monroe, R. C. (1979) Improving Cooling Tower Fan System Efficiencies Seventh *Turbomachinery Symposium Shamrock Hilton Hotel*, 50(11).

Muiyser, J. (2012). *Simultaneous measurement of air flow conditions and the resultant blade and gearbox loading at large-scale cooling system fans*. Master's thesis, Department of Mechanical and Mechatronic Engineering, University of Stellenbosch, South Africa.

Muiyser, J. *et al.* (2014) Measurement of air flow and blade loading at a large-scale cooling system fan, *Journal of the South African Institution of Mechanical Engineering*, 30, pp. 30-38.

O'Connor, P. D. T. and Kleyner, A. (2012). *Practical reliability Engineering.* 5th ed. West Sussex: John Wiley & Sons, LTd.

Owen, M. (2010). *A numerical investigation of air-cooled steam condenser performance under windy conditions*. Master's thesis, University of Stellenbosch. South Africa.

Salta, C.A. and Kröger, D.G. (1995). Effect of inlet flow distortions on fan performance in forced draft air-cooled heat exchangers. *Heat recovery systems and CHP*, vol. 15, pp. 555-561.

Stinnes, W. (1998). *The performance of axial fans subjected to forced cross-flow at Inlet*. Master's thesis, Department of Mechanical Engineering, University of Stellenbosch. South Africa.

Van Rooyen, J. (2007). *Performance trends of an air-cooled steam condenser under windy conditions*. Master's thesis, University of Stellenbosch. South Africa.

Venter S.J. (1990). *The Effectiveness of Axial Flow Fans in A-Frame Plenums.* Ph.D thesis, Department of Mechanical and Mechatronic Engineering, University of Stellenbosch, South Africa.

Venter, S.J. and Kröger, D.G. (1992). The Effect of Tip Clearance on the Performance of an Axial Flow Fan, *Energy Conversion and Management*, 33(2), pp. 89-97.

Wilkinson, M.B. and Van der Spuy, S. J. (2015).The effect of fan tip configuration on air-cooled condenser axial flow fan performance, *Fan2015*, pp. 1-12.

Wilkinson, M.B. (2017). *The design of an axial flow fan for air-cooled heat exchanger applications*. Master's thesis, Department of Mechanical Engineering, University of Stellenbosch. South Africa.

Zapke, A. (1997). *Characteristics of gas-liquid counterflow in inclined ducts with particular reference to reflux condensers*. Ph.D. thesis, Department of Mechanical and Mechatronic Engineering, University of Stellenbosch, South Africa.

# Appendix A: Fan drive system calculations

This chapter provides the reader with information regarding calculations performed during the design of the fan drive system.

## A.1) Shaft strength calculations

Data obtained from Wilkinson and Van der Spuy (2015) provided the maximum power consumption for the B2-fan. The maximum power consumption at the design blade angle of 31° equalled 5122 W at a tip clearance of 2 mm. Equation A1 is used to calculate the shaft torque.

$$P = \omega \times T \tag{A1}$$

Where $\omega$ represents the shaft rotational speed in radians per second, $P$ the power and $T$ the applied torque. Rearranging equation A1 to equation A2 gives the fan shaft torque.

$$T = \frac{P}{\omega} \tag{A2}$$

With a maximum fan shaft torque of 65.22 N.m the maximum shear stress in the shaft is calculated using equation A3.

$$\tau = \frac{Tr}{J} \tag{A3}$$

Where r represents the shaft radius, which is selected to be 20 mm, and $J$ the polar moment of inertia of the shaft which can be calculated using equation A4.

$$J = \frac{\pi d^4}{32} \tag{A4}$$

The maximum shear stress that will be experienced by the shaft equals 5.2 MPa. With a yield strength of 500 MPa for 410 stainless steel, this diameter of 40 mm is more than strong enough in torsion and will not yield. With the use of equation A5 the maximum axial load that may be experienced by the shaft can be calculated.

$$F_{axial} = \sigma_{yield} \times A \tag{A5}$$

With a yield strength of 500 MPa the maximum load that may be applied the fan shaft may not exceed 628 kN. This is much more than will ever be experienced and it is thus concluded that the fan shaft of 40 mm diameter is more than sufficient to be used at the A-frame ACC.

## A.2) Belt and pulley selection calculations

a) Speed ratio 750/750 = 1.
a) Service factor = 1.1 for fans over 7.5 kW operating less than 10 hours per day.
b) Design power = 1.1×15 kW = 16.5 kW
c) Belt selection: with the use of the design power and fastest shaft revolution speed the SPA belt type is selected for the application.
d) Minimum pulley diameter = 132 mm
e) Pulley pitch diameter = 132 mm and above
f) Centre distance should be as close as possible to 1.3 m due to design constraints. 1.292 m is the closest centre distance to 1.3 m and will be achieved by 2×180 mm diameter pulleys. A correction factor of 1.05 is noted.

$$\text{Trip rate} = \frac{0.0542 \times 180\text{mm} \times 750\ \text{r/min}}{3150\text{mm}} = 2.323$$

This value is lower than the maximum recommended of 12 which is acceptable.
g) Power per belt = 6.84 kW
h) Number of belts required

$$\text{Belts} = \frac{\text{Total power}}{\text{Power per belt}} = \frac{15\ \text{kW}}{6.84\ \text{kW}} = 2.19\ \text{belts}$$

The selected parts are listed below:

- Motor pulley: 180x5 SPA
- Taper Lock Bush: 2517x48mm
- Fan pulley: 180x3 SPA
- Taper Lock Bush: 2517x40mm
- Fenner wedge belts 3x(13N)SPA 3150
- Initial Centre Distance 1292mm

# Appendix B: Sensor calibration test results

This chapter provides an overview of the use of the induced draft wind tunnel along with the test results and graphs for the calibration of the load cell, torque transducer, pressure transducers and anemometers.

## B.1 Induced draft wind tunnel

Appendix B.1 refers to Figure 3.11.

Placing an inlet bell mouth in front of the test section at 1, with tests being performed at 2, helps to achieve a uniform flow field. The mass flow rate through the test section is calculated by measuring the pressure drop across the elliptical nozzles at 7. A single or combination of nozzles may be used for calculating the flow rate.

$$\dot{m} = C_n \Phi_g Y A_n (2\rho_n \Delta p_n)^{0.5} \quad \text{(B1)}$$

$C_n$ is the nozzle discharge coefficient and is a function of the Reynolds number. For 30000 < $Re_n$ < 100000 the discharge coefficient is

$$C_n = 0.954803 + 6.37817 \times 10^{-7} Re_n - 4.65394 \times 10^{-12} {Re_n}^2 + 1.33514 \times 10^{-17} {Re_n}^3 \quad \text{(B2)}$$

For 100000 < $Re_n$ < 350000

$$C_n = 0.9758 + 1.08 \times 10^{-7} Re_n - 1.6 \times 10^{-13} {Re_n}^2 \quad \text{(B3)}$$

and $C_n = 0.994$ for $Re_n$ > 350000

The gas expansion factor $\Phi_g$ may be approximated by

$$\Phi_g = 1 - 3\Delta p_n / \left(4 p_{up} C_p / C_v\right) \quad \text{(B4)}$$

The ratio $C_p/C_v$ for air is 1.4 and $p_{up}$ is the pressure upstream from the nozzle. The approach velocity factor $Y$, for a compressible fluid, can be approximated by

$$Y = 1 + 0.5(A_n/A_{tus})^2 + 2(A_n/A_{tus})^2 \Delta p_n / \left(p_{up} C_p / C_v\right) \quad \text{(B5)}$$

$A_{tus}$ is the upstream cross sectional area of the wind tunnel. With the nozzle coefficients dependent on the Reynolds number and the Reynolds number dependent on the flow rate, it was necessary to estimate an initial Reynolds number

to calculate the mass flow rate. After convergence of the equations through an iterative process, the mass flow rate is calculated.

## B.2 Load Cell calibration

With the drive shaft of the ACC fan orientated vertically, it was decided that a lever arm with a load cell connected perpendicularly to the arm would be used to calibrate the torque transducer. This was decided to prevent measurement errors caused by friction in a cable-, pulley- and weight calibration setup. The load cell used to calibrate the torque transducer first had to be calibrated using known weights as seen in Figure B.1. Apparatus used in the calibration is listed below:

- Load Cell HBM S2 500N
- HBM QuantumX MX840B
- Laptop
- Calibration masses
- Loading platform

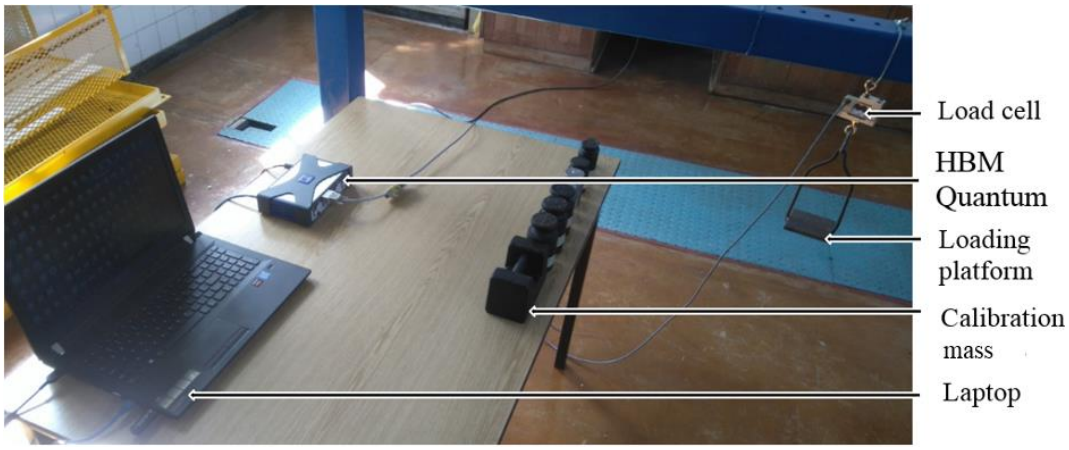


Figure B.1: Load cell calibration setup

The load cell was suspended from a horizontal beam and the platform below the load cell was used for carrying the weights for each measurement. Results from the load cell calibration can be seen in Figure B.2.

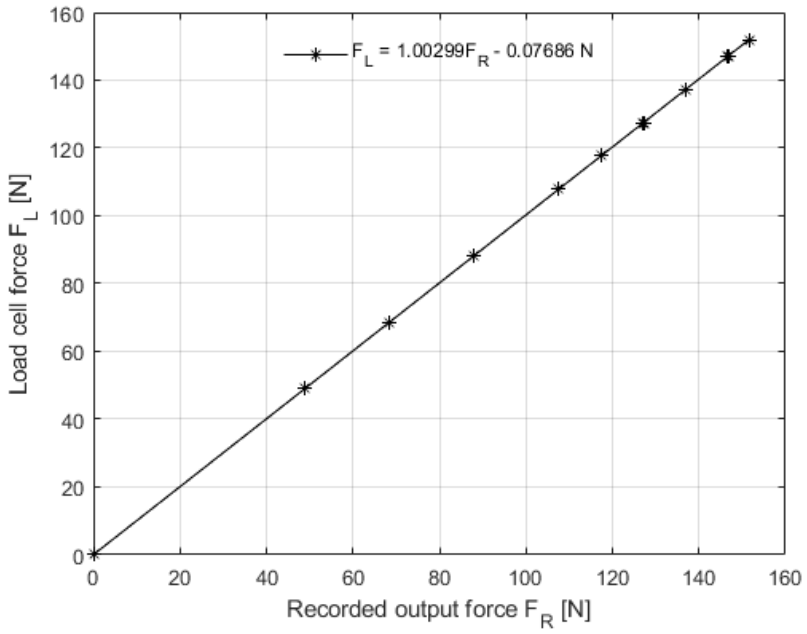


Figure B.2: Load cell calibration

From loading and unloading the load cell three times, equation B6 was calculated for the applied load versus the measured load. With an $R^2$ value of 0.999 the measured results from the load cell can be well approximated by

$$F_L = 1.00299x - 0.07686 \text{ N} \quad \text{(B6)}$$

It was important to zero the load cell with the suspended platform hanging from it. This ensured that the measurements start at zero for each loading of the load cell.

### B.3 Torque transducer calibration

A schematic representation of the torque transducer calibration setup can be seen in Figure B.3. With the use of the calibrated load cell it was possible to know the applied force $F_L$ at a distance of 0.613 m on the lever arm attached to the fan hub. The other end of the load cell was connected to a fixed point as seen in Figure B.5. Apparatus used in the calibration is listed below.

- Load Cell HBM S2 500N
- Torque transducer HBM T22/200 N.m
- HBM QuantumX MX840B
- Laptop
- Lever arm
- 3mm cable
- Cable clamps

Applying the torque to the top shaft, above the torque transducer, resulted in the load cell always being perpendicular to the lever arm. This gave the applied torque, which was then plotted against the measured voltage from the torque transducer. For repeatability of the calibration tests, loading and unloading was repeated three times. Equation B7 shows the relationship between the voltage and the torque as seen in Figure B.4.

$$T_F = 39.89305V - 0.1783 \text{ N.m} \quad \text{(B7)}$$

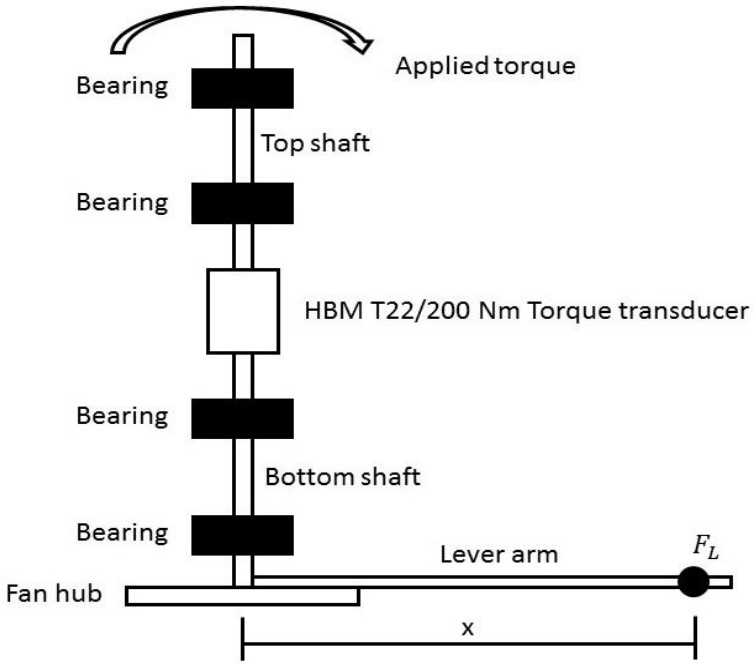


Figure B.3: Schematic torque transducer calibration setup

With an $R^2$ value of 0.999 equation B7 can be considered as an accurate representation of the measured torque. Figure B.4 shows the measured results and calibration curve. Figure B.5 shows the torque transducer calibration setup.

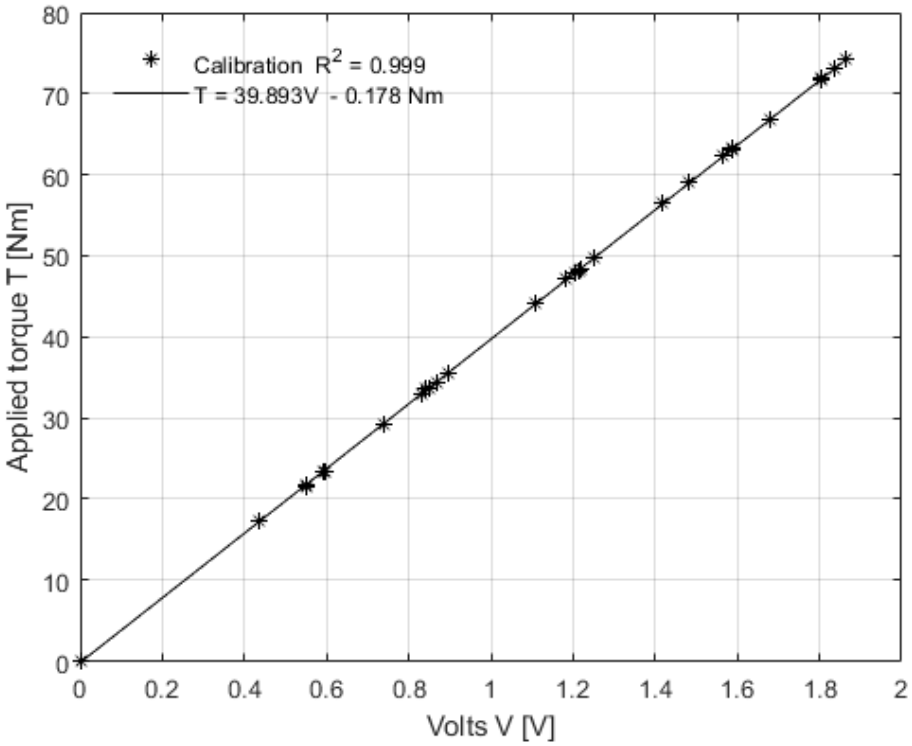


Figure B.4: Resulting torque at voltage output

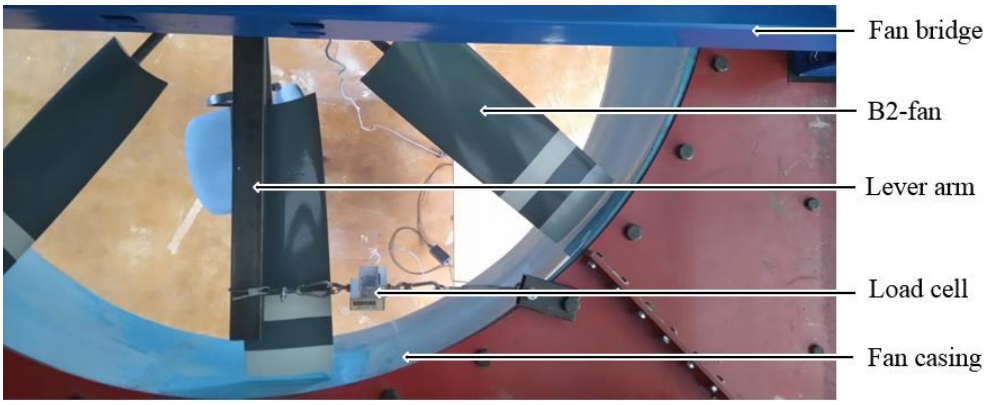


Figure B.5: Torque transducer calibration setup

The calibration data for the torque transducer installed at the small scale A-frame ACC facility is listed in Table B.1. This data is given as it is a time consuming exercise to calibrate the installed torque transducer.

Table B.1 : A-frame ACC facility torque transducer results

| Test 1 | | Test 2 | | Test 3 | |
|---|---|---|---|---|---|
| Torque $T$ [N.m] | Voltage $V$ [V] | Torque $T$ [N.m] | Voltage $V$ [V] | Torque $T$ [N.m] | Voltage $V$ [V] |
| -0.0045 | -0.0012 | -0.0055 | -0.001 | -0.003 | -0.0013 |
| -35.6074 | -0.5492 | -35.169 | -0.5498 | -38.2084 | -0.5946 |
| -54.625 | -0.8421 | -55.8377 | -0.8684 | -57.8224 | -0.8972 |
| -76.7993 | -1.1838 | -78.4589 | -1.216 | -78.7731 | -1.2175 |
| -101.527 | -1.5649 | -102.676 | -1.5893 | -103.048 | -1.5899 |
| -120.853 | -1.8654 | -119.101 | -1.8386 | -116.967 | -1.8064 |
| -120.744 | -1.864 | -96.0488 | -1.4819 | -116.842 | -1.8046 |
| -108.844 | -1.6795 | -71.7535 | -1.1075 | -91.8839 | -1.4172 |
| -78.0544 | -1.2038 | -54.8681 | -0.8515 | -81.0663 | -1.2509 |
| -53.6252 | -0.8322 | -38.1388 | -0.5943 | -47.7638 | -0.7405 |
| -35.125 | -0.5492 | -0.0043 | -0.0012 | -28.0914 | -0.4376 |

## B.4 Pressure transducer calibration

Before calibration of the anemometers, the pressure transducers shown in Figure B.6 had to be calibrated. They were used to measure the upstream pressure and the pressure drop across the flow nozzle in the induced draft wind tunnel as described in Appendix B.1. A Betz Manometer was used to calibrate the two pressure transducers used. The apparatus used in the calibration is listed below.

- Pressure transducers
- Betz manometer
- Plastic tubing
- Valve

Calibration was done by connecting the negatives of the transducers together after setting the manometer to 1100 Pa. The negatives were then connected to the negative of the manometer. Different data points were obtained by opening and closing the valve to obtain new pressure measurements on the manometer. The pressure on the Betz manometer and pressure transducers were documented at each measured pressure.


Figure B.6: Induced draft wind tunnel pressure transducers

The calibration results for the upstream and nozzle pressure measurements are shown in Figure B.7 and Figure B.8 respectively.

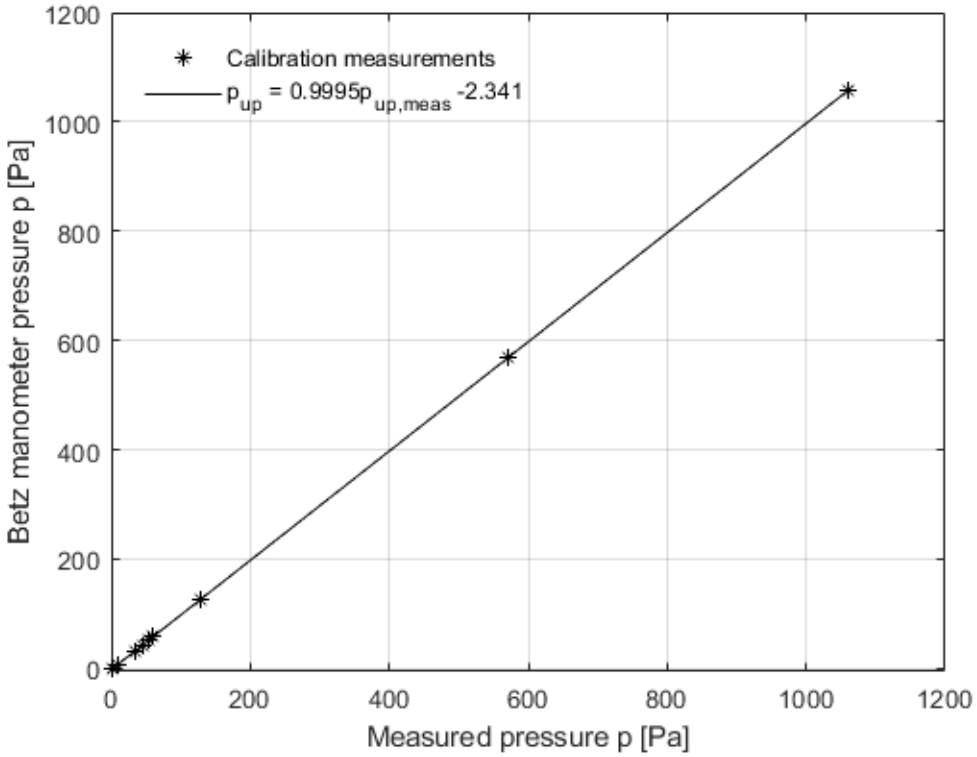


Figure B.7: Wind tunnel upstream pressure transducer calibration

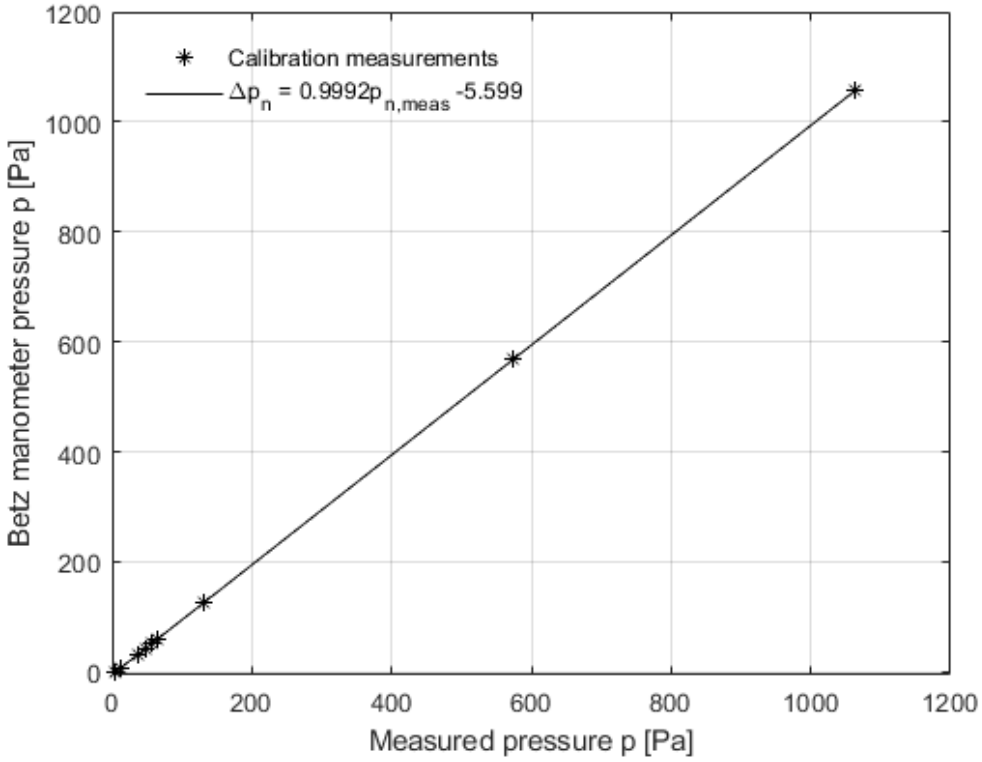


Figure B.8: Wind tunnel nozzle pressure transducer calibration

Equations B8 and B9 show the upstream and pressure difference across the nozzles respectively.

$$p_{up} = 0.9995 \times p_{up,meas} - 2.341 \quad \text{(B8)}$$

$$\Delta p_n = 0.9992 \times p_{n,meas} - 5.599 \quad \text{(B9)}$$

The positive side of the nozzle pressure transducer $\Delta p_n$ was connected to the upstream and the negative to the downstream side of the nozzles respectively to get the pressure drop across the flow nozzles. The negative side of the upstream pressure transducer $p_{up}$ was connected to the upstream pressure tap and the positive side left open to atmospheric pressure.

### B.5 Propeller anemometer calibration

Calibration of the eight propeller anemometers was done in an atmospheric open-loop induced draft wind tunnel as described by Kröger (2004, 5.2.1) that is shown in Figure 3.11 and described in Appendix B.1.

Figure B.9 shows an anemometer held in place with a laboratory stand inside the wind tunnel. This allowed for rigid mounting and also little flow disturbance in the test section.

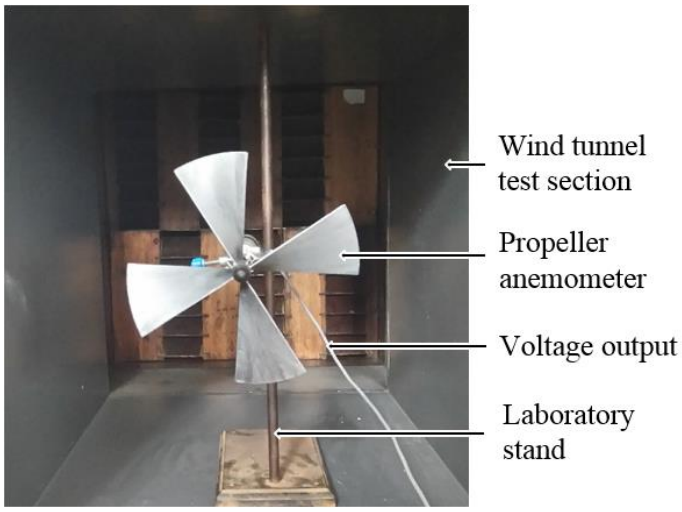


Figure B.9: Anemometer calibration inside induced draft wind tunnel

The calibration tests conducted on the eight anemometers were done by changing the flow rate by means of setting the variable speed drive to different frequency settings. Nozzle and upstream pressures along with the voltage output from the anemometers were documented over an extended period of time to achieve an average reading at each frequency setting and to ensure that all measurements taken were at steady state conditions. The resulting anemometer calibration values and the difference from the design output are listed in Table B.2 respectively.

Table B.2: Anemometer calibration results

| Anemometer # | Calibration slope [m/s/mV] | % Calibration difference from data sheet | Anemometer standard deviation [m/s] |
|---|---|---|---|
| A1 | 0.0167 | 7.32 | 0.0632 |
| A2 | 0.0173 | 3.94 | 0.0483 |
| A3 | 0.0174 | 3.61 | 0.0487 |
| A4 | 0.017 | 5.35 | 0.0499 |
| A5 | 0.0171 | 4.78 | 0.0352 |
| A6 | 0.0172 | 4.5 | 0.0335 |
| A7 | 0.017 | 5.58 | 0.0359 |
| A8 | 0.0168 | 6.63 | 0.0405 |

The calibration curve of propeller anemometer number A3 is shown in Figure B.10. Measured atmospheric conditions are listed below:

Atmospheric pressure $p_a$ = 100900 Pa
Air temperature $T_a$ = 21 ºC
Wetbulb temperature $T_{wb}$ = 15 ºC

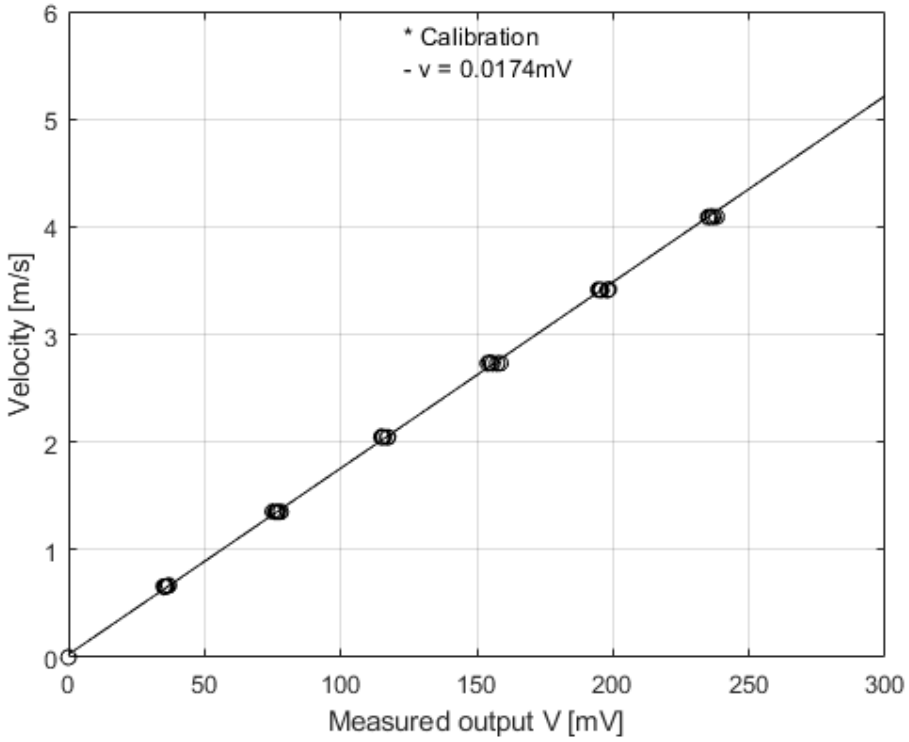


Figure B.10: Anemometer A3 calibration curve

Validation of the anemometer calibration was done with the use of a wind tunnel with a uniform velocity profile across the cross section. Testing each of the eight anemometers, again recording the voltage output of the anemometer and also the air velocity right in front of the anemometer with a pitot tube. The Pitot tube pressure measurements were done with the use of an alcohol manometer. It has the function of being angled so that the measurements can be done 20 times more accurate than when it is positioned vertically. The alcohol had a specific gravity of 0.8. The total pressure equals

$$p_t = p_s + \frac{\rho V^2}{2} \tag{B10}$$

The velocity will then equal

$$V = \sqrt{\frac{2(p_t - p_s)}{\rho}} \tag{B11}$$

Where the difference between the total and static pressure, $p_t$ and $p_s$, is measured by the manometer by reading off the height in millimetres and calculating the dynamic pressure by

$$p_d = \frac{0.8 \times g \times 1000 \times h}{20} \quad \text{(B12)}$$

Where $g$ is 9.81 and h the height of alcohol measured in millimetres. The slope for the anemometers is shown in Table B.3.

Table B.3: Anemometer recalibration results

| Anemometer # | Calibration slope [m/s/mV] |
|---|---|
| A1 | 0.01668 |
| A2 | 0.0173 |
| A3 | 0.01735 |
| A4 | 0.01705 |
| A5 | 0.01708 |
| A6 | 0.01716 |
| A7 | 0.01704 |
| A8 | 0.01688 |

From these results it was found that anemometers A3, A4 and A8 differed the most from the initial calibration results, but the difference was decided to be negligible. The results from the induced draft wind tunnel was chosen to be used rather than the recalibration results as the volumetric flow rate through the test section could more accurately and with more certainty be calculated than the small pressures measured by the pitot tube and the manometer.

## B.6 ISO 5801 (2007) Type-A fan test facility torque transducer calibration

Measurement of the torque applied to the shaft is done by means of a HBM T22/100 torque transducer. Before any measurements were taken it was necessary to first calibrate the torque transducer used. An already manufactured tool for calibration was used. This tool consists of a lever arm, balancing weight and weight loading platform as shown in Figure B.11.

The calibration tool first had to be balanced before attachment to the fan shaft. Balancing was done by inserting a shaft through the middle of the tool which was fixed and allowed the tool to rotate to its equilibrium position. The balancing weight was adjusted and fixed in position when the digital protractor on top of the tool measured 0º.

A zero load reading was taken to ensure that the torque transducer was indeed experiencing no initial torque, after which weights were added. A reading was taken

after each added weight and the whole process was repeated to confirm the measured values. The calibrated equation for the torque transducer is shown in equation B10.

$$T = -0.0568V^2 + 20.477V - 1.6871 \quad \text{(B10)}$$


Figure B.11: Torque transducer calibration setup

## B.7 ISO 5801 (2007) Type-A fan test facility pressure transducer calibration

Calibration of the pressure transducers was done in a similar fashion as in 3.3.1 with the use of a Betz manometer. Applying a pressure to the pressure transducers and documenting the voltage output and the pressure reading on the Betz manometer is shown in Figure B.12. The relationships for the nozzle and settling chamber pressures is given by equations B11 and B12 respectively.

$$p_n = -0.1981V^2 - 121.55V - 170.42 \quad \text{(B11)}$$

$$p_{sc} = 0.2629V^2 - 117.22V + 8.387 \quad \text{(B12)}$$

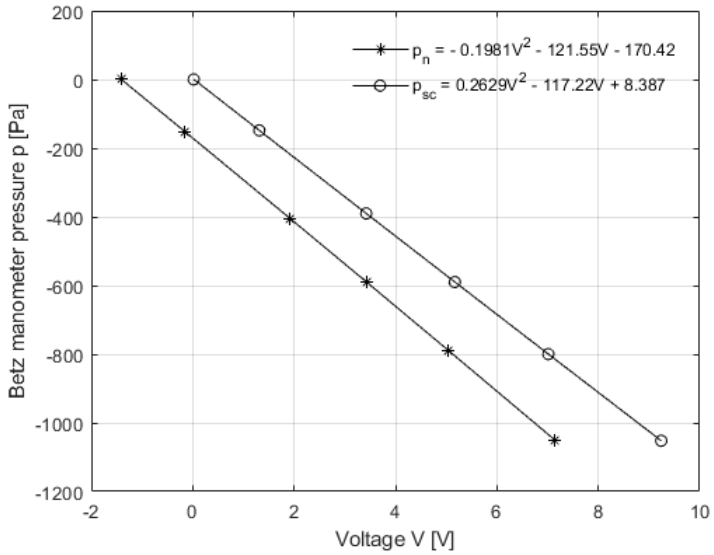


Figure B.12: Pressure transducer calibration

## B.8 Rotational speed calibration

The fan shaft rotational speed is given as a voltage output. With the use of a tachometer and reflective tape, it was possible to measure the rotational speed and document it along with the voltage output. The relationship is shown in equation B13. Figure B.13 shows the calibration curve for the rotational speed.

$$N_{sh} = -86.658V - 0.577 \quad \text{(B13)}$$

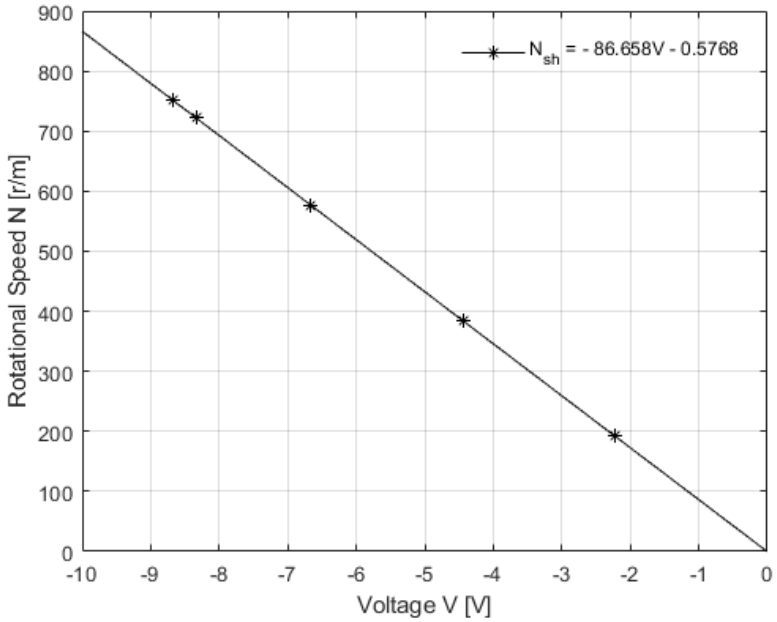


Figure B.13: Shaft rotational speed calibration

## B.9 Fan blade angle setting

Three different blade angles were selected to be tested in both the standardised test facility and the small scale ACC facility for the B2-fan. The blade angle settings selected to be tested included 28º, 31º, and 34º respectively. Changing of the blade angles were done on a flat steel table. A digital protractor was placed on the flat surface and zeroed to the surface angle. The fan was placed on the surface and with the use of a jig, fitting over the blade at the blade root and the blade angles were individually set to the desired angle.

The M-fan was also tested at three different blade angle settings which included 34º, 35º and 36º respectively. For this fan however, setting of the blade angles is simply done by moving a locator pin between different holes which sets the blade angle to the desired position.

# Appendix C: Pressure loss and gain coefficients

This chapter provides the sample calculations on the pressure loss and gain coefficients used in the system draft equation.

## C.1 ACC supports loss coefficient

**Parameters**

$L_s = 2\ m$

$d_s = \sqrt{0.1^2 + 0.1^2}$

$n_s = 4$

$A_2 = \left(\sqrt{0.3^2 + 0.3^2}/2\right)^2 \times \pi L_s$

$v_s = V/A_2$

$Re_s = \rho v_s\, d_s/\mu$

$C_{d,s} = -6.813 \times 10^{-6} Re_s + 1.841$ (Figure 5.3)

$K_s = C_{d,s} L_s d_s\, n_s/A_2$

$A_2$ in this context is the area through which the air flows measured in a cylindrical fashion as shown in Figure 5.2. The values for the support loss coefficient at the different blade angle settings tested are listed in Table C.1 along with the standard deviation as a result of the normal distribution of the volumetric flow rate. Figure C.1 shows the loss coefficient as a function of volumetric flow rate.

Table C.1: Vertical supports loss coefficients

| Parameter | 28º Blade angle setting | 31º Blade angle setting | 34º Blade angle setting |
|---|---|---|---|
| Volumetric flow rate V [$m^3/s$] | 13.117 | 14.615 | 15.929 |
| $K_s$ | 0.0768 | 0.0767 | 0.0765 |
| $\sigma$ | $3.522\times10^{-6}$ | $3.696\times10^{-6}$ | $3.658\times10^{-6}$ |

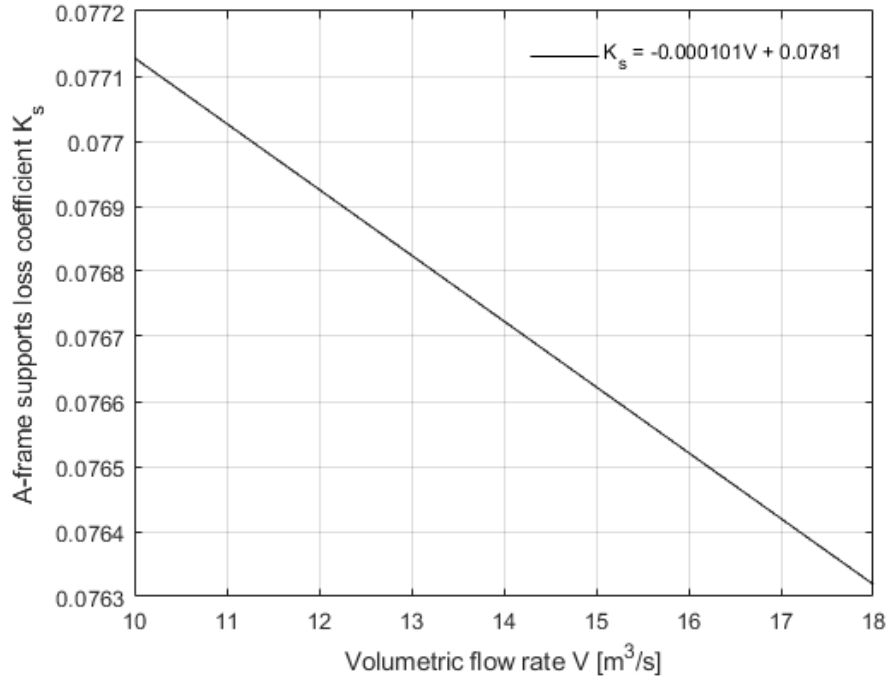


Figure C.1: A-frame supports loss coefficient

## C.2 Fan Bridge loss coefficient

**Parameters**

$d_b = 0.05$ m

$Re_b = \rho(V/A_e)\, d_b/\mu$

$L_{act} = 2.55$ m

$C_d = 2.365 \times 10^{-5} Re_b + 1.496$ (Figure 5.3)

$F_{d,b} = C_d L_{act} d\rho\, ((V/A_e)^2)/2$

$p_b = F_{d,b}/(L_1 L_2)$

$K_b = 2\rho p_b/((V/A_e)^2)$

The values for the bridge loss coefficient at the different blade angle settings tested are listed in Table C.2 along with the standard deviation as a result of the normal distribution of the volumetric flow rate. Figure C.2 shows the fan bridge loss coefficient as a function of volumetric flow rate.

Table C.2: Fan bridge loss coefficients

| Parameter | 28º Blade angle setting | 31º Blade angle setting | 34º Blade angle setting |
|---|---|---|---|
| Volumetric flow rate V [$m^3/s$] | 13.117 | 14.615 | 15.929 |
| $K_b$ | 0.345 | 0.356 | 0.367 |
| $\sigma$ | $2.758\times10^{-4}$ | $2.894\times10^{-4}$ | $2.864\times10^{-4}$ |

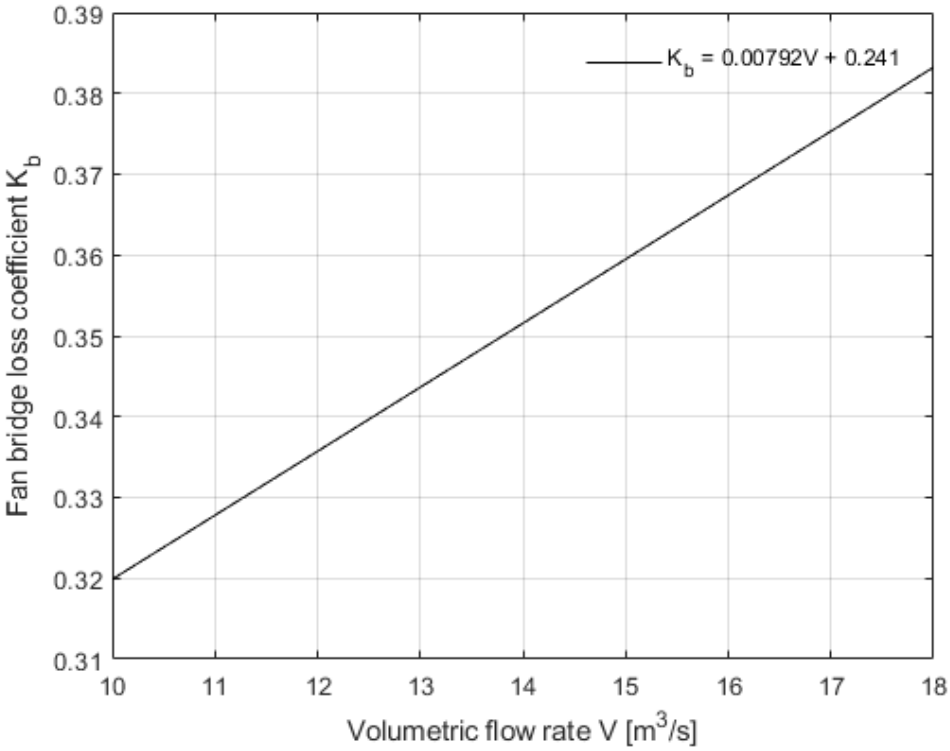


Figure C.2: Fan bridge loss coefficient

## C.3 Heat exchanger loss coefficient

The calibrated heat exchanger loss coefficient along with the standard deviation at the different blade angle settings, which includes the turning loss of the flow, is shown in Table C.3.

Table C.3: Heat exchanger loss coefficient

| Parameter | 28º Blade angle setting | 31º Blade angle setting | 34º Blade angle setting |
|---|---|---|---|
| Volumetric flow rate V [$m^3$/s] | 13.117 | 14.615 | 15.929 |
| $K_{he\theta}$ | 37.733 | 37.288 | 36.995 |
| $\sigma$ | 0.1619 | 0.0832 | 0.0828 |

From these results it is seen that the heat exchanger standard deviation can be expected to be higher at lower volumetric flow rates. This can be due to a small disturbance in the inlet flow, during calibration or facility tests, resulting in a greater percentage deviation in the measured result at lower volumetric flow rates.

## C.4 Fan static pressure rise coefficient

Tests performed at the standardised fan testing facility were used to calculate the fan static pressure rise coefficient and standard deviation of these values in the region in which tests were performed at in the A-frame test facility. Table C.4 shows the calculated results.

Table C.4: Fan static pressure rise coefficient

| Parameter | 28º Blade angle setting | 31º Blade angle setting | 34º Blade angle setting |
|---|---|---|---|
| Volumetric flow rate V [$m^3/s$] | 13.117 | 14.615 | 15.929 |
| $K_{Fs}$ | 4.732 | 4.602 | 4.9 |
| $\sigma$ | 0.0766 | 0.1249 | 0.0487 |

# Appendix D: B2-fan test data

This chapter provides the plots of the B2-fan tested in the small scale ACC setup as well as the results from the fan tests according to the ISO 5801 (2007) Type-A tests.

## D.1 B2-fan ISO 5801 (2007) Type-A test results

The characteristic curves for the tests performed and repeated for the different blade angle settings is shown in Figures D.1-D.3.

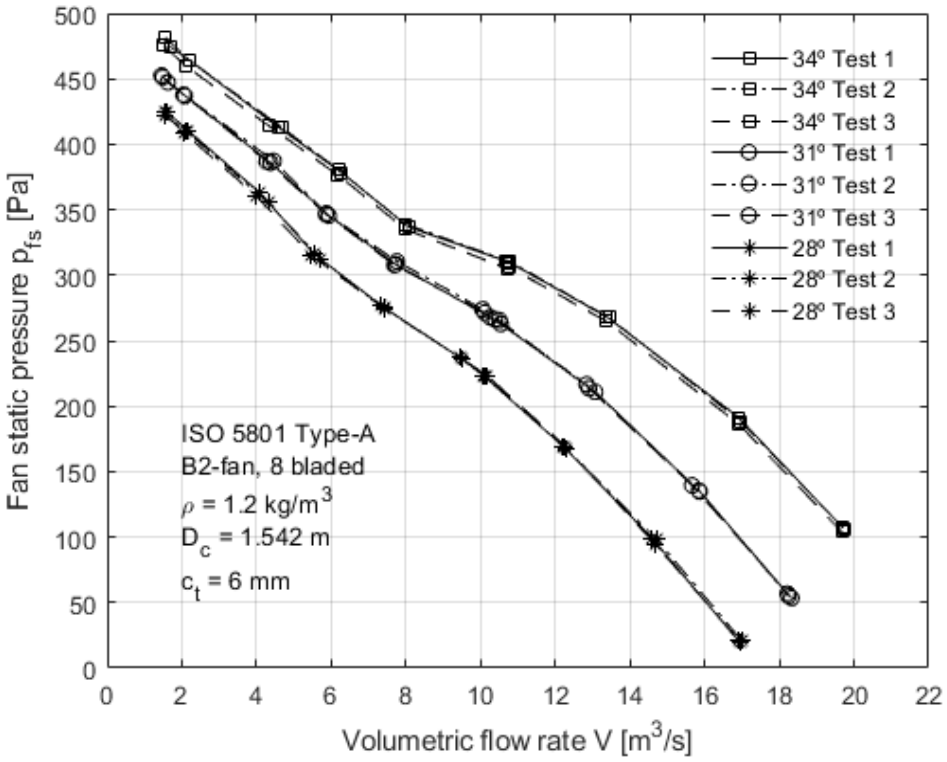


Figure D.1: Fan static pressure rise tests at different blade angle settings

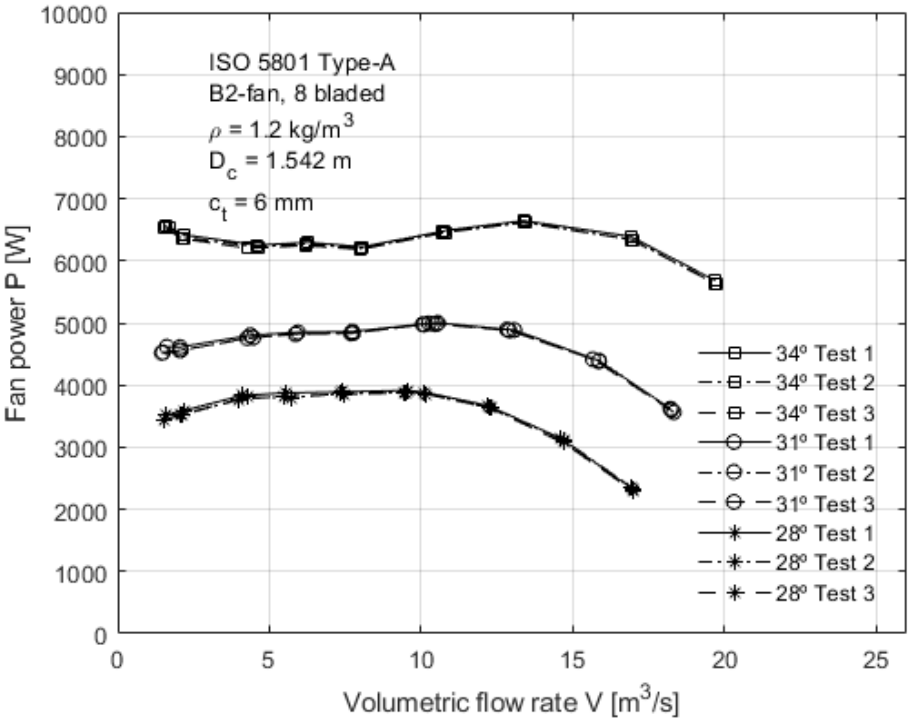


Figure D.2: Fan power consumption tests at different blade angle settings

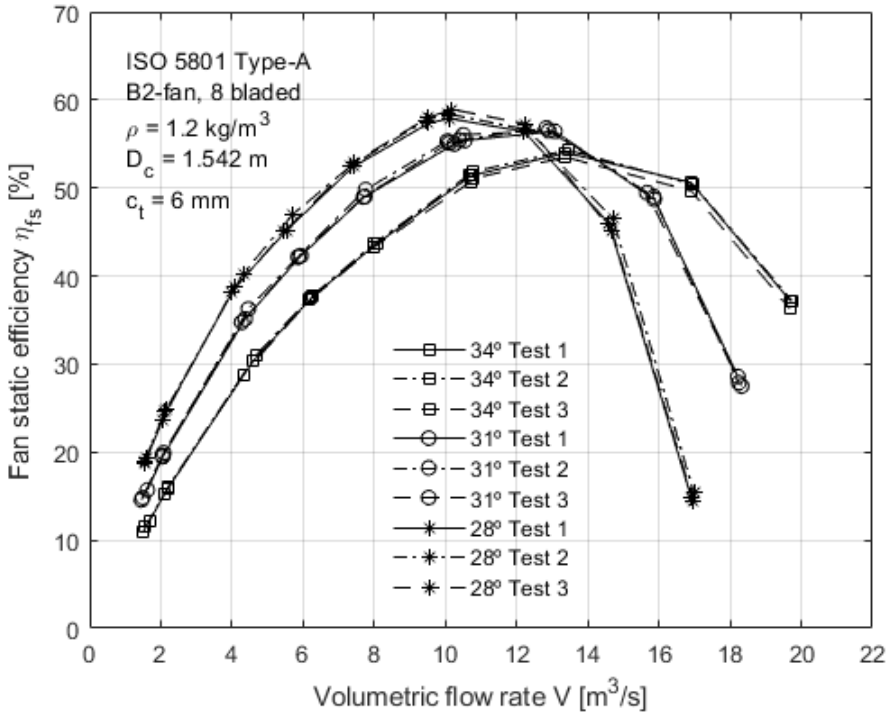


Figure D.3: Fan static efficiency tests at different blade angle settings

The data from the B2-fan tests at 28º blade angle according to ISO 5801 (2007) in a Type-A test facility is shown in Table D.1.

Table D.1: B2-fan tests at 28º blade angle according to ISO 5801 (2007)

| Volumetric flow rate $V$[m$^3$/s] | Fan static pressure $P_{Fs}$ [Pa] | Fan power $P$[W] | Fan static efficiency $\eta_{Fs}$ |
|---|---|---|---|
| 1.552024833 | 423.7359891 | 3463.411 | 18.9869 |
| 2.107906119 | 409.7401105 | 3544.074 | 24.36849 |
| 4.131403152 | 359.5955116 | 3802.307 | 39.06114 |
| 5.569356154 | 314.6538933 | 3830.613 | 45.74982 |
| 7.393098298 | 275.2564552 | 3868.187 | 52.60812 |
| 9.488784636 | 236.3837871 | 3890.542 | 57.65309 |
| 10.12656565 | 223.0437652 | 3867.032 | 58.40955 |
| 12.26302287 | 168.5789411 | 3642.79 | 56.74993 |
| 14.65983015 | 97.33279597 | 3109.981 | 45.8752 |
| 16.95359081 | 20.48739584 | 2330.297 | 14.90383 |

The data from the B2-fan tests at 31º blade angle according to ISO 5801 (2007) in a type-A test facility is shown in Table D.2.

Table D.2: B2-fan tests at 31º blade angle according to ISO 5801 (2007)

| Volumetric flow rate $V$[m$^3$/s] | Fan static pressure $P_{Fs}$ [Pa] | Fan power $P$[W] | Fan static efficiency $\eta_{Fs}$ |
|---|---|---|---|
| 1.52194429 | 450.3060196 | 4554.547 | 15.03932 |
| 2.058847296 | 437.4800947 | 4577.892 | 19.67569 |
| 4.367285982 | 386.7380086 | 4773.83 | 35.3808 |
| 5.888326267 | 346.4258122 | 4830.211 | 42.23089 |
| 7.728232842 | 308.8131401 | 4843.473 | 49.27513 |
| 10.13854284 | 271.0657122 | 4982.635 | 55.15179 |
| 10.47623037 | 264.9522103 | 4989.583 | 55.62867 |
| 12.93596952 | 213.7382753 | 4886.076 | 56.5828 |
| 15.79467997 | 136.5631902 | 4395.992 | 49.06157 |
| 18.26344173 | 55.07362987 | 3594.008 | 27.98203 |

The data from the B2-fan tests at 34º blade angle according to ISO 5801 (2007) in a type-A test facility is shown in Table D.3.

Table D.3: B2-fan tests at 34º blade angle according to ISO 5801 (2007)

| Volumetric flow rate $V$[m$^3$/s] | Fan static pressure $P_{Fs}$ [Pa] | Fan power $P$[W] | Fan static efficiency $\eta_{Fs}$ |
|---|---|---|---|
| 1.588689635 | 477.0650146 | 6551.475 | 11.56723 |
| 2.163336419 | 462.7857182 | 6383.662 | 15.68389 |
| 4.52774937 | 413.4049487 | 6226.616 | 30.05729 |
| 6.217625737 | 378.3762228 | 6271.841 | 37.50998 |
| 8.015013576 | 336.9954246 | 6202.982 | 43.54334 |
| 10.70577152 | 308.9138986 | 6457.827 | 51.21098 |
| 10.78586661 | 308.6022996 | 6467.994 | 51.4616 |
| 13.39280834 | 266.8954343 | 6626.301 | 53.94395 |
| 16.92652372 | 188.670677 | 6357.831 | 50.22883 |
| 19.70441139 | 105.6765864 | 5646.966 | 36.87425 |

## D.2 A-frame facility test results

The data from the A-frame facility outlet velocity tests for the B2-fan at a blade angle of 28º on the Eastern and Western bundles is shown in Table D.4 and Table D.5 respectively. A total of 80 velocity measurements are documented for each heat exchanger of which the whole test is repeated three times and averaged to give the values shown. All of the velocity measurements tabled are done in such a matter that shows the velocities if one were to look at the heat exchanger outlet perpendicularly on the outer surface.

Table D.4: Eastern side outlet velocity measurements at 28º blade angle

| A1 | A2 | A3 | A4 | A5 | A6 | A7 | A8 |
|---|---|---|---|---|---|---|---|
| 2.759362 | 2.790511 | 2.772869 | 2.601226 | 3.038026 | 2.59315 | 2.67478 | 2.918107 |
| 2.438679 | 2.353959 | 2.245095 | 2.239491 | 2.619667 | 2.371343 | 2.453253 | 2.63762 |
| 2.308104 | 2.255013 | 2.161121 | 2.131489 | 2.440634 | 2.27176 | 2.300832 | 2.473751 |
| 2.296258 | 2.246311 | 2.102668 | 2.168408 | 2.427443 | 2.264907 | 2.22919 | 2.423642 |
| 2.509902 | 2.306504 | 2.289566 | 2.255549 | 2.330063 | 2.287536 | 2.290519 | 2.416394 |
| 2.658854 | 2.339441 | 2.345207 | 2.317827 | 2.342771 | 2.328661 | 2.312104 | 2.491285 |
| 3.04142 | 2.554442 | 2.507954 | 2.465547 | 2.545734 | 2.594691 | 2.621415 | 2.767161 |
| 3.078326 | 2.716387 | 2.733769 | 2.7095 | 2.795453 | 2.81912 | 2.785799 | 2.774424 |
| 2.836737 | 2.646373 | 2.83419 | 2.741467 | 2.779027 | 2.794906 | 2.804039 | 2.853696 |
| 2.801432 | 2.721022 | 3.019326 | 2.803129 | 2.895909 | 2.826722 | 2.866859 | 2.888153 |

Table D.5: Western side outlet velocity measurements at 28º blade angle

| A1 | A2 | A3 | A4 | A5 | A6 | A7 | A8 |
|---|---|---|---|---|---|---|---|
| 2.773471 | 2.658997 | 2.502605 | 2.556281 | 2.565363 | 2.584322 | 2.69223 | 2.967977 |
| 2.380766 | 2.272912 | 2.178143 | 2.242847 | 2.224664 | 2.28435 | 2.446487 | 2.607413 |
| 2.292133 | 2.179153 | 2.115593 | 2.242784 | 2.153165 | 2.16522 | 2.282911 | 2.503042 |
| 2.352817 | 2.167398 | 2.089908 | 2.167628 | 2.076511 | 2.10719 | 2.299808 | 2.424626 |
| 2.397196 | 2.282687 | 2.197424 | 2.267596 | 2.142983 | 2.178015 | 2.354646 | 2.486004 |
| 2.559964 | 2.473261 | 2.311624 | 2.36047 | 2.215087 | 2.232123 | 2.462081 | 2.70519 |
| 2.768928 | 2.466345 | 2.277418 | 2.348317 | 2.165521 | 2.356849 | 2.537141 | 2.675872 |
| 2.722743 | 2.498697 | 2.404378 | 2.509044 | 2.385465 | 2.536131 | 2.716451 | 2.742413 |
| 2.679136 | 2.72486 | 2.709652 | 2.734248 | 2.633063 | 2.795989 | 2.820465 | 2.851578 |
| 2.757445 | 2.713575 | 2.877887 | 2.734242 | 2.897307 | 2.846281 | 2.880849 | 2.909451 |

The data from the A-frame facility outlet velocity tests for the B2-fan at a blade angle of 31º on the Eastern and Western bundles is shown in Table D.6 and Table D**.7** respectively.

Table D.6: Eastern side outlet velocity measurements at 31º blade angle

| A1 | A2 | A3 | A4 | A5 | A6 | A7 | A8 |
|---|---|---|---|---|---|---|---|
| 2.944624 | 2.983701 | 3.007134 | 2.788516 | 3.39767 | 2.919018 | 2.999441 | 3.282518 |
| 2.61318 | 2.539313 | 2.473916 | 2.420501 | 2.924476 | 2.663548 | 2.726435 | 2.943079 |
| 2.500279 | 2.443257 | 2.364985 | 2.309932 | 2.712633 | 2.531736 | 2.538887 | 2.732839 |
| 2.506213 | 2.470568 | 2.33845 | 2.377751 | 2.704274 | 2.524287 | 2.506374 | 2.668195 |
| 2.76016 | 2.514105 | 2.553923 | 2.474002 | 2.604196 | 2.54149 | 2.581249 | 2.662842 |
| 2.931473 | 2.574635 | 2.611756 | 2.539072 | 2.591375 | 2.544195 | 2.572574 | 2.742433 |
| 3.357712 | 2.798313 | 2.762502 | 2.686568 | 2.791974 | 2.818478 | 2.889471 | 3.04702 |
| 3.397531 | 2.923339 | 2.956932 | 2.858086 | 3.065126 | 3.088426 | 3.06799 | 3.080862 |
| 3.195286 | 2.941306 | 3.112103 | 2.970403 | 3.134762 | 3.1659 | 3.206076 | 3.223208 |
| 3.247219 | 3.1552 | 3.536902 | 3.246005 | 3.352721 | 3.304573 | 3.337058 | 3.358124 |

Table D.7: Western side outlet velocity measurements at 31º blade angle

| A1 | A2 | A3 | A4 | A5 | A6 | A7 | A8 |
|---|---|---|---|---|---|---|---|
| 2.988634 | 2.821811 | 2.687169 | 2.713729 | 2.842548 | 2.906788 | 2.987343 | 3.286719 |
| 2.624867 | 2.460426 | 2.372072 | 2.487982 | 2.507809 | 2.585926 | 2.721592 | 2.894122 |
| 2.533259 | 2.408679 | 2.343931 | 2.490746 | 2.415643 | 2.44554 | 2.538424 | 2.797022 |
| 2.61072 | 2.403639 | 2.334598 | 2.406332 | 2.333639 | 2.368002 | 2.560575 | 2.69233 |
| 2.647622 | 2.539895 | 2.469383 | 2.524667 | 2.381567 | 2.436449 | 2.609031 | 2.764626 |
| 2.838043 | 2.734253 | 2.587395 | 2.609096 | 2.437687 | 2.463346 | 2.721267 | 3.036596 |
| 3.0772 | 2.69841 | 2.498076 | 2.568251 | 2.364347 | 2.558744 | 2.795257 | 3.034147 |
| 3.061417 | 2.768521 | 2.65074 | 2.720427 | 2.582487 | 2.747175 | 3.012343 | 3.11941 |
| 3.106264 | 3.109948 | 3.030395 | 3.046351 | 2.926796 | 3.14046 | 3.222152 | 3.262983 |
| 3.210766 | 3.153075 | 3.34124 | 3.161753 | 3.297101 | 3.22746 | 3.316083 | 3.369072 |

The data from the A-frame facility outlet velocity tests for the B2-fan at a blade angle of 34º on the Eastern and Western bundles is shown in Table D.8 and Table D.9 respectively.

Table D.8: Eastern side outlet velocity measurements at 34º blade angle

| A1 | A2 | A3 | A4 | A5 | A6 | A7 | A8 |
|---|---|---|---|---|---|---|---|
| 3.336151 | 3.361893 | 3.374818 | 3.051393 | 3.697999 | 3.181884 | 3.273049 | 3.583297 |
| 2.894315 | 2.816789 | 2.748783 | 2.645798 | 3.12512 | 2.887144 | 2.929021 | 3.187816 |
| 2.768146 | 2.711349 | 2.616225 | 2.52154 | 2.899233 | 2.736219 | 2.740119 | 2.95671 |
| 2.756292 | 2.729591 | 2.556948 | 2.591188 | 2.901821 | 2.732024 | 2.727104 | 2.862709 |
| 3.061731 | 2.798367 | 2.783194 | 2.712994 | 2.803675 | 2.74855 | 2.804846 | 2.833675 |
| 3.264641 | 2.849695 | 2.856854 | 2.790901 | 2.80061 | 2.725782 | 2.778526 | 2.905884 |
| 3.683414 | 3.051213 | 2.972473 | 2.908081 | 2.95134 | 2.94691 | 3.039477 | 3.21 |
| 3.77023 | 3.247538 | 3.181192 | 3.104418 | 3.298442 | 3.288505 | 3.262032 | 3.285669 |
| 3.537491 | 3.222688 | 3.382481 | 3.257111 | 3.44391 | 3.468692 | 3.517173 | 3.499719 |
| 3.483292 | 3.381341 | 3.896384 | 3.572078 | 3.77109 | 3.735166 | 3.757053 | 3.772337 |

Table D.9: Western side outlet velocity measurements at 34º blade angle

| A1 | A2 | A3 | A4 | A5 | A6 | A7 | A8 |
|---|---|---|---|---|---|---|---|
| 3.313759 | 3.127461 | 3.048714 | 3.001631 | 3.122385 | 3.184099 | 3.262594 | 3.623975 |
| 2.837115 | 2.700853 | 2.62162 | 2.694146 | 2.703335 | 2.80242 | 2.944985 | 3.169557 |
| 2.754628 | 2.631503 | 2.539085 | 2.692092 | 2.602804 | 2.635749 | 2.743744 | 3.024014 |
| 2.811878 | 2.628831 | 2.528367 | 2.612267 | 2.519505 | 2.574301 | 2.757542 | 2.939354 |
| 2.859469 | 2.763575 | 2.667547 | 2.742552 | 2.582568 | 2.653519 | 2.807031 | 3.008104 |
| 3.031627 | 2.981086 | 2.808256 | 2.839315 | 2.643315 | 2.657914 | 2.914348 | 3.295162 |
| 3.281079 | 2.926188 | 2.697836 | 2.770434 | 2.524536 | 2.679226 | 2.957518 | 3.255796 |
| 3.301016 | 2.969874 | 2.779764 | 2.901507 | 2.728824 | 2.873027 | 3.19384 | 3.353482 |
| 3.365282 | 3.352726 | 3.202302 | 3.282118 | 3.140899 | 3.377462 | 3.546823 | 3.552356 |
| 3.482983 | 3.48799 | 3.692654 | 3.513658 | 3.636506 | 3.590001 | 3.696311 | 3.724924 |